

Master's degree thesis

IP501909 MSc thesis, discipline oriented master

**Investigation in Scale Effects on Propellers with
Different Magnitude of Skew by CFD Methods**

2106

Number of pages including this page: 94

Aalesund, 25.05.2015

Mandatory statement

Each student is responsible for complying with rules and regulations that relate to examinations and to academic work in general. The purpose of the mandatory statement is to make students aware of their responsibility and the consequences of cheating. **Failure to complete the statement does not excuse students from their responsibility.**

Please complete the mandatory statement by placing a mark <u>in each box</u> for statements 1-6 below.		
1.	I/we hereby declare that my/our paper/assignment is my/our own work, and that I/we have not used other sources or received other help than is mentioned in the paper/assignment.	<input checked="" type="checkbox"/>
2.	I/we hereby declare that this paper <ol style="list-style-type: none"> 1. Has not been used in any other exam at another department/university/university college 2. Is not referring to the work of others without acknowledgement 3. Is not referring to my/our previous work without acknowledgement 4. Has acknowledged all sources of literature in the text and in the list of references 5. Is not a copy, duplicate or transcript of other work 	Mark each box: 1. <input checked="" type="checkbox"/> 2. <input checked="" type="checkbox"/> 3. <input checked="" type="checkbox"/> 4. <input checked="" type="checkbox"/> 5. <input checked="" type="checkbox"/>
3.	I am/we are aware that any breach of the above will be considered as cheating, and may result in annulment of the examination and exclusion from all universities and university colleges in Norway for up to one year, according to the Act relating to Norwegian Universities and University Colleges, section 4-7 and 4-8 and Examination regulations paragraph 31.	<input checked="" type="checkbox"/>
4.	I am/we are aware that all papers/assignments may be checked for plagiarism by a software assisted plagiarism check	<input checked="" type="checkbox"/>
5.	I am/we are aware that Aalesund University college will handle all cases of suspected cheating according to prevailing guidelines.	<input checked="" type="checkbox"/>
6.	I/we are aware of the University College's rules and regulation for using sources paragraph 30.	<input checked="" type="checkbox"/>

Publication agreement

ECTS credits: 30

Supervisor: Karl Henning Halse

Agreement on electronic publication of master thesis

Author(s) have copyright to the thesis, including the exclusive right to publish the document (The Copyright Act §2).

All theses fulfilling the requirements will be registered and published in Brage HiÅ, with the approval of the author(s).

Theses with a confidentiality agreement will not be published.

I/we hereby give Aalesund University College the right to, free of charge, make the thesis available for electronic publication: yes no

Is there an [agreement of confidentiality](#)? yes no

(A supplementary confidentiality agreement must be filled in and included in this document)

- If yes: Can the thesis be online published when the period of confidentiality is expired? yes no

This master's thesis has been completed and approved as part of a master's degree programme at Aalesund University College. The thesis is the student's own independent work according to section 6 of Regulations concerning requirements for master's degrees of December 1st, 2005.

Date: 25.05.2015

TITLE:

Investigation in Scale Effects on Propellers with Different Magnitude of Skew by CFD Methods

CANDIDATE NAME:

2106

DATE: 25.05.2015	COURSE CODE: IP501909	COURSE TITLE: MSc thesis	RESTRICTION:
STUDY PROGRAM: Master-Ship Design		PAGES/APPENDIX: 90/9	LIBRARY NO.:

SUPERVISOR(S):

Karl Henning Halse

ABSTRACT:

Scale effects on the open-water performance of marine propellers are the problems to be investigated to the researchers and ship designers. Present thesis analyse the scale effects of marine propellers by CFD methods. The main focus is on the aspects related to propeller blade skews. The ambient flow around the propeller is assumed to be fully turbulent and the Reynolds-averaged Navier-Stokes (RANS) equations are applied in the turbulent flow. Propellers with different scales and skew angles operating in open-water conditions will be simulated in the CFD software – STAR-CCM+. The differences in open-water characteristics (e.g. thrust coefficient K_T , torque coefficient K_Q and efficiency η_0) of propellers with different skew angles are demonstrated and explained through the analysis of simulated flow patterns around the blades, as well as through the reasonable estimations of percentage of pressure and friction force contributions. The CFD results are compared with some experimental data for verifications.

This thesis is submitted for evaluation at Ålesund University College.

Postal address:

 Høgskolen i Ålesund
 N-6025 Ålesund
 Norway

Visit adress

 Larsg årdsvegen 2
Internett
www.hials.no
Telephone

70 16 12 00

E-mail
yaning.zhao@stud.hials.no
Fax

70 16 13 00

Bank

7694 05 00636

Enterprise no.

NO 971 572 140

MASTER THESIS 2015
FOR
STUD.TECHN. Yaning Zhao

Investigation in Scale Effects on Propellers with Different Magnitude of Skew by CFD Methods

In nowadays, to achieve the best propulsion performance for commercial ship owners, an excellent propeller design is one of the most economical saving ways. In most experimental tests, only the model scale propellers will be tested. The full-scale propeller performance is corrected and derived from that of model scale data and take the scale effects into account. Computational fluid dynamics (CFD) are becoming an increasingly important way for propeller tests in the propeller pre-design phase.

The scale effects of open-water propellers in different scales and magnitude of skew will be investigated by CFD methods with turbulent flow model. The objective of this thesis is to provide a reference of scale effects on propellers with various of skew angles for propeller designers.

- Pre-study:
 - Skew definition of propellers and theoretical propeller scale effects
 - CFD method investigations
 - ITTC 78's scale correction for open water propellers
- Simulations in STAR-CCM+
 - Validation process for propeller by comparing with experimental data
 - Develop proper CFD setups for propellers with different skew and scales
 - Simulate all the propellers in STAR- CCM+ and collect results
- Data processing
 - Compare the open-water performance of propellers with different scales
 - Compare the open-water performance of propellers with different magnitude of skew
 - Flow pattern analysis
 - Compare the ITTC correction with the CFD results
- Conclude the scale effects results from CFD methods

Supervision at Aalesund UC.: Karl Henning Halse

Finish: 25. May 2015

Signature

candidate: 


PREFACE

Propeller performance is an important metric of the ship propulsion system. To get the propeller performance, open water tests are usually carried out. There are many geometric factors that affect the properties of the propellers, for instance, the pitch, the blade ratio of the propeller, the skew angle and the blade number. The PROSCALE project provided by MARINTEK is targeted to study the scale effects on these factors. This thesis will discuss the “skew series” of the project, which means the scale effects on propellers with different magnitude of skew will be studied.

During the work of last six month, there are many problems have been experienced. Thanks to my supervisor Mr. Halse, who provided suggestions and guidance for the project and imparting knowledge in my two years’ master study life. Also thank MARINTKE who provides so interesting topic and technical supports for the project. A thank is also given to all my families and friends who make the two years’ master life wonderful.

ABSTRACT

Scale effects on the open-water performance of marine propellers are the problems to be investigated to the researchers and ship designers. Present thesis analyse the scale effects of marine propellers by CFD methods. The main focus is on the aspects related to propeller blade skews. The ambient flow around the propeller is assumed to be fully turbulent and the Reynolds-averaged Navier-Stokes (RANS) equations are applied in the turbulent flow. Propellers with different scales and skew angles operating in open-water conditions will be simulated in the CFD software– STAR-CCM+. The differences in open-water characteristics (e.g. thrust coefficient K_T , torque coefficient K_Q and efficiency η_0) of propellers with different skew angles are demonstrated and explained through the analysis of simulated flow patterns around the blades, as well as through the reasonable estimations of percentage of pressure and friction force contributions. The CFD results are compared with some experimental data for verifications.

Table of contents

SYMBOLS.....	IX
ABBREVIATIONS.....	X
1 INTRODUCTION.....	1
1.1 PROJECT BACKGROUND.....	1
1.2 PROBLEM FORMULATION	2
1.2.1 Target cases.....	2
1.2.2 Calculation conditions for CFD analyses	3
1.3 OBJECTIVES.....	4
2 THEORETICAL BASIS.....	5
2.1 BLADE SKEW.....	5
2.2 PROPELLER SCALE EFFECTS	6
2.3 CFD.....	7
2.3.1 Governing equations of fluid dynamics – Basic laws of physics	7
2.3.2 Turbulence model and RANS.....	8
2.3.3 Near-wall treatment.....	10
2.3.4 Moving Reference Frame.....	10
2.3.5 Mesh generation	11
3 METHODS	13
3.1 PROPELLER CHARACTERISTICS	13
3.2 ITTC78 OF SCALE EFFECT CORRECTIONS	14
3.3 TEST ARRANGEMENT AND PLAN	16
3.4 METHOD DESCRIPTIONS	16
3.4.1 Test and analysis parameters	17
3.4.2 Calculating new propellers and changing scale.....	34
3.4.3 Analysis methods	36
4 RESULTS.....	37
4.1 RESULTS VALIDATION.....	37
4.1.1 Experimental results	37
4.1.2 STAR-CCM+ results.....	38
4.2 CFD RESULTS.....	42
4.2.1 Scale effects on open water characteristics	42
4.2.2 Open water characteristics for different skews	45

4.2.3	<i>Pressure distribution on blade section</i>	47
4.2.4	<i>Flow patterns</i>	51
4.2.5	<i>Vortex</i>	54
4.2.6	<i>ITTC correction for propeller scale effects</i>	58
5	DISCUSSION	60
5.1	WORK QUALITY	60
5.1.1	<i>CFD results compared with experimental data</i>	60
5.1.2	<i>Scale effects on propellers with different skew angles</i>	64
5.2	PROJECT PROCESS	68
6	CONCLUSIONS	70
7	FURTHER WORK	71
	REFERENCES	72
	APPENDIX A EXPERIMENTAL DATA OF P1374 AT P/D=0.90	73
	APPENDIX B PUBLICATION VERSION OF THE THESIS	74

LIST OF FIGURES

Figure 2.1.1 Skew definition	5
Figure 2.1.2 Reference frames: (a) global reference frame and (b) local reference frame.....	6
Figure 2.3.1 Schematic illustration of turbulence scales resolved by DNS, LES and RANS methods	9
Figure 2.3.2 Cell types in modern CFD codes	12
Figure 3.1.1 Open water diagram for Wageningen B5-75 screw series.....	14
Figure 3.4.1 Two variants of the domain setup with one blade passage	18
Figure 3.4.2 Establish the segment domain.....	18
Figure 3.4.3 Boundary assignment of the domain.....	19
Figure 3.4.4 Introduction of feature curves in the one blade passage domain	20
Figure 3.4.5 Volume mesh of the domain in a whole view	22
Figure 3.4.6 Volume mesh around P1374, model scale	22
Figure 3.4.7 Model selection dialog	23
Figure 3.4.8 Selected model of P1374.....	24
Figure 3.4.9 Near-wall cell of the prism layer.....	24
Figure 3.4.10 Boundary definition	25
Figure 3.4.11 Establishment of MRF for the open water propeller.....	29
Figure 3.4.12 Residual plot	31
Figure 3.4.13 Torque coefficient plot.....	32
Figure 3.4.14 All kinds of available reports	32
Figure 3.4.15 Scene node in the simulation tree	33
Figure 3.4.16 The derived parts manager node	34
Figure 4.1.1 Relative differences of experimental data and CFD results.....	41
Figure 4.1.2 open water diagram for P1374, n=9 Hz, CFD & Exp.....	41
Figure 4.2.1 open water diagrams of scale effects study.....	44
Figure 4.2.2 open water diagrams for propellers with different skews in both model and full scales	46
Figure 4.2.3 Pressure distribution on the section 0.7R for propellers with the same skews and different scales.....	48
Figure 4.2.4 Pressure distribution of section 0.50R, 0.70R, 0.90R, 0.95R, model scale, J=0.10..	49
Figure 4.2.5 Pressure distribution on both pressure side and suction side (model scale, J=0.10).	51
Figure 4.2.6 Axial velocity of model scale propellers (Propeller skew0, skew23, skew46) under J=0.10.....	53
Figure 4.2.7 Velocity vectors around blades, Model scale (Propeller skew0, skew23, skew46) under J=0.10.....	54

Figure 4.2.8 Vortex around the propellers with different skew angles (skew0, skew23, skew46) in model scale (coloured by the magnitude of vorticity).....	55
Figure 4.2.9 Vortex around the propellers with different scales (MS, FS10, FS20) and skew angle 23 deg (coloured by the magnitude of vorticity).....	57
Figure 4.2.10 Vortex around the propeller with skew angle 23 deg in model scale under different advance velocities (coloured by the magnitude of vorticity)	58
Figure 5.1.1 Thrust coefficient K_T for P1374 with different pitch ratios (0.70, 0.90, 1.10) (experimental data and CFD data).....	61
Figure 5.1.2 Torque coefficient K_Q for P1374 with different pitch ratios (0.70, 0.90, 1.10) (experimental data and CFD data).....	62
Figure 5.1.3 Open water efficiency η_0 for P1374 with different pitch ratios (0.70, 0.90, 1.10) (experimental data and CFD data).....	63
Figure 5.1.4 Relative differences for thrust coefficient K_T , skew angle 0 deg	64
Figure 5.1.5 Relative differences for torque coefficient K_Q , skew angle 0 deg	65
Figure 5.1.6 Relative differences for efficiency η_0 , skew angle 0 deg	65
Figure 5.1.7 Relative differences for thrust coefficient K_T , skew angle 23 deg	66
Figure 5.1.8 Relative differences for torque coefficient K_Q , skew angle 23 deg	66
Figure 5.1.9 Relative differences for efficiency η_0 , skew angle 23 deg	67
Figure 5.1.10 Relative differences for thrust coefficient K_T , skew angle 46 deg	67
Figure 5.1.11 Relative differences for torque coefficient K_Q , skew angle 46 deg	68
Figure 5.1.12 Relative differences for efficiency η_0 , skew angle 46 deg	68

TERMINOLOGY

As a general rule, the symbols and abbreviations in the thesis are explained the first time when they are introduced, and they are listed here.

Symbols

A_E	Expanded area
A_0	Disc area
C_p	Pressure coefficient
c	Chord length of blade section
$c_{(r/R)}$	Blade chord length at the reference radius r
D	Diameter of the propeller
Fr	Froude number
g	Acceleration of gravity
L	Characteristic length of the object
K_T	Thrust coefficient
K_Q	Torque coefficient
M	Scale factor
n	Rotational speed
P	Propeller pitch
P/D	Pitch Ratio
p	Pressure
Q	Torque
R	Propeller radius
r	Radius at any point
R_{nco}	Local Reynolds number
T	Thrust
t	Maximum thickness
V	Inflow speed
V_a	Advance velocity of the propeller
Z	Number of Blades
ρ	Fluid density
μ	Dynamic viscosity
ν	Kinematic viscosity
$\vec{U} = (u, v, w)$	Fluid velocity
τ_{nm}	Viscous stresses

$\vec{F} = (F_x, F_y, F_z)$	Body force
η_0	Open water efficiency
θ_{sp}	Propeller skew angle
x_i	i-th Cartesian component of the absolute velocity vector
δ_{ij}	Kronecker delta

Abbreviations

BAR	Blade Area Ratio, A_E / A_0
CFD	Computational Fluid Dynamics
CPP	Controllable Pitch Propeller
DES	Detached Eddy Simulations
DNS	Direct Numerical Simulations
FPP	Fixed-Pitch Propeller
FS	Full Scale
LES	Large Eddy Simulation
MS	Model Scale
MRF	Moving Reference Frame
RANS	Reynolds Averaged Navier–Stokes
RPS	Revolution Per Second
TE	Trailing Edge

1 INTRODUCTION

1.1 *Project background*

In nowadays, to achieve the best propulsion performance for commercial ship owners, an excellent propeller design is one of the most economical saving ways. A large numbers of factors may affect the characteristics and performance of propellers e.g. the levels of periodic forces, blade structural strengths, cavitation, as well as the noises and vibrations induced by the propellers. Among those factors, the different magnitudes and distributions of blade skews and the overall influence on the propeller performance by these parameters will be investigated in details in the thesis. Skewed propellers have been used for many years. However, the scale effects of different magnitudes of blade skews need further investigations.

There are model tests for the both model scale and full scale propellers such as open water tests and behind-hull propeller tests. Behind-hull tests are more realistic comparing to the open water tests, because it takes the free-surface effects into considerations when the propeller is submerged, and it also accounted for the propeller-hull interactions. The full scale tests for propellers are performed in the open seas and are carried out on the real ships; therefor the costs for such tests are very high. On the other hand, the model-scale tests for propellers are usually take place either in the ocean basins or in the wind-tunnel laboratories. The tested models of propellers are made smaller (or scaled by a length scale) comparing to the full-scale propellers. The scale effects must take into considerations because the tested results and all the tested and measured parameters will be scale by a length scale. The hydrodynamics of flow around model-scale propellers need to be analysed and results have to be transformed to the full scale.

Computational fluid dynamics (CFD) are becoming an increasingly important way for propeller tests in the propeller pre-design phase. Because, CFD takes the advantages of powerful modern computers, and make the CPU consuming, numerical time-domain simulations of flow around propellers, possible.

Considerable improvements have been made in the applications of computational fluid dynamics to the analysis and design of marine propellers during the last several years. Modelling the flow physics is one of the most crucial problems during the CFD applications, and some methods have been developed. The analysis of flow around propellers are the Reynolds-Averaged Navier – Stokes (RANS) method, the Large Eddy Simulation (LES) techniques, Detached Eddy Simulations (DES) and Direct Numerical Simulations (DNS). In terms of practical propeller-flow computations, the applications of many above-mentioned methods are limited by the huge amount of computational efforts in order to

obtain reasonable solutions. Among those propeller-flow simulation techniques, the RANS method are found to be the most favorable because the computational times are rather lower than the other methods.^[1]

One of the studies on scale effect of skewed propellers using a RANS code was made by Vladimir Krasilnikov, Jiaying Sun and Karl Henning Halse (2009). They calculated a large series of propellers by varying skew at a number of advance coefficients around the design point and studied about the pressure distribution and velocity field around the blades in the both model and full scales.^[2]

1.2 Problem formulation

In this project, propellers with different skew (0 deg, 23 deg, 46 deg) are investigated in both model scale and full scale (with the scale number 10 and 20). Their thrust characteristics such as thrust coefficient K_T , Torque coefficient K_Q , open water efficiency η_0 , pressure and velocity of the flow in the wake field will be obtained and compared to get the scale effect of different magnitude of blade skew. The flow are assumed to be 100% turbulent in the whole analysis process.

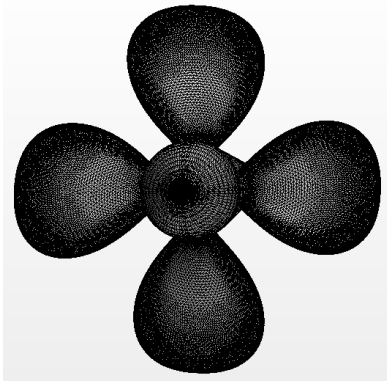
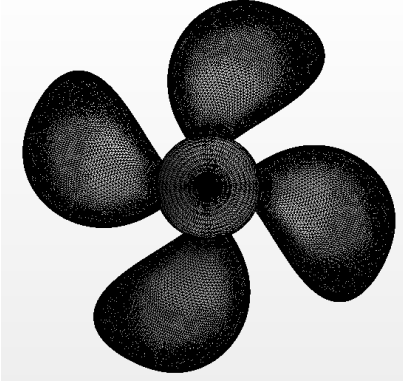
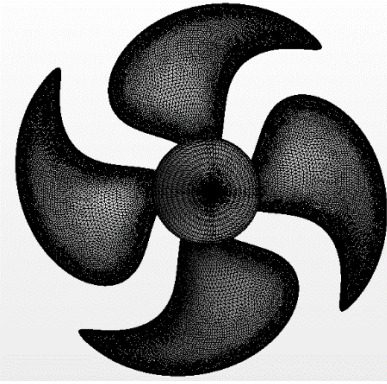
1.2.1 Target cases

The original parent propeller P1374 is a controllable pitch propeller (CPP). It has four blades, and the blade area ratio is 0.60. Skew angle 23 deg (balanced skew distribution) and design pitch i.e. $P(0.7)/D=1.10$. It's hub ratio at the propeller plane is 0.24 and direction of propeller rotation is right-handed. The model tests performed with this propeller in the PROPSCALE project are those of CPP propeller. In the systematic CFD analyses, propellers are considered as fixed-pitch propellers (FPP). The parameters of the propeller series are shown in Table 1.1.

Table 1.1 Skew series parameters

Skew Series	
A_E/A_o	0.60
P/D	0.70 (FPP - Fixed Pitch Propeller)
Skew	0 deg; 23 deg; 46 deg
Z	4

Table 1.2 Model scale propellers with different magnitude of skew (rear view)

		
Skew 0°	Skew 23°	Skew 46°
D=0.25m; Z=4; $A_E/A_0=0.60$; P(0.7)/D=0.70		

1.2.2 Calculation conditions for CFD analyses

Preliminary calculations done with the parent propeller P1374 have shown quite heavy loading of the outer blade sections, resulting in strong tip vortex. This result is thought to be related to the radial distributions of chord length and pitch at the outer blade sections, which may not be typical for conventional open propeller designs (it should be remembered that propeller P1374 was conceived as a compromise design to be used in the tests with both open and ducted propulsors). Obviously, the aforementioned phenomena may have considerable influence on scale effects. Therefore, it is planned to include in the investigations some alternative distributions of chord length and pitch along the radius.

Model scale conditions

Propeller diameter: $D=0.25$ [m]

RPS (revolution per second): $n= 20$ [Hz], 15 [Hz] (main), 9 [Hz], 5 [Hz]

The RPS value of 15 [Hz] is recommended as the reference value in model scale in present scale effect studies. Calculations at other RPS values in model scale can be used in the studies of flow transition effects. These RPS values correspond to the ones used in model tests with the parent propeller.

Recommended calculation conditions

All propellers are fully immersed in a straight uniform flow with several different advance numbers (advance coefficients: $J = 0.1; 0.3; 0.5; 0.7; 0.9, 1.1$ are recommended).

The above J values are suggested for the calculations with the parent propeller at the pitch setting $P(0.7)/D = 1.1$. Therefore, in the case of $P(0.7)/D = 0.70$, the value of required J maybe varied. Minimum five J values per curve are recommended. For different pitch settings, the J values

corresponding to free sailing operation conditions may be adjusted, so that one point is located below the point of maximum efficiency, one point is close to the point of maximum efficiency, and one point is behind the point of maximum efficiency.

Water properties

- Density: $\rho=999.1$ [kg/m³]
- Dynamic viscosity: $\mu=0.00114$ [Pa-s]

The values of water properties are the same in model scale and full scale calculations.

Geometrical elements of systematic series propellers

- Blade area ratio: $A_E/A_0=0.60$,
- Pitch settings (FPP): $P(0.7)/D=0.7$,
- Skew: total skew angle 0; 23 (parent); 46 [deg],
- Number of blades: $Z=4$.

1.3 Objectives

The information about scale effect on different magnitude and distribution of marine blade skew is still limited. Hopefully, the results of the project can be a valid reference for propeller designers or engineers, as there will be a validation process of the results compared with the information from Norwegian Marine Technology Research Institute (MARINTEK).

One concern is that this project is a complete CFD application in studies of open water propellers and the results are either compared with some experimental data or some CFD results. In expectations, there are differences for the results may come from the different settings of CFD software or even the exact test condition. But with a larger database, we can always try to find a way to get propeller characteristics as accurate as possible.

2 THEORETICAL BASIS

As in real operation, the flow around the propeller is always turbulent; the analysis is performed on the bases of only turbulent flow. In this project, a RANS solver of the commercial CFD code STAR-CCM+ and the original pre-processing code customized for modeling of marine propulsors will be applied.

2.1 Blade Skew

In the Cartesian reference frame, there are some different definitions of skew used by engineers. In this paper, the following definition is adopted which has a good accordance with ITTC standards and is used by some other researchers in Europe, the USA and the Far East. The skew angle $\theta_s(x)$ of a particular section, Figure 2.1.1, is the angle between the directrix and a line drawn through the shaft center line and the mid-chord point of a section at its non-dimensional radius (x) in the projected propeller outline; that is, looking normally, along the shaft centre line, into the y - z -plane of Figure 2.2. Angles forward of the directrix, that is in the direction of rotation, in the projected outline are considered to be negative. The propeller skew angle (θ_{sp}) is defined as the greatest angle, measured at the shaft centre line, in the projected plane, which can be drawn between lines passing from the shaft centre line through the mid-chord position of any two sections. Propeller skew also tends to be classified into two types: balanced and biased skew designs. The balanced skew design is one where the locus of the mid-chord line generally intersects with the directrix at least twice in the inner regions of the blade. In contrast, in the biased skew design the mid-chord locus intersects with the directrix not more than once; normally only in the inner sections.^[3] In this project, only the characteristics of balanced skew propellers are discussed.

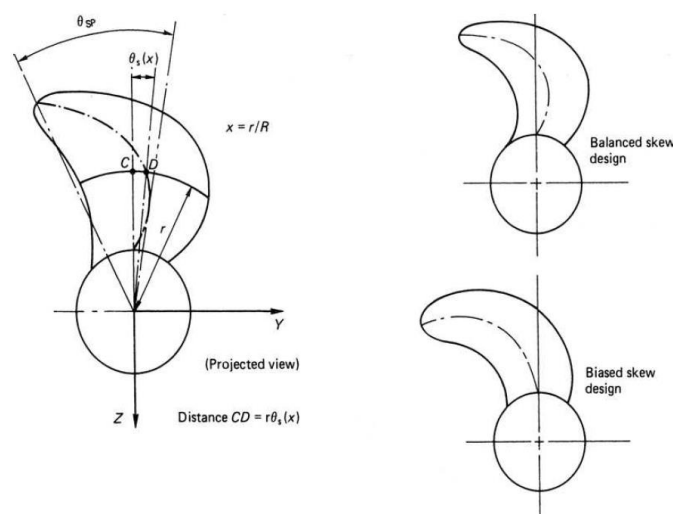


Figure 2.1.1 Skew definition
(The figure is found in Reference [3])

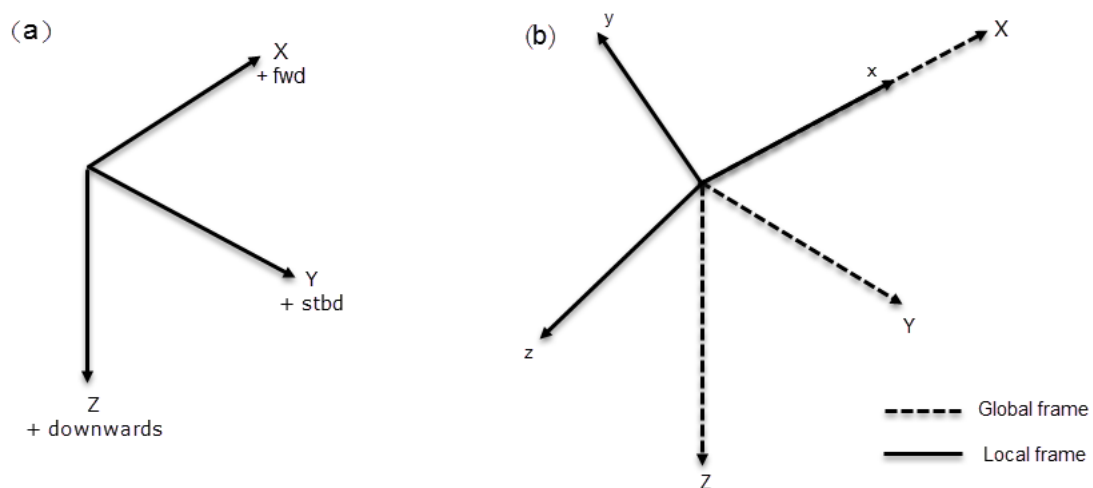


Figure 2.1.2 Reference frames: (a) global reference frame and (b) local reference frame

2.2 Propeller scale effects

In marine propeller related hydrodynamics, the two fundamental non-dimensional governing-flow parameters are the Froude number and the Reynolds number. In both the model scale and full scale cases for propellers rotating in an open-water, we want to keep the Froude number and Reynolds number the same, at the same time, due to the dynamic similarity of water. Froude number is a non-dimensional parameter that represents the ratio of inertia force of water to the gravity force. The Reynolds number represents the viscous of water and flow separations.

Roughly speaking, the Froude number equality for the both model and full scale is “in a global sense”. Because the water displaced behind the propeller in every propeller revolution equals to the force the propeller delivered to the ship. The Reynolds number equality, is more or less “in a detailed sense” for the flow. Since the propeller force is a lift force which is associated with vortex shedding in the trailing edge of blades, the blade roughness and flow patterns in the wake. Comparing the model scale to the full scale, it is almost impossible to keep equality for the both Froude number and Reynolds number.

Open water characteristics are determined from model experiments on propeller models run at high speed and with diameters of 200 to 300 mm. It arouses a topic of how the propeller performance characteristics will be changed if we reduce the propeller speed and increase its diameter at full scale. The boundary layer phenomena makes viscous property of water the main scale effects which affect the propeller performance characteristics.

There are some different procedures used by practitioners to predict the scale effects from model test. The main one is the ITTC procedure which take only take Reynolds number into consideration, as

Reynolds number is always applied to measure the boundary layer phenomena. Some other methods also take propeller loading into account. Significantly different results can arise from the various procedures. To get more accurate results about scale effect of model propeller performance characteristics, much more analysis about the flow structure within the boundary layer and the lift and drag properties in the flow field is needed. [4]

2.3 CFD

Computational Fluid Dynamics, or *CFD*, is the computational technology for the analysis of systems involving fluid flow, heat transfer and associated phenomena by means of computer-based simulation.

The equations that describe fluid flows and heat transfer are solved by numerical methods and algorithms with this technology. The governing equations – conservation of mass, momentum and energy – are used to describe the dynamics of fluid. Data preparation, building the computational domain, establishing the grid and mesh, solving all the equations and analysis of results are all performed by computers. Thus, CFD offers an opportunity for the engineers to perform “numerical experiments” in a “virtual laboratory” .

2.3.1 Governing equations of fluid dynamics – Basic laws of physics

The three basic laws of physics which describe the dynamic of fluid will be simply introduced.

The first law is mass conservation law stating that the mass of fluid is conserved (shown in (Equ. 2.1)). Momentum conservation law indicates that the rate of change of momentum is equal to the sum of forces acting on a fluid particle (shown as (Equ. 2.2)). Energy conservation law states that the rate of change of energy is equal to the sum of the rate of heat addition to and the rate of work done on a particle.

Mass conservation – Continuity equation

$$\frac{\partial \rho}{\partial t} + \nabla(\rho \vec{U}) = 0 \quad (\text{Equ. 2.1})$$

Momentum conservation – Momentum equation (Navier-Stokes equation)

$$\frac{\partial(\rho u)}{\partial t} + \nabla(\rho u \vec{U}) = -\frac{\partial p}{\partial x} + \frac{\partial \tau_{xx}}{\partial x} + \frac{\partial \tau_{yx}}{\partial y} + \frac{\partial \tau_{zx}}{\partial z} + \rho F_x$$

$$\frac{\partial(\rho v)}{\partial t} + \nabla(\rho v \vec{U}) = -\frac{\partial p}{\partial y} + \frac{\partial \tau_{xy}}{\partial x} + \frac{\partial \tau_{yy}}{\partial y} + \frac{\partial \tau_{zy}}{\partial z} + \rho F_y$$

$$\frac{\partial(\rho w)}{\partial t} + \nabla(\rho w \vec{U}) = -\frac{\partial p}{\partial x} + \frac{\partial \tau_{xz}}{\partial x} + \frac{\partial \tau_{yz}}{\partial y} + \frac{\partial \tau_{zz}}{\partial z} + \rho F_z \quad (\text{Equ. 2.2})$$

Where

ρ – water density [kg/m³];

$\vec{U} = (u, v, w)$ – fluid velocity [m/s];

p – pressure [Pa];

τ_{nm} – viscous stresses [Pa];

$\vec{F} = (F_x, F_y, F_z)$ – body force [N].

Energy conservation – Energy equation:

$$\begin{aligned} \frac{\partial}{\partial t} \left(\rho \left(e + \frac{\vec{U}^2}{2} \right) \right) + \nabla \left(\rho \vec{U} \left(e + \frac{\vec{U}^2}{2} \right) \right) &= \rho \cdot \dot{q} + \frac{\partial}{\partial x} \left(k \frac{\partial T}{\partial x} \right) + \frac{\partial}{\partial y} \left(k \frac{\partial T}{\partial y} \right) + \frac{\partial}{\partial z} \left(k \frac{\partial T}{\partial z} \right) \\ &- \frac{\partial(up)}{\partial x} - \frac{\partial(vp)}{\partial y} - \frac{\partial(wp)}{\partial z} + \frac{\partial(u\tau_{xx})}{\partial x} + \frac{\partial(u\tau_{yx})}{\partial y} + \frac{\partial(u\tau_{zx})}{\partial z} \\ &+ \frac{\partial(v\tau_{xy})}{\partial x} + \frac{\partial(v\tau_{yy})}{\partial y} + \frac{\partial(v\tau_{zy})}{\partial z} + \frac{\partial(w\tau_{xz})}{\partial x} + \frac{\partial(w\tau_{yz})}{\partial y} + \frac{\partial(w\tau_{zz})}{\partial z} + \rho \vec{F} \cdot \vec{U} \end{aligned} \quad (\text{Equ. 2.3})$$

2.3.2 Turbulence model and RANS

In the simulation process of marine propellers, the flow is almost turbulent except a small part of fluid near the wall. Therefore, find a proper way to model the turbulent flow is the critical issue. There are some different kinds of modelling concepts in numerical methods, such as Direct Numerical Simulation (DNS), Large Eddy Simulation (LES) and Reynolds Averaged Navier-Stokes equations (RANS).

As the most general and conceptually simple CFD methods, DNS methods imply that the Navier-Stokes equations describe both laminar and turbulent regimes of fluid flow. However, it is far too complicated for universal numerical application which can only be used on supercomputers. The LES methods are based on the concept of partial averaging of the Navier-Stokes equations. It takes the largest eddies under consideration. The RANS approach is based on complete averaging of Navier-Stokes equations and the flow characteristics, such as the velocity and pressure, are represented as a sum of averaged and fluctuating values. The turbulent stresses are modeled by one or another turbulence model.^[6]

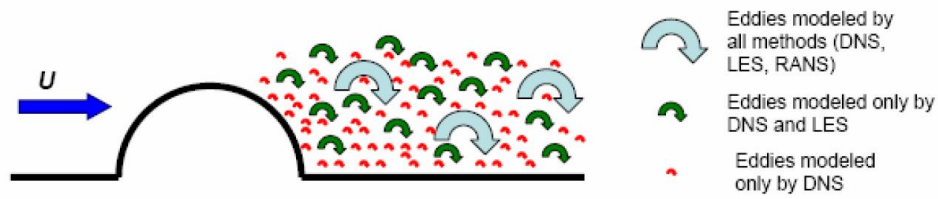


Figure 2.3.1 Schematic illustration of turbulence scales resolved by DNS, LES and RANS methods

(The figure is found in Reference [6])

The equations of the RANS method for incompressible viscous flow are derived by averaging of the Navier-Stokes equations. The governing equations of the method to be solved are written in the following form:

$$\frac{\partial \rho}{\partial t} + \frac{\partial(\rho u_i)}{\partial x_i} = 0 \quad (\text{Equ. 2.4})$$

$$\frac{\partial(\rho u_i)}{\partial t} + \frac{\partial(\rho u_i u_j)}{\partial x_j} = -\frac{\partial p}{\partial x_i} + \frac{\partial}{\partial x_j} \left[\mu \left(\frac{\partial u_i}{\partial x_j} + \frac{\partial u_j}{\partial x_i} - \frac{2}{3} \delta_{ij} \frac{\partial u_l}{\partial x_l} \right) \right] + \frac{\partial}{\partial x_j} (-\rho \overline{u'_i u'_j}) \quad (\text{Equ. 2.5})$$

Where

x_i is the i -th Cartesian component of the absolute velocity vector

p is the static pressure

μ is the molecular viscosity

δ_{ij} is the Kronecker delta

$-\rho \overline{u'_i u'_j}$ is the Reynolds stress. The Reynolds stress must be modeled to close the governing equation by using an appropriate turbulence model.

In the present work, the SST (Shear Stress Transport) k - ω turbulence model is chosen for turbulence closure. The k - ω turbulence models represent a group of two-equation turbulence models in which the transport equation are solved for the turbulent kinetic energy k and its specific dissipation rate ω . The SST k - ω model is currently one of the most widely used turbulence models for blade row machinery applications. As far as the subject of the present research is concerned, the advantages of this model are seen in its ability to handle simultaneously lower-Re and higher-Re zones in the flow, and to predict more accurately non-equilibrium regions in the boundary layer with adverse pressure gradients such as observed when separation occurs. The above considerations are important when modeling model scale propellers, model and full scale propellers operating at heavy loading. One can also expect more adequate location of vortical structures such as leading edge vortex and tip vortex,

although, as any isotropic two equation turbulence model, the SST $k-\omega$ model shows lower accuracy in resolving flows near and inside vertical structures compared to second-moment closure RSTM models. [6]

2.3.3 Near-wall treatment

Applying CFD methods to the analysis of scale effects on propeller characteristics in open water one should be aware that in model scale laminar flow domains can exist on propeller blades and influence blade force measured during the tests, while most of CFD methods available for engineers (mainly, these are RANS methods) imply fully turbulent flow. Furthermore, in model scale laminar flow separation can develop at the leading edge under some conditions. The extent of laminar flow domains and zones of laminar separation varies with blade configuration (first of all, skew) and loading distribution along the radius. Capturing these effects in RANS simulation would require a reliable transition model.

Turbulent flows are significantly affected by the presence of walls. The mean velocity field is affected through the no-slip condition that has to be satisfied at the wall.

Very close to the wall, viscous damping reduces the tangential velocity fluctuations, while kinematic blocking reduces the normal fluctuations. Toward the outer part of the near-wall region, however, the turbulence is rapidly augmented by the production of turbulence kinetic energy due to the large gradients in mean velocity. [6]

Semi-empirical formulas called "wall functions" are used to bridge the viscosity-affected region between the wall and the fully-turbulent region. The use of wall functions obviates the need to modify the turbulence models to account for the presence of the wall. A Y^+ factor (local Reynolds number) is used to indicate the near-wall treatment characteristic and the value of it should be in the range of 30-300.

2.3.4 Moving Reference Frame

With a moving reference frame (MRF), the flow around the moving part can (with certain restrictions) be modeled as a steady-state problem with respect to the moving frame.

The MRF modeling capability allows user to model problems involving moving parts by allowing you to activate moving reference frames in selected cell zones. When a moving reference frame is activated, the equations of motion are modified to incorporate the additional acceleration terms which occur due to the transformation from the stationary to the moving reference frame. The additional acceleration terms also mean when we rewrite equation of motions in a non-inertia frame, some terms must be introduced since the Newton's second law is only valid in an inertia frame. By solving these equations in a steady-state manner, the flow around the moving parts can be modeled.

Open water propeller analysis in straight flow is a steady-state problem, and one can benefit from employing a Moving Reference Frame (MRF) approach to solve the equations in the reference frame rotating together with propeller. In addition, only one blade passage is included in the simulation domain provided with appropriate periodicity conditions on the side boundaries of the passage sector.

2.3.5 Mesh generation

In this thesis, the finite volume methods (FVM) are applied which is a procedure for solving the stress and displacement calculations in the analysis process. With this method, a three-dimensional (3D) water domain is established as a region that the flow simulation will be performed. Computation domain will be restricted by some different kinds of boundaries. The most common types are walls, inlet boundaries, exit boundaries, symmetry boundaries, periodic boundaries and interface boundaries. Which kind of boundary will be used depends on the simulation setup and on functions to be performed by these boundaries in the solution.

Computation mesh is a discrete geometrical representation of computational water domain which will be divided into finite cells. These aforementioned domain boundaries are also parts of computation mesh. Many meshing methods begin with the mesh generations on the domain boundaries (surfaces) which enclosed the computational water domain. Surface mesh consists of many two-dimensional planar or curvilinear elements called faces. A face is comprised of vertices and edges. A volume mesh will be built from the surface mesh consisting of three-dimensional elements called cells. The density of faces on a domain boundary (i.e. the size of every faces and the distributions) depend on the boundary type, and will affect the CFD results

There are different kinds of cell types in modern CFD codes, such as tetrahedron, hexahedron, pyramid, prism/wedge and polyhedron. With different cell types, the required computational efforts (such as time required for mesh generation, memory and time consumption during numerical solution, complexity of numerical solution algorithm, convergence speed) may significantly differ in a particular simulation. It is important to know all the advantages and limitations of all the cell types to choose an appropriate cell type in a simulation. ^[6]

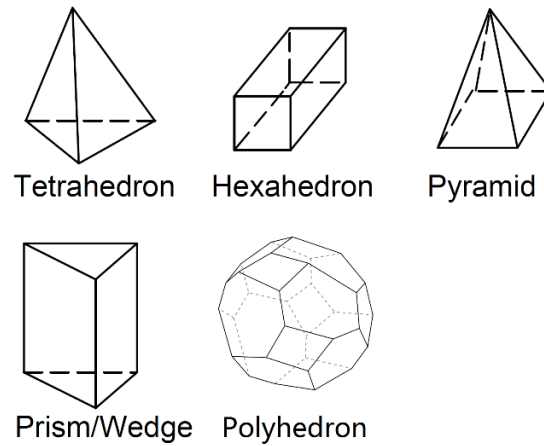


Figure 2.3.2 Cell types in modern CFD codes

Table 2.1 Advantages and limitations of all types of mesh cells

Cell type	Advantages	Limitations
Hexahedral cell	<ol style="list-style-type: none"> 1. Low numerical diffusion when a mesh aligned with flow can be built 2. Suited for boundary layers because of little sensitivity to stretching 3. Accurate approximation 	For complex geometries, get poor cell quality
Tetrahedral cell	<ol style="list-style-type: none"> 1. Well suitable for automatic mesh generation 2. Good cell quality for complex geometries 	Having only 4 neighbours makes it insufficient to achieve the accuracy offered by a mesh cell with 6 faces
Wedge/Prisms&Pyramids	<ol style="list-style-type: none"> 1. Use in “transition” mesh layers between boundaries and main core mesh, and between mesh blocks featuring different cell types 	In comparison with hexahedral cells, more numerically diffusive.
Polyhedral cells	<ol style="list-style-type: none"> 2. Greater automatic meshing benefits than tetrahedral cells 3. Variable gradients can be much better approximated because of many neighbour cells 4. Cells can easily be joined, split, or modified by introducing additional points, edges and faces. 5. More accurate results 	<ol style="list-style-type: none"> 1. Memory usage for polyhedral mesh is approximately four times more compared to a tetrahedral mesh of similar cell count 2. General polyhedral mesh takes longer time for one iteration, compared to a tetrahedral mesh of similar cell count.

3 METHODS

3.1 Propeller characteristics

Open-water performance characteristics for a series of propellers with the similar geometric shapes are normally expressed by some non-dimensional terms. They are important references used by engineers to measure whether the propeller performance is good enough for a specific ship or not. Typical terms are shown as follows:

$$\begin{aligned} \text{thrust coefficient } K_T &= \frac{T}{\rho n^2 D^4} \\ \text{torque coefficient } K_Q &= \frac{Q}{\rho n^2 D^5} \\ \text{advance coefficient } J &= \frac{V_a}{nD} \end{aligned} \quad (\text{Equ. 3.1})$$

where

T – thrust [N]

Q – torque [N · m]

ρ – fluid density [kg/m³]

n – rotational speed [RPS, Hz]

D – diameter of the propeller [m]

V_a – advance velocity of the propeller [m/s]

The open water efficiency η_0 of the propeller can also be expressed by these non-dimensional terms:

$$\eta_0 = \frac{TV_a}{2\pi nD} = \frac{K_T \rho n^2 D^4 V_a}{2\pi n K_Q \rho n^2 D^5} = \frac{K_T}{K_Q} \cdot \frac{V_a}{2\pi nD} = \frac{K_T}{K_Q} \cdot \frac{J}{2\pi} \quad (\text{Equ. 3.2})$$

For a specific propeller, the performance characteristics (K_T, K_Q, η_0) are functions of the advance coefficient J . In an open-water diagram, (K_T, K_Q, η_0) are usually plotted against J , with varying the pitch ratios P/D (see Figure 3.1.1). Without losing generality, values of Wageningen B5-75 screw series are used. The figure indicates that, the open-water characteristic curves of the propeller under a steady condition with positive advance coefficients varies with the pitch ratio P/D .^[7] However, for a certain geometric form of propellers, the values in the curves can be affected by the propeller diameter, the fluid density and advance coefficient. Therefore, in this thesis, the scale effect will be discussed for propellers performed in the same in flow conditions (water density and advance coefficient are kept constant). In this case, the propeller diameter D is the only variable in a fixed pitch P simulation. The

open water diagrams can be obtained by experimental methods and CFD calculations. In this thesis, the CFD calculations are applied in a commercial CFD software STAR-CCM+ with the version of 10.02.

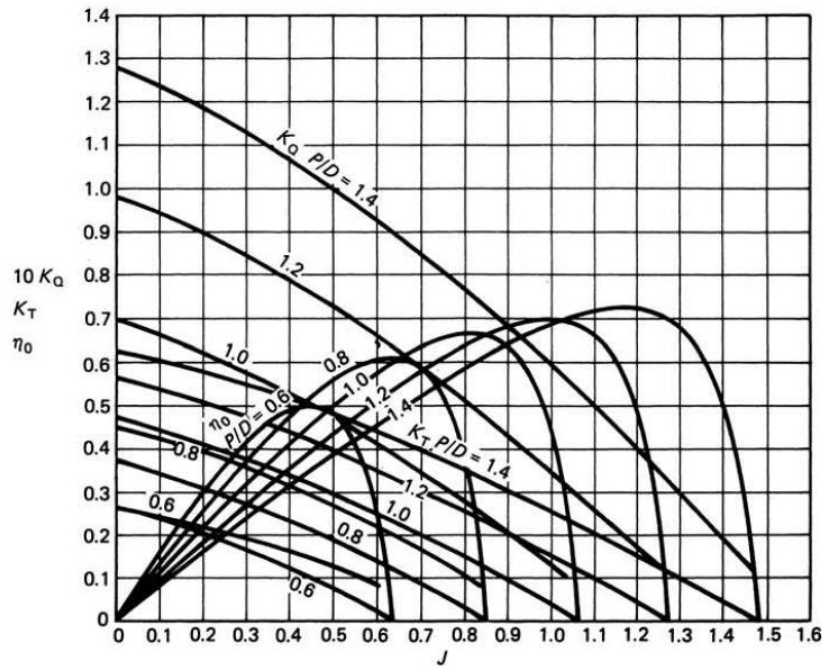


Figure 3.1.1 Open water diagram for Wageningen B5-75 screw series
(The figure is found in Reference [7])

The pressure distribution around the propeller blade can be represented by pressure coefficient, which is defined as:

$$C_p = \frac{p - p_\infty}{\frac{1}{2} \rho_\infty V_\infty^2} \quad (\text{Equ. 3.3})$$

Where

p – the pressure at the point at which pressure coefficient is being evaluated [Pa];

p_∞ – the pressure in the freestream (i.e. remote from any disturbance) [Pa];

ρ_∞ – the freestream fluid density (in this project, fluid density is a constant, 999.1 kg/m³)

V_∞ – the velocity of the body through the fluid [m/s].

3.2 ITTC78 of Scale effect corrections

According to ITTC 78's recommendation, the full scale propeller characteristics can be obtained from the model scale characteristics in the following algorithm.

$$\begin{aligned} K_{TS} &= K_{TM} - \Delta K_T \\ K_{QS} &= K_{QM} - \Delta K_Q \end{aligned} \quad (\text{Equ. 3.4})$$

Where

$$\begin{aligned}\Delta K_T &= -\Delta C_D \cdot 0.3 \cdot \frac{P}{D} \cdot \frac{c}{D} \cdot Z \\ \Delta K_Q &= -\Delta C_D \cdot 0.25 \cdot \frac{c \cdot Z}{D}\end{aligned}\quad (\text{Equ. 3.5})$$

The difference in drag coefficient ΔC_D is

$$\Delta C_D = C_{DM} - C_{DS}$$

Where

$$C_{DM} = 2 \left(1 + 2 \frac{t}{c} \right) \left[\frac{0.04}{(R_{nco})^{\frac{1}{6}}} - \frac{5}{(R_{nco})^{\frac{2}{3}}} \right]$$

and

$$C_{DS} = 2 \left(1 + 2 \frac{t}{c} \right) \left(1.89 + 1.62 \cdot \log \frac{c}{k_p} \right)^{-2.5} \quad (\text{Equ. 3.6})$$

In Equ. 3.4 to Equ. 3.6, c is the chord length, t is the maximum thickness, P/D is the pitch ratio and R_{nco} is the local Reynolds number at the reference radius $r/R = 0.75$. The blade roughness k_p is $k_p = 30 \cdot 10^{-6} \text{ m}$. R_{nco} must not be lower than $2 \cdot 10^5$ at the open water test. In this project, the pitch ratio P/D at $r/R = 0.75$ will be approximated as the value at $r/R = 0.70$, which is 0.70.^[8]

From Equ. 3.4 to 3.6, we can see that, in ITTC78, modifications of non-dimensional thrust and torque coefficients from model scale to full scale are based on semi-empirical formulas of drag difference coefficients ΔC_D .

In this project, the local Reynolds number is calculated as:

$$R_{nco} = \frac{\sqrt{V^2 + [(r/R) \cdot \pi \cdot RPS \cdot D]^2} \cdot c_{(r/R)}}{\nu} = \frac{\sqrt{V^2 + [(r/R) \cdot \pi \cdot RPS \cdot D]^2} \cdot \rho \cdot c_{(r/R)}}{\mu} \quad (\text{Equ. 3.7})$$

Where

V – the inflow speed (m / s);

$c_{(r/R)}$ – the blade chord length at the reference radius (according to ITTC, $r/R = 0.75$) (m);

RPS – the rotational speed, revolution per second (Hz);

D – propeller diameter (m);

ρ – density of the fluid (in this project, $\rho = 999.1 \text{ kg / m}^3$);

μ – dynamic viscosity of the fluid (in this project, $\mu = 0.00114 \text{ Pa} \cdot \text{s}$),

ν – kinematic viscosity of the fluid, $\nu = \frac{\mu}{\rho}$, (m^2 / s);

In Equ. 3.7, local Reynolds number, the $c_{(r/R)}$ is used as the characteristic length. The characteristic velocity in R_{nco} is a bit complicated, since this reference velocity is the combinations of inflow velocity and the propeller rotation parameters.

3.3 Test arrangement and plan

At the beginning of this PROPSCALE project, some simulation examples, experimental data, setup recommendations and numerical blade models are received from MARINTEK. All these experimental data is for the propeller 1374, the parent propeller of all the simulated ones, and the parameters of it is shown in Table 3.1. The experimental data is from open water test in the towing tank or cavitation tunnel.

Table 3.1 Parameters of P1374

Parameters of P1374	
Propeller diameter, D [m]	0.25 (model scale)
Number of blades, Z [-]	4
Skew angle, θ_{sp} [deg]	23
Blade area ratio, A_E/A_0 [-]	0.60
Pitch ratio, P/D [-]	1.10, 0.90
Rotational speed RPS, n [Hz]	5, 9, 15, 20

The tests in this project can be classified as two parts.

The first part is validation. To ensure the results of STAR-CCM+ for this project is reliable and all the settings are appropriate for the specific simulation condition, the propeller in a model scale with a rotational speed RPS, $n = 9$ Hz, pitch ratio $P/D = 1.10$, will be calculated in a series of advance ratio J. The results from the CFD method will be compared with that of the experimental method as a validation.

The second part is the main part of this project: simulations of propeller with different skew angles (0 deg, 23 deg and 46 deg), different diameters (model scale propeller with the diameter of 0.25 m, full scale propeller with the scale factor of 10 and 20, and the propeller diameters for full scale propellers are 2.5 m and 5 m respectively) and the pitch ratio of $P/D = 1.10$ under all work conditions (with different advance ratio J).

3.4 Method descriptions

In this part, both the simulation methods and analysis methods will be expressed. Some import settings of STAR-CCM+ during the simulation process will be explained as references for duplication of other practitioners afterwards. Generally, the CFD simulation process involves three stages:

- Pre-processing

- Solving
- Post-processing

In the following contents, these three stages will be explained based on the simulation of the particular propeller P1374 with an advance ratio of $J = 0.70$. The other parameters about the propeller are shown in Table 3.1.

3.4.1 Test and analysis parameters

3.4.1.1 Pre-processing

In this stage, the user needs to input all the data and setup for the simulation into the pre-processor. The following activities need to be finished.

- 1) Preparation of the propeller models that need to be tested. In this project, all the blade geometry models with different skew angle ($\theta_{sp} = 0, 23, 46 \text{ deg}$) and pitch ratio ($P/D = 0.70, 1.10$) in model scale have been provided by MARINTEK. With a simple transformation of the models, we can also get the full scale propeller model and the transformation process will be introduced afterwards.
- 2) Definition and sub-division of computation domain.

When modelling propeller in a straight-flow open-water condition, one can take advantage of flow's axial symmetric property, and use only one blade passage domain with setting up appropriate periodic boundaries. The most straightforward setup for one blade passage flow simulation implies the use of a fan-shaped sector, having angular dimension of $360/Z \text{ deg}$ (Z is the number of propeller blades). The sector is cut from a cylinder and includes only one whole blade, as shown in Figure 3.1.1a). Such a setup also makes the post-processing work simpler. However, if propeller blades are wide, they may not be entirely accommodated in the domain as described above.

The simplest way to solve the problem is to use an alternative one blade passage setup that includes the same cylindrical sector, but instead splits two neighbouring blades. Such a setup will ensure that complete blade geometry will be accommodated in the one blade passage domain, and flow periodicity will be observed.

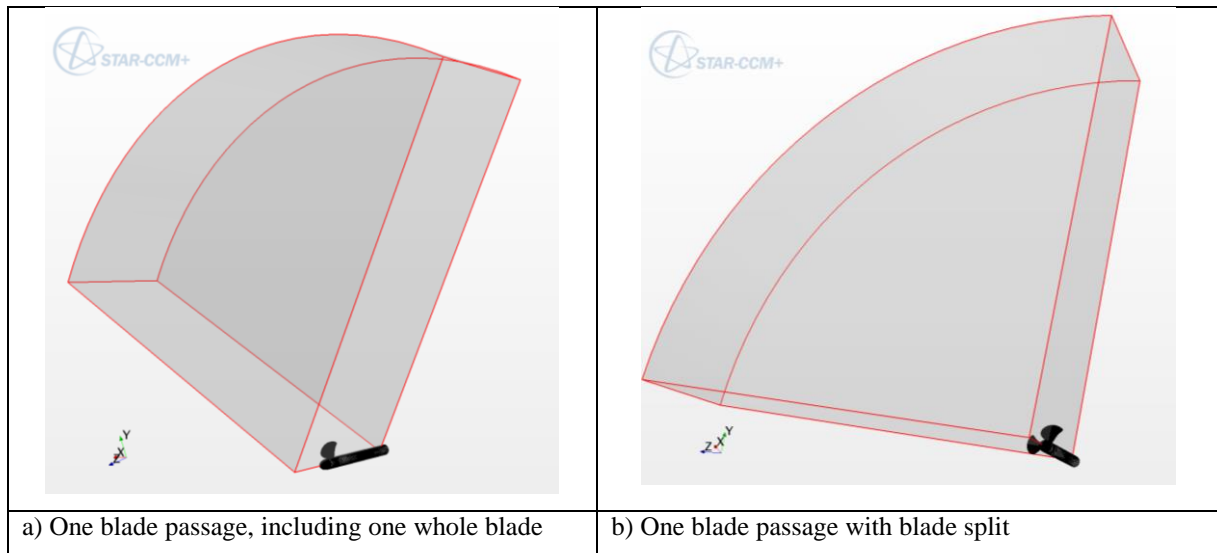


Figure 3.4.1 Two variants of the domain setup with one blade passage

In the PROSCALE project, all propellers have 4 blades. Therefore, we can get the angle of the domain as:

$$360/Z = 360/4 = 90 \text{ deg}$$

The segment domain is subtracted from a cylinder sharing the same centerline with the propeller shaft by two blocks which intersect at the shaft centerline as shown in Figure 3.4.2. The domain must be large enough to avoid the effects of boundaries. For the model scale cases, the radius of the segment domain is set to be 2.5 m while the length after the blades in the flow inlet direction is 0.3 m and the length behind the propeller in the flow outlet direction is 0.4 m. Therefore, the domain is short and this will be fixed by Extruder meshing tool as explained in the later content about mesh generation.

After the establishment of the domain, it need to be assigned to the simulated region and divided into some different faces for the later boundary definition. The domain is divided into five faces (Inlet, Outlet, Outward, Symmetry plane 1 and Symmetry plane 2) as shown in Figure 3.4.3.

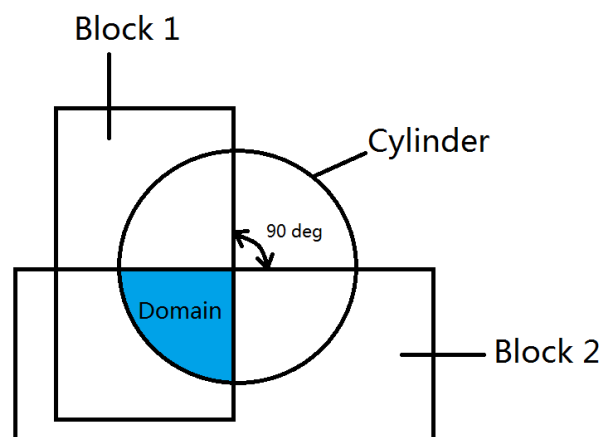


Figure 3.4.2 Establish the segment domain

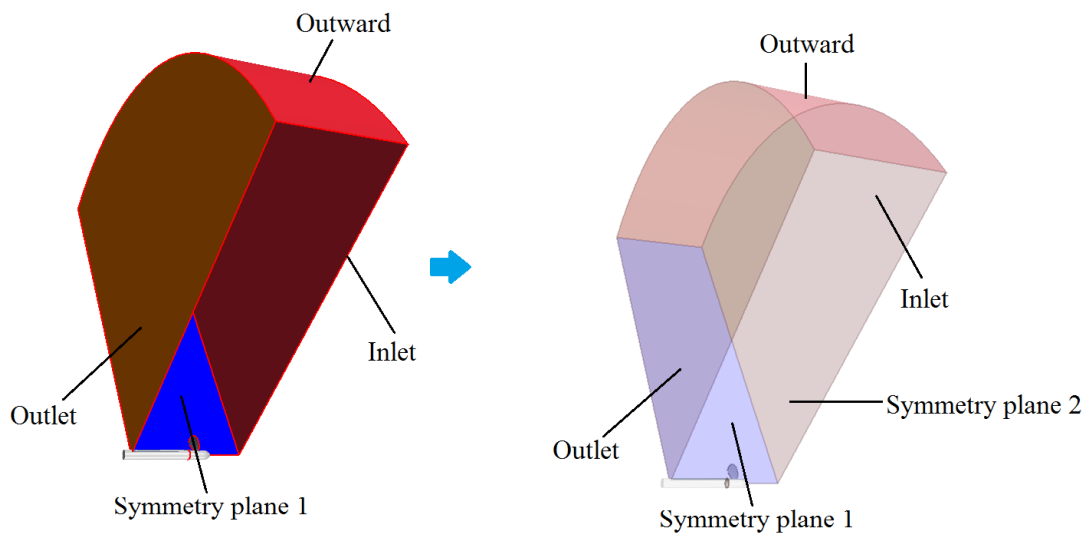


Figure 3.4.3 Boundary assignment of the domain

- 3) Choice of the mesh model and mesh generation. In PROSCALE project, four different kinds of mesh models are selected: Surface Remesher, Prism Layer Mesher, Polyhedral Mesher and Extruder.

The intersection of blade surface with periodicity boundaries may create some problems. In older versions of STAR-CCM+ it sometimes caused incomplete boundary intersection at creation of periodic interfaces, especially when using Trim mesher. In the recent versions, it seems to be fixed, but depending on complexity of the blade surface, minor surface flaws may still occur at the intersection of the blade with periodic boundaries. The Surface Remesher tries to repair these flaws, often resulting in unnecessary locally increased mesh density and higher overall cell count, if special treatment is not applied to the blade surface mesh.

One remedy is to make use of feature curves. The setup with the first variant of one blade passage domain allows in principal only one (combined) feature curve for all geometry parts. Surface remeshing on the blade is then entirely guided by the values of target size and minimum surface size set up for blade, tip and TE (Trailing Edge) boundaries. Such meshing model may result in the aforementioned issues when using the alternative setup with blade split. To remedy this one can, at the stage of preparation of geometry parts, produce a separate set of feature curves describing blade patch perimeters and following the blade edges. The blade edges and tip region are the areas where finer mesh is needed. Then one can set up both the target size and minimum size for the blade surface to the same desired value and instruct Surface Remesher to do mesh refinement only along the Blade Patch Perimeter feature curves, on the blade tip and blade TE. The rest of the blade surface and regions on the periodic boundaries where they intersect with the blade will be unaffected, resulting in uniform,

good quality mesh as shown in Figure 3.4.4. The general mesh reference values is laid out in Table 3.2. Except these values, to perform a fine volume mesh during calculation, there are some special customize settings for boundaries as shown in Table 3.3.

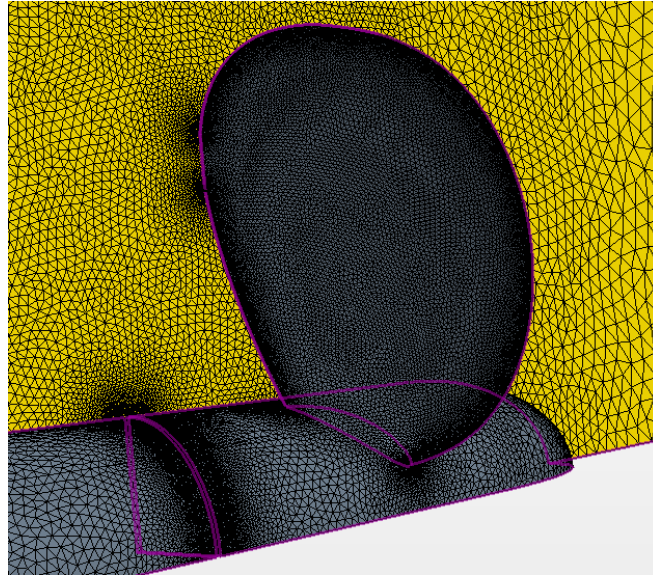


Figure 3.4.4 Introduction of feature curves in the one blade passage domain

Table 3.2 General mesh reference values

Properties		Unit	Values
Base size		m	0.25
Automatic surface repair	Minimum proximity	-	0.05
	Minimum quality	-	0.01
Number of prism layers		-	10
Prism layer stretching		-	1.4
Prism layer thickness		percentage of base	0.25
Surface size	Relative minimum size	percentage of base	50
	Relative target size	percentage of base	50

Table 3.3 Customize mesh setup for boundaries

Boundary	Customize Prism Mesh	Custom Surface Size	Relative Minimum size (percentage of base)	Relative Target size (percentage of base)
Blade	Use default values	Enable	0.125	0.5
Blade TE	Use default values	Enable	0.125	0.125
Blade tip	Use default values	Enable	0.125	0.125
Inlet	Disable	Disable	-	-
Outlet	Disable	Disable	-	-
Outward	Disable	Disable	-	-
Symmetry plane	Disable	Disable	-	-
Hub	Use default values	Enable	1.00	3.00
Shaft	Use default values	Enable	1.00	3.00

Regarding the simulation domain it should be mentioned that the initial geometry part imported in the simulation is a short domain. When generating volume mesh, the Inlet and Outlet boundaries of this initial domain are extruded using the Extruder meshing tool, in order to place the final Inlet and Outlet boundaries at a sufficient distance from propeller. The use of Extruder helps to reduce the total cell count without compromising mesh quality by using the prismatic mesh in the extrusion domains. Flow aligned prismatic meshes are well suitable for modelling flows with one prevailing direction, such as jets and propulsor slipstreams. In the used version of STAR-CCM+, the Extruder option is not supported by the Parts Based Meshing, and for that reason the meshing in the present simulation is done as Region Based Meshing. In present example, the Extruder tool is applied on two boundaries – Inlet and Outlet – to extend the domain and the parameters for the Extruder mesh is shown in Table 3.4.

Table 3.4 Normal Extrusion Parameters

Properties	Boundaries	
	Inlet	Outlet
Magnitude	1.25 m	3.75 m
Number of layers	15	35
Stretching	20.0	40.0
Use average normal	Disable	Disable
Specify a new region	None	None

As the properties of the flow around the propeller is the main research object to get the propeller characteristics, this part of domain requires more accurate calculations. In STAR-CCM+, volumetric control mesh is meant to solve this problem. Volumetric control can be applied to specify the mesh density in a specific zone for both surface and volume meshes. Therefore, specific cell sizes can be set within the zone for each mesh generation stage by the use of volume shapes and geometry parts. If two or more volumetric controls overlap, the smallest user-defined cell size takes priority.

In the example case, seven volumetric control cylinders are established around the propeller with different size and mesh settings. All the cylinders possess the same centerline as the propeller shaft. Surface remesher, prism layer mesher and polyhedral mesher are selected to model the volumetric control cylinders. The customize surface mesh size will increase as the radius of the cylinder increasing, for example, the custom mesh size of a cylinder with the radius of 0.14 m is 1.0% of the base size while another cylinder with the radius of 1.0 m is set a mesh size of 25.0% of the base size.

After all the settings done, a surface mesh will be established before the volume mesh. The final volume mesh scene is observed as Figure 3.4.6 and Figure 3.4.6.

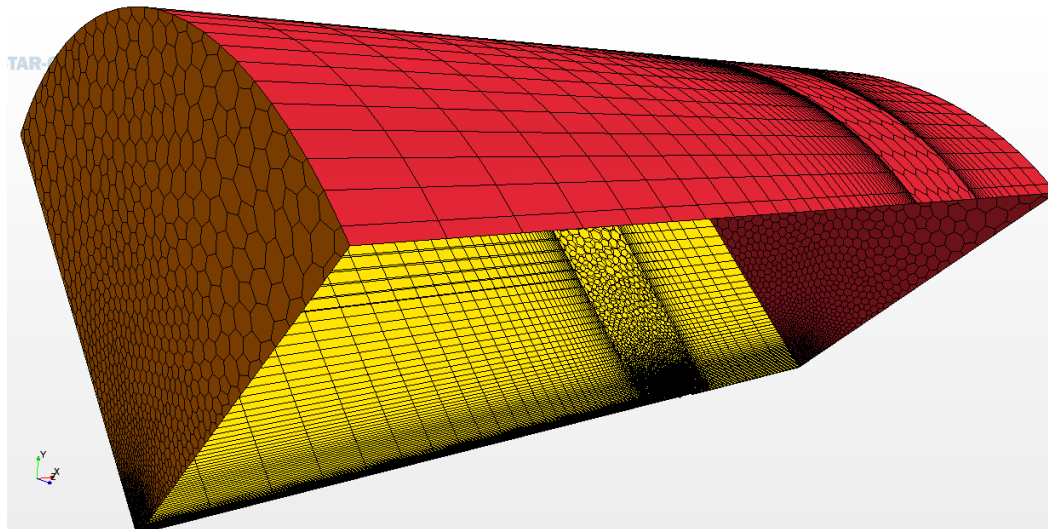


Figure 3.4.5 Volume mesh of the domain in a whole view

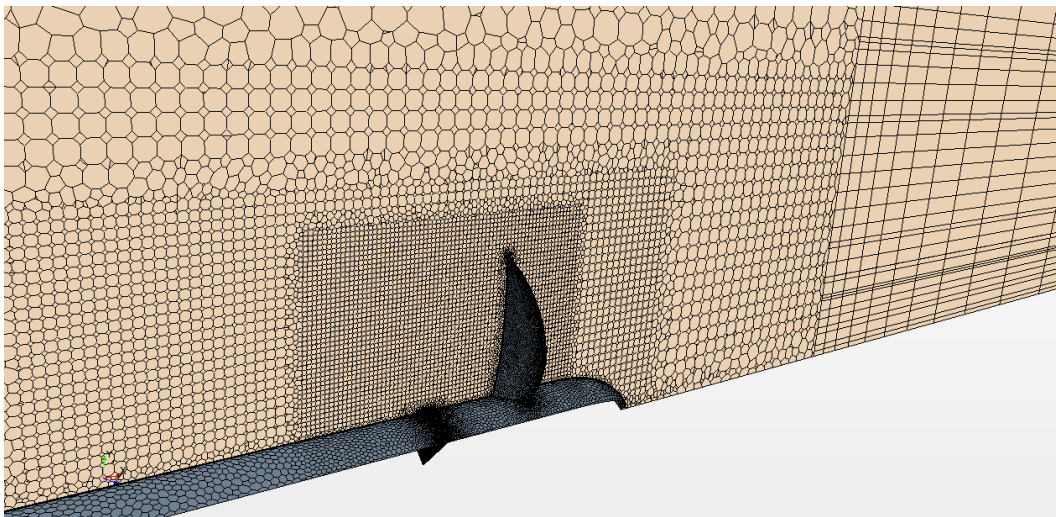


Figure 3.4.6 Volume mesh around P1374, model scale

4) Definition of fluid properties.

In PROSCALE project, there is only one fluid – water – is taken into account as the cavitation condition is out of consideration. According to the theory explained in Chapter 2, the viscous property of the water is the main factor for propeller scale effects. For both model scale and full scale propellers, the water is set to have the following properties:

Water density $\rho = 999.1 \text{ kg/m}^3$

Dynamic viscosity $\mu = 0.00114 \text{ Pa} \cdot \text{s}$

5) Selection and setup of the adequate solution models. Solution models are the language using which we tell the solver what type of problem is simulated and what methods are to be used in the solution. The numerical solution setup should reflect the real simulated flow regime.

In the representative example, when choosing the solution model, a dialog (see Figure 3.4.7) will show up. Firstly, the blank box before “Auto-select recommended models” on the bottom left corner of the dialog will be selected. After this operation, the STAR-CCM+ can choose some recommended models that the engineers always use automatically. The solution models can be selected in the following order:

Three dimensional → Implicit unsteady → Liquid → Segregated flow → Constant density → Turbulent → K-Omega turbulence. Combined with the automatic selection of the pre-processor, the selected models are shown in Figure 3.4.8.

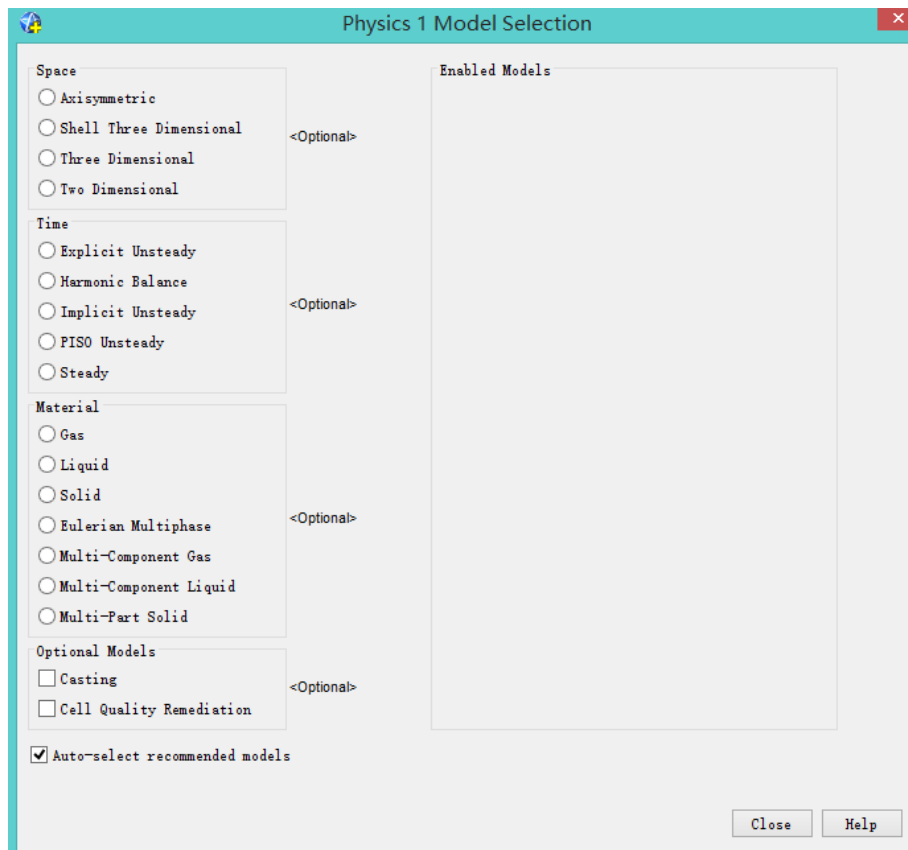


Figure 3.4.7 Model selection dialog

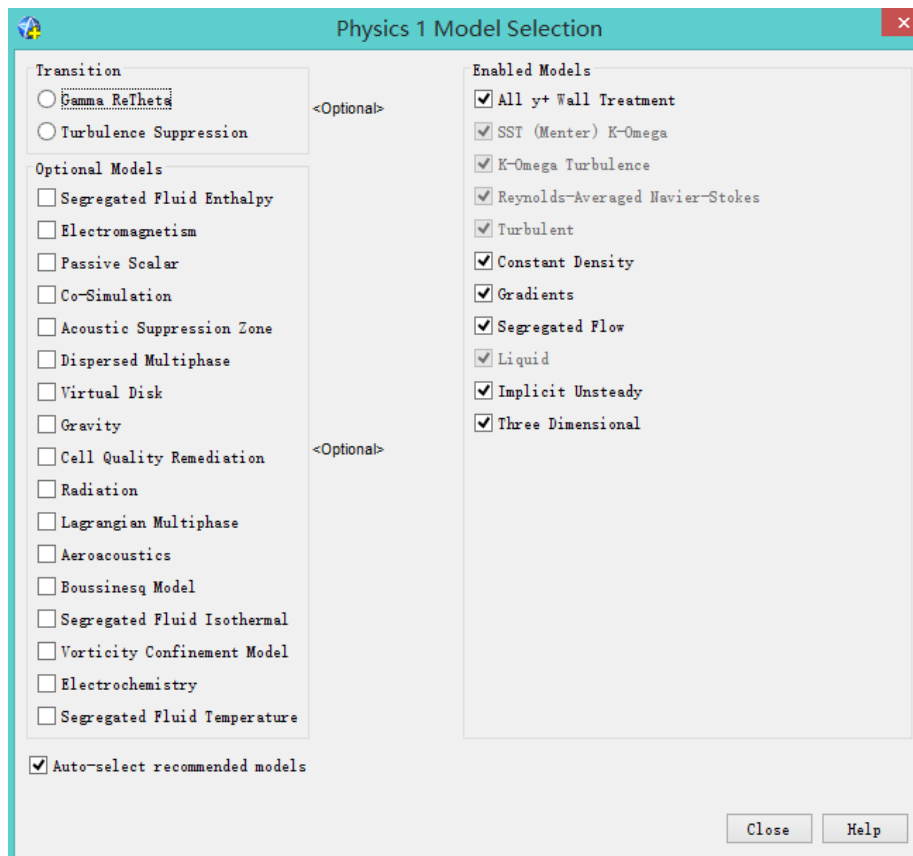


Figure 3.4.8 Selected model of P1374

According to Figure 3.4.8, all Y^+ wall treatment is selected by the processor to solve the near-wall problem as mentioned in Chapter 2. Y^+ function represents the local Reynolds number and for normal simulation, the appropriate range of value is 30-300.

$$Y^+ = \frac{VL}{\nu} \quad (\text{Equ. 3.8})$$

Where

V is the velocity of the cell centroid (m / s);

L is the distance between the cell centroid and the solid boundary (m);

ν is the kinematic viscosity of the fluid ($\nu = \mu/\rho$) (m^2 / s).

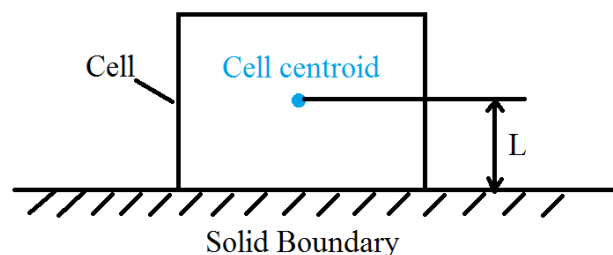


Figure 3.4.9 Near-wall cell of the prism layer

The RANS (Reynolds-Averaged Navier-Stokes) is selected when choosing “K-Omega turbulence”.

6) Specification of appropriate boundary conditions.

The domain has been divided into 5 closed surfaces assigned to region. In order to express the experimental flow region, the boundary conditions need to be defined and all these boundaries of the domain are shown in Figure 3.4.10. To simulate the whole propeller, a periodic internal interface is assigned to the two symmetry planes. The periodicity of the interface is set to be rotational and the x-axis (in this project, it has the same direction as the propeller shaft) is set to be the rotational axis. The boundary type wall is set as the boundary condition for all parts of the propulsor (Blade, tip, TE, Hub and shaft).

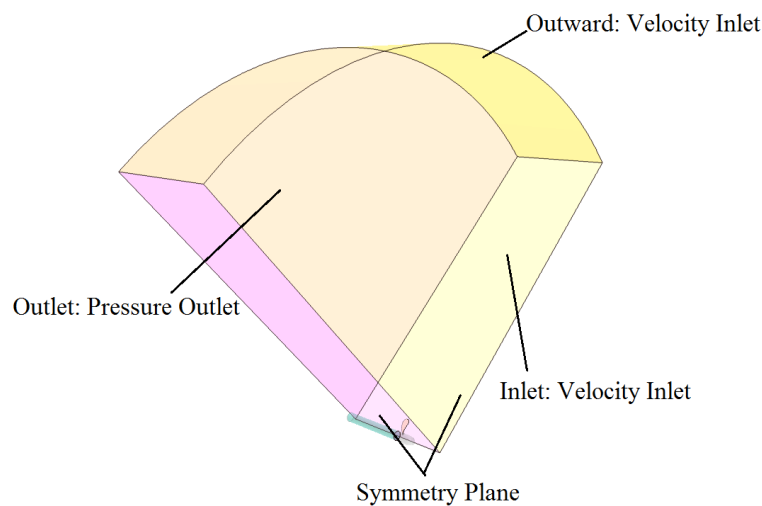


Figure 3.4.10 Boundary definition

Table 3.5 Boundary conditions for the domain and propeller

Boundary name	Boundary type
Blade	Wall
TE	Wall
Tip	Wall
Inlet	Velocity Inlet
Outlet	Pressure Outlet
Outward	Velocity Inlet
Symmetry plane 1	Symmetry Plane (with periodic internal interface)
Symmetry plane 2	Symmetry Plane (with periodic internal interface)

	interface)
Hub	Wall
Shaft	Wall

For the two velocity inlet boundaries, the velocity needs to be input into the pro-processor. In the model scale simulation example of P1374 with an advance ratio of $J = 0.70$, the advance velocity of propulsor is 2.625 m/s. According to Equ. 3.1, we can get the propeller velocity as:

$$V_a = nD * J = 15 * 0.25 * 0.70 = 2.625 \text{ m/s}$$

Similarly, the velocity for both model scale and full scale propellers under a different advance ratio can be summarized as Table 3.6. In this table, M indicates the scale factor of full scale propellers compared with the model scale ones. In this project, not all the conditions with different advance velocities are simulated. Only the conditions with the advance ratio $J = 0.1, 0.3, 0.5, 0.6, 0.7, 0.8$ are calculated as a result of the time limitation.

Table 3.6 Advance velocities for model scale and full scale propellers

J	Advance velocity [m/s]		
	Model scale (MS)	Full scale, M=10 (FS10)	Full scale, M=20 (FS20)
0.1	0.375	1.186	1.677
0.2	0.750	2.372	3.354
0.3	1.125	3.558	5.031
0.4	1.500	4.743	6.708
0.5	1.875	5.929	8.385
0.6	2.250	7.115	10.062
0.7	2.625	8.301	11.739
0.8	3.000	9.487	13.416
0.9	3.375	10.673	15.093
1.0	3.750	11.859	16.771
1.1	4.125	13.044	18.448
1.2	4.500	14.230	20.125
1.3	4.875	15.416	21.802
1.4	5.250	16.602	23.479
1.5	5.625	17.788	25.156
1.6	6.000	18.974	26.833

3.4.1.2 Solving

There are four different numerical techniques – finite difference methods, finite element methods, spectral methods and finite volume methods – used to solve the governing flow equations (Equ. 2.4 and Equ. 2.5) in CFD methods. When processing the equations, all these methods follow three stages:

- Approximation of the unknown variables by means of simple functions;
- Discretization of governing flow equations by substitution of these approximations and subsequent reduction to a system of algebraic equations;
- Solution of the algebraic equations.

The distinct ways in which the approximations of the variables are obtained and the discretization is handled can express the main differences between all these aforementioned solution techniques.

In the finite difference methods, the unknown variables of the partial derivative of the transport equations are approximated by the truncated Taylor series expansions. In the solution process, an algebraic equation for the flow at each grid point and its immediate neighbors is generated. The essential condition is a high degree of mesh regularity to get accurate partial derivatives, which means the unstructured mesh is beyond the applicability.

In the finite element methods, simple piece-wise polynomial functions are applied on local elements to describe the variations of unknown variables (we usually call those polynomial functions the shape functions). The concept of residuals is also introduced during the process to measure the error when the approximations substituted into the transport equations. These residuals are then minimized by several special weighing functions and integrating with results in a set of algebraic equations for the unknown coefficients of approximating functions. Generally speaking, they are slower and require more memory in comparison with finite volume methods, and their application is limited.

Spectral methods are based on the same principals as finite difference and finite element methods. The difference is that, the unknown variables are approximated by truncated Fourier series and series of Chebyshev polynomials through the entire domain, not the local approximation as in the previous two methods. The Fourier series and Chebyshev polynomials have their own advantages. The residual minimization technique is similar to finite element methods and, as in the aforementioned methods, it results in a set of algebraic equations for the unknown coefficients of approximating series. For large-scale computations, spectral methods have shown great advantages, for example, direct numerical simulation (DNS) of homogeneous turbulence, computation of transition in shear flows, and global weather modeling. However, compared to finite volume methods, the spectral methods occupy much smaller room in modern commercial CFD codes.

The finite volume method employs discretization of the integral form of the conservation equations directly in physical space. Therefore, the resulting equations express the exact conservation of relevant fluid characteristics for each finite cell volume. This is probably the most essential difference of this method – it works with cell volumes, but not with grid points. The clear relationship between the numerical algorithm and the underlying physical conservation principle makes the concept of the finite volume method simple to understand and to program, in comparison with the finite element and spectral methods. The finite volume method is suitable for all mesh types (structured, unstructured or hybrid), and it is valid for arbitrary shape of cells, which makes it suitable for complex geometries. It has to be noted that the mesh, which divides the solution domain into a finite number of contiguous control volumes defines, actually, only the control volume boundaries, so it does not have to be related to a specific coordinate system. Finite difference type approximations are applied to build a discrete analog of the transport equations and arrive at the set of algebraic equations which are solved by an iterative procedure. STAR-CCM+, as a commercial CFD code, applies the finite volume methods to form the basis for the solution algorithms.

Discretization of governing flow equations results in a large system of non-linear algebraic equations. The method of their solution depends on the problem, but in all cases, since the equations are non-linear, an iterative solution approach is required. The iterative approaches use successive linearization of the equations and the resulting linear systems are solved, as a rule, by iterative techniques. Special algorithms are used to ensure correct coupling between pressure and velocity. As any iterative approach, solution algorithms in CFD need a set of convergence criteria to control convergence. It is customary to distinguish the two levels of iterations: inner iterations, within which the linear equation systems are solved, and outer iterations that deal with non-linearity of the problem and coupling of the equations. Convergence monitoring on both levels is very important as it tells the user whether the desired converged solution is obtained and when it is possible to stop the iterative process.

3.4.1.3 Post-processing

Post-processing in CFD serves the purposes of facilitation of solution setup, execution control and interpretation of simulation results. With constantly improving graphics capabilities of modern personal computers and workstations, visualization tools in CFD play more and more important role and become more elaborate and, at the same time, user friendly. Enforced by specialized utilities for surface quality and mesh quality analyses, simple visual check of geometry and mesh can be extremely helpful in avoiding critical mistakes, saving project time and ensuring accurate, converged solution. As solution goes on, the monitors of residuals and desired integral flow characteristics (forces, surface averaged and volume averaged fluxes, etc.) are used to control the convergence of the

iterative processes. After the solution is obtained, post-processing tools allow for the extraction and visualization of quantities of interest in the form of values, distribution tables, 2D and 3D surface plots, contour plots, vector diagrams, streamline and particle tracking, as well as various geometrical manipulations (translation, rotation, scaling, creation of the new surfaces, etc.). The most advanced post-processing tools allow for the animation of dynamic computation results, which can be both the post-execution and runtime. In addition to graphics, all codes produce alphanumeric output and provide data converters to save results in formats that can further be used by external programs. Post-processing makes CFD results sufficiently illustrative and understandable even for non-specialists.

1) Definition of rotational speed RPS of propellers.

In PROSCALE project, the rotation of the open water propeller is simulated by a moving reference frame (MRF) as introduced in Chapter 2. The reference frame can be set up in the tag “Tools – Reference Frames”, where more reference frames can be established following the steps shown in Figure 3.4.11. For the model scale propellers, the rotational speed RPS is set to be 15 Hz, which can be defined in the property window of the rotational reference frame.

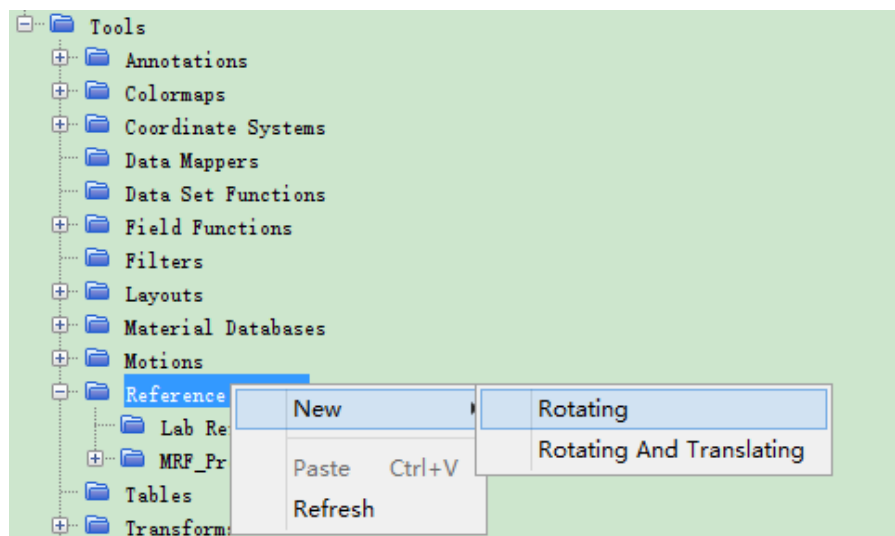


Figure 3.4.11 Establishment of MRF for the open water propeller

For the full scale propellers (scale factor $M = 10, 20$), the diameters for them are shown in Table 3.7.

Table 3.7 Propeller diameters of different scales

Propeller scale	Model scale	Full scale (M=10)	Full scale (M=20)
Diameter [m]	0.25	2.5	5.0

The rotational speed is defined from the Froude scaling:

$$\text{Froude number: } Fr = \frac{V}{\sqrt{gL}} \quad (\text{Equ. 3.9})$$

Where

V – characteristic flow velocity (m/s);

g – acceleration of gravity (m^2/s);

L – characteristic length of the object (m).

In this project,

$$V = \pi \cdot n \cdot D \quad (\text{Equ. 3.10})$$

Where

n – rotational speed RPS of propellers (Hz)

D – propeller diameter (shown in Table 3.7) (m).

Therefore, we can get the following equation:

$$Fr = \frac{\pi n_M \cdot D_M}{\sqrt{g \cdot D_M}} = \frac{\pi n_S \cdot D_S}{\sqrt{g \cdot D_S}} \Rightarrow n_S = n_M \cdot \sqrt{\frac{D_M}{D_S}} = \frac{n_M}{\sqrt{M}} \quad (\text{Equ. 3.11})$$

In Equ. 3.6, the subscripts M and S represent model scale and full scale respectively. And the rotational speed for the propellers with different scales are summarized in Table 3.8.

Table 3.8 Rotational speed of propellers with different scales

Propeller scale	Model scale	Full scale (M=10)	Full scale (M=20)
Rotational speed RPS, n, [Hz]	15.0	4.7434	3.3541

2) Setting up initial condition.

Initial condition provides flow information for all the cells in the simulated region. The initial values should be as close as possible to the expectation values in order to minimize the computation time. However, in practice, the recommendation of initial condition should be as close as possible to inlet boundary conditions. Thus, in this project, all the velocities of initial conditions are set to be the same values as the advance velocity of the propellers (refer to Table 3.6).

3) Control of solvers and stopping criteria.

In the present analyses we use the time step corresponding to propeller turn to 2 degrees. Since the simulations are done using Implicit Unsteady solver, one should change the Time-Step under Solvers->Implicit Unsteady and Maximum Physical Time under Stopping Criteria, in order to adjust them to

propeller RPS used in full scale. The simulation time covers the period of 30 complete propeller revolutions (although, at higher J values, i.e. lower propeller loading, the time can be significantly reduced). And this can be set at Maximum Physical Time under Stopping Criteria. Both the time-step and simulation time for different scale propellers are shown in Table 3.9.

Table 3.9 Time-step for solvers and maximum simulation criteria for different scale propellers

Propeller scale	Model scale	Full scale (M=10)	Full scale (M=20)
Time-step [s]	$3.7037 \cdot 10^{-4}$	$1.1712 \cdot 10^{-3}$	$1.6563 \cdot 10^{-3}$
Maximum Physical Time [s]	2.0	6.325	8.944

There are two indications for converged results. If all the residuals, which show the difference of the value (pressure, velocity, etc.) between the current iteration and the previous one, go down with every iteration or the overall trend for the residuals are going down, that means a good convergence is achieved as shown in Figure 3.4.12. Another indication of a good convergence is the behavior of one of the key parameters, for example, the force coefficient for airfoil, thrust and torque coefficients, resistance coefficient of ship hull. This parameter should be constant at every iteration step when convergence is achieved as shown in Figure 3.4.13.

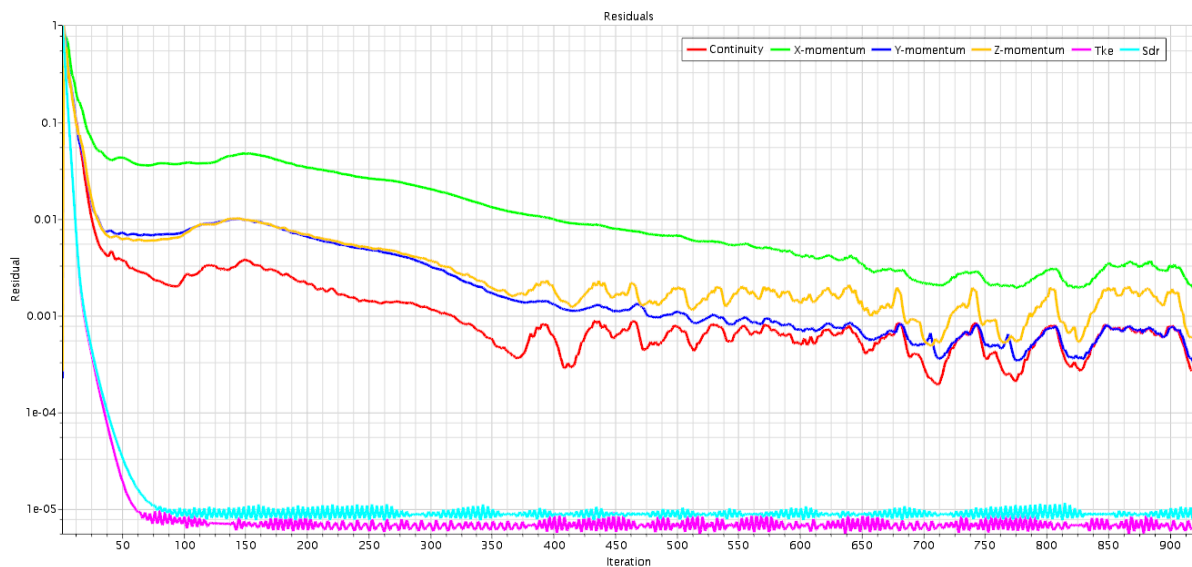


Figure 3.4.12 Residual plot

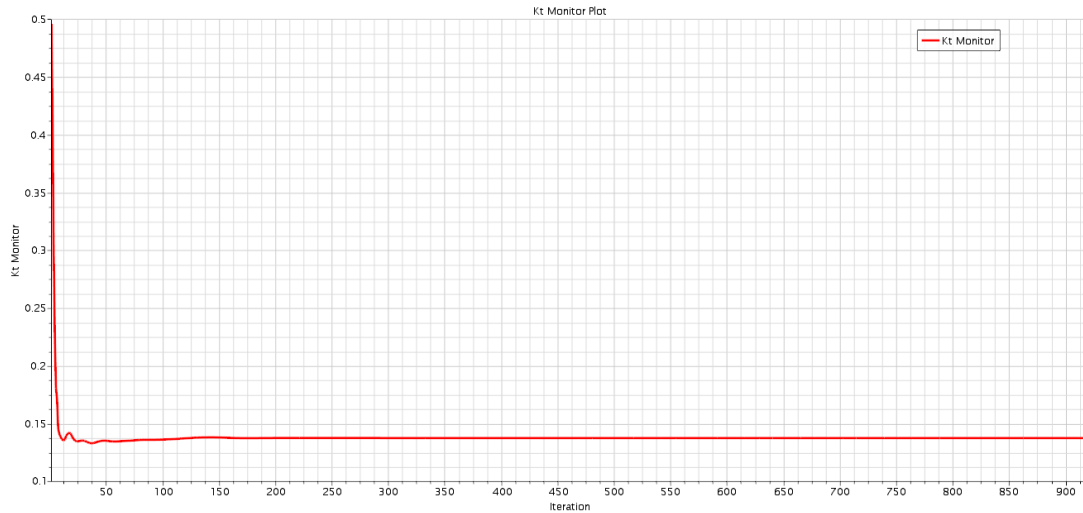


Figure 3.4.13 Torque coefficient plot

4) Interpretation of simulation results.

In this section, the reports for both thrust coefficient K_T and torque coefficient K_Q are established by the use of field functions in STRA-CCM+ code. In the Simulation tab, by right click on the Reports node, some new reports can be established and the user can choose the report type in STAR-CCM+.

There are different kinds of reports that are available as shown in Figure 3.4.14. In this project, only the force coefficient is chosen to express the torque and thrust coefficients.

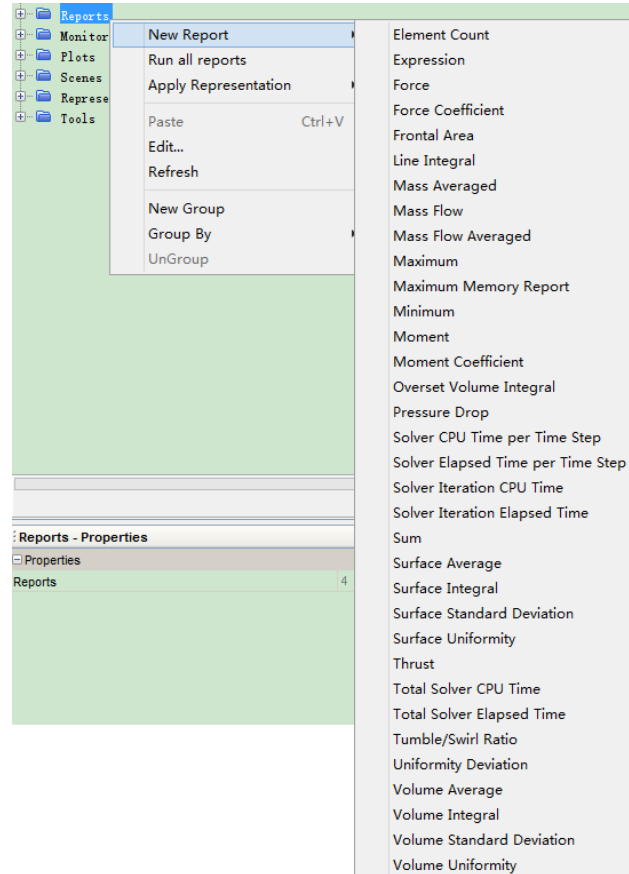


Figure 3.4.14 All kinds of available reports

The property parameters for the reports are summarized in Table 3.10 and all these parameters can be obtained by Equ. 3.7.

$$\begin{aligned} \text{Reference velocity: } V_{ref} &= n \cdot D \\ \text{Reference area: } S_{ref} &= \frac{2 \cdot D^2}{Z} \\ \text{Reference radius: } R_{ref} &= D \end{aligned} \quad (\text{Equ. 3.12})$$

Table 3.10 Reference parameters for force coefficient reports

Propeller scale	Model scale	Full scale (M=10)	Full scale (M=20)
Reference velocity, (nD), [m/s]	3.75	11.8585	16.7705
Reference area, S_{ref} , [m ²]	0.03125	3.125	12.5
Reference radius, for K_Q , [m]	0.25	2.5	5.0

5) Setting up scenarios and plots to visualize results.

Visualization tools are important as previously mentioned. All the reports can be intuitively displayed in plots by an operation named “create monitor and plot from reports”. To display the interested values (for example, in this project, the velocities and pressure in the domain), some scenes and plots can be established. The **Scenes** node, which has a pop-up menu, is the manager object for working with scenes in the simulation tree. Usually, the geometry is used to display the simulated object and monitor the edition process while the mesh scene is always utilized to display the surface mesh and volume mesh. The scalar or vector scenes play an important role when the target parameters is expressed by some field functions.

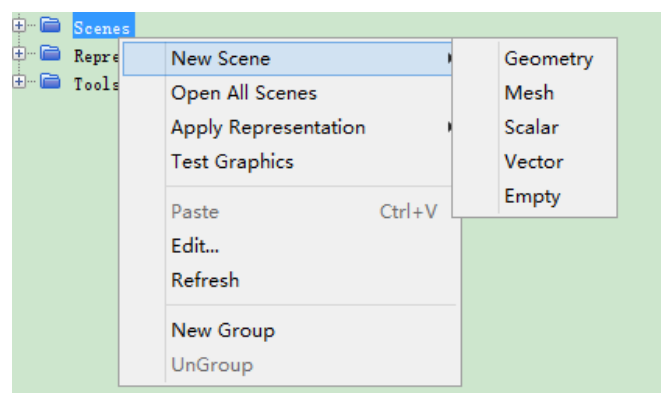


Figure 3.4.15 Scene node in the simulation tree

Derived parts are used to analyze data within a STAR-CCM+ simulation. The Derived Parts manager node, which has its own pop-up menu, contains all of the derived part nodes in the object tree.

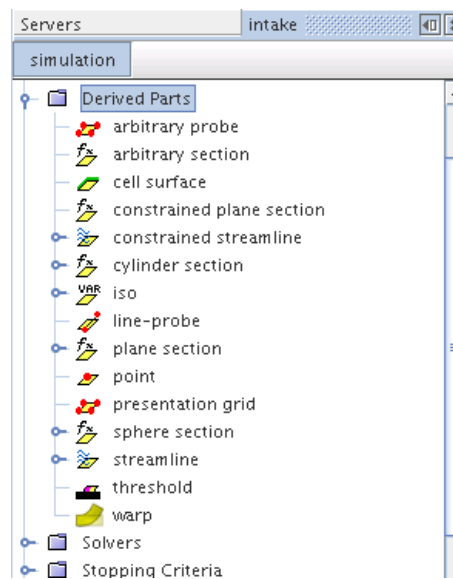


Figure 3.4.16 The derived parts manager node

Any of various derived parts can be edited and used to examine solution data. Creating and editing can be done visually using the powerful in-place dialog. A derived part gets its data when you select input (parent) parts for it. Certain derived parts can be defined using local coordinate systems. Derived parts make the illustration of results more flexible and comprehensive.

In the simulation example, it contains scenes for visualizing wall Y^+ distribution, Velocity field at longitudinal plane, Constrained streamlines on propeller blades and hub, Boundary layer flow visualization, and Vorticity field around propeller by Volume Rendering. The Plots group contains an X-Y plot to output pressure distribution along a given cylindrical section of propeller blade. When estimating scale effect on propeller characteristics, it is very useful to compare the Pressure and Friction (Shear) components of propeller thrust and torque, which are output by default in the Reports.

3.4.2 Calculating new propellers and changing scale

The enclosed simulation examples can easily be used to set up a calculation with new propeller geometry and do calculations at different scales.

Since all domain geometry manipulations are performed at the Parts level, one can simply replace the Blade part in the Parts list with a new blade surface from a *Blade.dbs* file. The surface patch name conventions are observed in the prepared dbs-models. Additional operations (copying, transforming)

will be needed after importing a new blade part in the simulation according to the setup with blade split, to create the neighbouring blade. When done, one has to simply Update the resulting Fluid part and proceed with meshing. These steps are made automatic due to the Parts Based Operation functionality and Assign Parts to Region functionality of STAR-CCM+.

When performing simulations in full scale, one can also use conveniently the simulation examples done in model scale and the proper arrangement of the change can follow the subsequent steps:

- 1) The first step is to scale the necessary geometry parts defining the domain and volumetric controls used in meshing. These include:

Geometry Parts: Blade, Hub, Fluid_Cylinder_1BP

Volumetric Controls: VC_Cylinder-1, VC_Cylinder-2, VC_Cylinder-3, VC_Cylinder-4, VC_Cylinder-5, VC_Cylinder-6, VC_Cylinder-7, VC_Cylinder_Hub_Gap.

Scaling is done using the option Transform->Scale. After scaling, the domain Update operation should be repeated. Further, one has to modify the extrusion settings for the Inlet and Outlet boundaries under Regions-Fluid->Boundaries-Inlet(/Outlet)->Mesh Values ->Normal Extrusion Parameters. The Magnitude of extrusion should be changes according to the scale factor.

- 2) The mesh setup used in the simulations should allow for adequate near-wall (boundary layer) flow treatment in both the model scale and full scale conditions (full scale factors over 10) without modification of Prism Layer Mesher setting. In model scale, it will result in wall $Y+ < 5$, while in full scale, it will result in wall $30 < Y+ < 300$.
- 3) The Time-Step under Solvers->Implicit Unsteady and Maximum Physical Time under Stopping Criteria, should also be adjusted to propeller RPS used in full scale and the values are shown in Table 3.9.
- 4) The propeller RPS should be changes under Tools->Reference Frames->MRF_Propeller (all these RPS have been illustrated in Table 3.8). The simulation uses Moving Reference Frame (MRF) method. The inflow velocity should accordingly be adjusted to meet the same J value as in model scale calculation.

The velocity is input at three places: Physics->Initial Conditions->Velocity (to initialize the solution), Regions-Fluid->Boundaries-Inlet and Regions-Fluid->Boundaries-Outward (the two boundaries where the inlet boundary conditions are set).

- 5) Finally, modify the reference values for thrust and torque coefficients reports under Reports, by changing the value of Reference Velocity, Reference area and Reference radius parameters. All these parameters are illustrated in Table 3.10.

3.4.3 Analysis methods

The validation process will be performed at the beginning of the project by comparing the CFD results with the experimental data. The open water characteristics (thrust coefficient K_T , torque coefficient K_Q , efficiency η_0) are import metrics to measure the quality of CFD results. During the process, the feasible setups of STAR-CCM+ for this project will be obtained.

All the CFD results for propellers in the same skew angle but with different scales (model scale, full scales) will be compared to get the scale effects of open water performance. For the propellers with the same scale but various of skew angles (0 deg, 23 deg, 46 deg), the open water characteristics will be compared to get the different tendency along different advance velocities. All the scale effects will be analysed on the view of flow patterns around the propellers.

For the propeller P1374 (skew angle 23 deg), both the experimental data and geometry parameters can be obtained. Therefore, more analysis of scale effects will be based on this propeller. The ITTC corrections for scale effects of propellers will be carried out as a reference for the CFD results.

4 RESULTS

4.1 Results validation

The results obtained from CFD methods can be affected by some simulation errors and uncertainties, such as the model errors and uncertainties, discretization (numerical) errors, iteration (convergence) errors, round-off errors, application uncertainties, user errors and code errors. Therefore, the simulation results from STAR-CCM+ will be compared with some experimental data provided by MARINTEK. If the results errors are within the acceptable range, some detailed setups will be proceeded with in the following simulations.

4.1.1 Experimental results

The experimental data of open water propeller characteristics provided by MARINTEK are with the following parameters:

Table 4.1 Propeller parameters for experimental data

P1374	
Parameters	values
Pitch ratio : $P(0.70)/D$	1.10, 0.90
Skew angle	23 deg
Rotational speed, RPS, n	5 Hz, 9Hz, 15 Hz, 20 Hz

For the cases of $n = 5 \text{ Hz}$, 9 Hz , 15 Hz , the experimental results are obtained from open water test in towing tank in April, 2014. And the results for the case of $n = 20 \text{ Hz}$, the propeller model are tested in the cavitation tunnel in March, 2006. In this project, only the propellers of model scale with the pitch ratio of $P(0.70)/D = 1.10$ is simulated in STAR-CCM+ as a time limitation. Therefore, the open-water characteristics (thrust coefficient K_T , torque coefficient K_Q and open water efficiency η_0) for $P(0.70)/D = 1.10$ will be laid out in this section and more detailed experimental data of $P(0.70)/D = 0.90$ will be expressed in Appendix A.

Table 4.2 Experimental results of open water tests, $P/D=1.10$

n=5 Hz				n=9 Hz			
J	K_T	K_Q	η_0	J	K_T	K_Q	η_0
0.0	0.606	0.0924	0	0.0	0.611	0.0924	0

0.1	0.561	0.0867	0.103	0.1	0.568	0.087	0.104
0.2	0.516	0.0809	0.203	0.2	0.523	0.0813	0.205
0.3	0.47	0.0751	0.299	0.3	0.475	0.0754	0.301
0.4	0.423	0.0693	0.388	0.4	0.426	0.0693	0.391
0.5	0.375	0.0635	0.47	0.5	0.376	0.0632	0.474
0.6	0.326	0.0572	0.543	0.6	0.326	0.0569	0.547
0.7	0.276	0.0507	0.608	0.7	0.277	0.0506	0.61
0.8	0.226	0.0442	0.652	0.8	0.228	0.0441	0.658
0.9	0.175	0.0372	0.673	0.9	0.178	0.0374	0.684
1.0	0.117	0.0289	0.642	1.0	0.126	0.03	0.67
1.1	0.049	0.0191	0.45	1.1	0.069	0.0217	0.554
1.2	-0.024	0.0083	-0.552	1.2	0.001	0.0119	0.012
n=15 Hz				n=20 Hz			
J	K_T	K_Q	η₀	J	K_T	K_Q	η₀
-	-	-	-	0.1	0.58317	0.09039	0.10269
-	-	-	-	0.2	0.53204	0.08366	0.20242
-	-	-	-	0.3	0.47949	0.07705	0.29712
-	-	-	-	0.4	0.42736	0.07060	0.38538
-	-	-	-	0.5	0.37680	0.06429	0.46636
0.6	0.325	0.0566	0.548	0.6	0.32818	0.05809	0.53948
0.7	0.276	0.0502	0.613	0.7	0.28116	0.05187	0.60387
0.8	0.230	0.0439	0.666	0.8	0.23469	0.04548	0.65702
0.9	0.182	0.0373	0.700	0.9	0.18694	0.03870	0.69189
1	0.131	0.0301	0.692	1.0	0.13540	0.03127	0.68907
1.1	0.072	0.0218	0.579	1.1	0.07679	0.02288	0.58764
1.2	0.005	0.0122	0.077	1.2	0.00711	0.01314	0.10328

The test results from the towing tank at low J values, $n = 15$ Hz are absent and this is due to the limitation of current propeller dynamometer that cannot withstand very high loads. However, for this particular propeller, no (in the common measured range) significant differences are observed between $n = 15$ Hz and $n = 9$ Hz. So the results for $n = 9$ Hz can be used with confidence in comparisons. In the range of $n = 5$ Hz, the influence of laminar-turbulent transition already becomes large, thus the results for that will not be taken into use in this project. The results obtained at 20 Hz in the cavitation tunnel (atmospheric condition) show consistently higher values of K_T and K_Q compared to the towing tank measurements. This is probably due to the influence of tunnel walls (blockage effect). The use of towing tank results in our comparisons is therefore most appropriate.

4.1.2 STAR-CCM+ results

In the CFD simulation process, to find the proper setups of STAR-CCM+ in the aspects of results accuracy, time and computational power, two different mesh sizes are used. When changing the base

size of mesh from 0.20 m to 0.25 m in model scale simulation, the quantities of the mesh cells will change. As mesh quality is the main factor for results precision, for the same mesh method, more sophisticated the mesh is, more accurate the results possibly be obtained. The different volume mesh representations are shown in Table 4.3.

Table 4.3 Different mesh results for two mesh sizes

P/D = 1.10, skew angle $\theta_{sp} = 23^\circ$, model scale			
Base size of mesh [m]		0.20	0.25
Volume mesh representations	Cells	$2.17 \cdot 10^6$	$1.36 \cdot 10^6$
	Interior Faces	$12.0 \cdot 10^6$	$7.20 \cdot 10^6$
	Vertices	$8.96 \cdot 10^6$	$5.25 \cdot 10^6$

The simulation results of open water propellers in the case of $n = 9\text{ Hz}$ for these two mesh sizes from STAR-CCM+ are shown in Table 4.4.

Table 4.4 Simulation results of different mesh sizes

Skew23, P(0.7)/D=1.10, n=9 Hz, D=0.25 m						
J	K_T		K_Q		η_0	
	0.20 m	0.25 m	0.20 m	0.25 m	0.20 m	0.25 m
0.1	0.5787	0.5803	0.0902	0.0909	0.1021	0.1016
0.3	0.4787	0.4777	0.0769	0.0770	0.2974	0.2962
0.5	0.3743	0.3727	0.0636	0.0634	0.4686	0.4675
0.7	0.2710	0.2695	0.0502	0.0500	0.6013	0.6001
0.9	0.1699	0.1693	0.0364	0.0364	0.6683	0.6659
1.1	0.0557	0.0551	0.0204	0.0204	0.4791	0.4739
1.2	-0.0129	-0.0140	0.0105	0.0104	-0.2355	-0.2560

There is only a marginal difference between the results for a specific advance ratio J, for example, when $J = 0.70$, the difference of thrust coefficient expressed by percentage is:

$$\Delta K_T = \frac{0.2710 - 0.2695}{0.2710} \times 100\% = 0.55\%$$

However, the required time of the simulation for the case with the base size of 0.20 m (about 40 hours) is approximately twice of the case with the base size of 0.25 m. Therefore, the base size 0.25m will be

applied to all the simulations for model scale propellers and the base size of the full scale propellers will be this value multiplied by the scale factor ($M=10, 20$).

To validate the results of STAR-CCM+, the open water performance of the propeller P1374 with a model scale ($D = 0.25$ m) and rotational speed (RPS) of $n = 9$ Hz, $n = 15$ Hz will be compared with the corresponding experimental data. Because the experimental results are incomplete as mentioned before, the CFD results for the cases of $n = 15$ Hz will be compared with the experimental results of $n = 9$ Hz.

For P1374 of model scale, $n=9$ Hz, the results are shown in Table 4.5. The absolute differences for low advance coefficient (e.g. $J = 0.1$) and high advance coefficient (e.g. $J = 1.1$ and $J = 1.2$) is larger than that of the other advance ratios. The biggest difference of thrust coefficient happens at $J = 1.2$. The open water diagram states the differences in a more frank way (Figure 4.1.2).

Table 4.5 CFD results and experiment data of P1374, $n=9$ Hz

Skew23,P(0.7)/D=1.10, n=9 Hz, D=0.25									
J	CFD results			Experimental results			Relevant difference		
	K_T	K_Q	η_0	K_T	K_Q	η_0	ΔK_T	ΔK_Q	$\Delta \eta_0$
0.1	0.5803	0.0909	0.1016	0.568	0.087	0.104	-0.0123	-0.0039	0.0024
0.3	0.4777	0.0770	0.2962	0.475	0.0754	0.301	-0.0027	-0.0016	0.0048
0.5	0.3727	0.0634	0.4675	0.376	0.0632	0.474	0.0033	-0.0002	0.0065
0.7	0.2695	0.0500	0.6001	0.277	0.0506	0.610	0.0075	0.0006	0.0099
0.9	0.1693	0.0364	0.6659	0.178	0.0374	0.684	0.0087	0.0010	0.0181
1.1	0.0551	0.0204	0.4739	0.069	0.0217	0.554	0.0139	0.0013	0.0801
1.2	-0.0140	0.0104	-0.2560	0.001	0.0119	0.012	0.0150	0.0015	0.2680

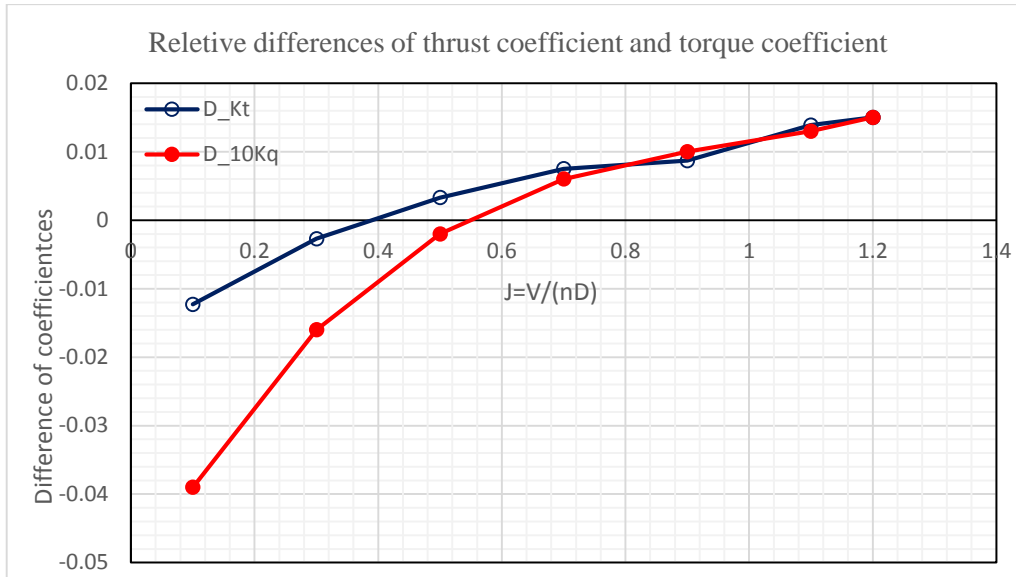


Figure 4.1.1 Relative differences of experimental data and CFD results

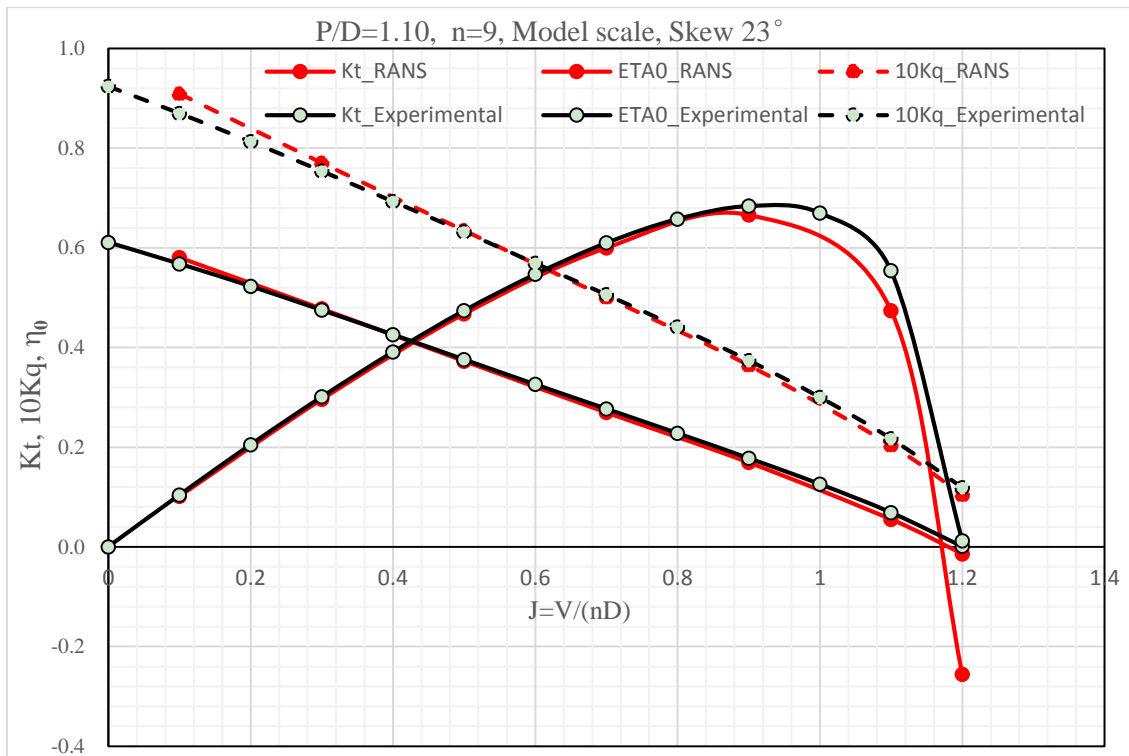


Figure 4.1.2 open water diagram for P1374, n=9 Hz, CFD & Exp.

The results obtained from STAR-CCM+ for P1374 at the case of $n = 15$ Hz will also be compared with the characteristics from towing tank ($n = 9$ Hz). The results are summarized in Table 4.6, which shows slight differences of results from CFD methods and experimental methods even they represented the different rotational speed.

Table 4.6 CFD results ($n=15$ Hz) and experiment data ($n=9$ Hz) of P1374

Skew23,P(0.7)/D=1.10, D=0.25

J	CFD results			Experimental results			Relevant difference		
	K_T	K_Q	η_0	K_T	K_Q	η_0	ΔK_T	ΔK_Q	$\Delta \eta_0$
0.1	0.5846	0.0911	0.1021	0.568	0.087	0.104	-0.0166	-0.0041	0.0019
0.3	0.4805	0.0770	0.2980	0.475	0.0754	0.301	-0.0055	-0.0016	0.0030
0.5	0.3751	0.0634	0.4710	0.376	0.0632	0.474	0.0009	-0.0002	0.0030
0.7	0.2723	0.0501	0.6059	0.277	0.0506	0.610	0.0047	0.0005	0.0041
0.9	0.1725	0.0365	0.6769	0.178	0.0374	0.684	0.0055	0.0009	0.0071
1.1	0.0583	0.0204	0.5002	0.069	0.0217	0.554	0.0107	0.0013	0.0538

Therefore, the CFD settings for the simulated cases in this project can yield proper results for open water tests and the settings will be used for all the simulations for propellers with different magnitude of skew in both model scale and full scales.

4.2 CFD results

4.2.1 Scale effects on open water characteristics

The open water characteristics of propellers (thrust coefficient K_T , torque coefficient K_Q and efficiency η_0) with different magnitude of skews in both model scale (MS) and full scales (FS10, FS20) are obtained by the simulations of STAR-CCM+. The scale effects on open water performance of propellers were analyzed by comparing the characteristics (thrust coefficient K_T , torque coefficient K_Q and efficiency η_0) of propellers with one specific skew angle (for example, skew0) but different sizes (MS, FS10, FS20). The detailed values for all the characteristics are shown in Table 4.7. The open water diagrams for that are shown in Figure 4.2.1.

The open water diagrams show the same tendency in the characteristics (thrust coefficient K_T , torque coefficient K_Q and efficiency η_0) of different scale propellers with the same skew angle. The thrust coefficient K_T and efficiency η_0 of the model scale propeller is always lower than that of the full scale propellers at the same skew. The propellers of two different full scales (FS10, FS20) show little difference in terms of thrust coefficient K_T and efficiency η_0 compared with that of propellers in corresponding model scale. The propeller with the largest diameter (FS20, $D = 5.0$ m) indicates the maximal thrust coefficient K_T , minimal torque coefficient K_Q and highest efficiency η_0 in comparison with the propellers in the other two scales at the same skew.

The reasons for the differences of thrust coefficient K_T is analyzed by studying the two components (pressure and friction) of total force (shown in Table 4.8). For the propellers in the same skew and advance velocity, the pressure coefficient will rise along with the increase of propeller scale while the absolute values of shear (friction) coefficient decrease. Therefore, the total thrust coefficient K_T will increase as the propeller scale get larger.

Table 4.7 Open water characteristics of CFD results for propellers with different scales and skew angles

Skew0									
J	MS			FS10			FS20		
	K_T	K_Q	η_0	K_T	K_Q	η_0	K_T	K_Q	η_0
0.1	0.3161	0.0357	0.1409	0.3239	0.0353	0.1461	0.3264	0.0352	0.1475
0.3	0.2327	0.0290	0.3828	0.2404	0.0286	0.4009	0.2425	0.0286	0.4055
0.5	0.1460	0.0220	0.5279	0.1533	0.0216	0.5651	0.1553	0.0215	0.5744
0.6	0.0989	0.0183	0.5171	0.1059	0.0178	0.5679	0.1078	0.0177	0.5812
0.7	0.0459	0.0139	0.3682	0.0525	0.0134	0.4375	0.0543	0.0133	0.4561
0.8	-0.015	0.0087	-0.2190	-0.0090	0.0082	-0.1319	-0.0067	0.0081	-0.1048
Skew23									
J	MS			FS10			FS20		
	K_T	K_Q	η_0	K_T	K_Q	η_0	K_T	K_Q	η_0
0.1	0.3344	0.0379	0.1406	0.3425	0.0374	0.1459	0.3441	0.0372	0.1471
0.3	0.2526	0.0311	0.3878	0.2616	0.0307	0.4066	0.2631	0.0306	0.4108
0.5	0.1649	0.0239	0.5491	0.1736	0.0234	0.5893	0.1749	0.0233	0.5977
0.6	0.1173	0.0200	0.5606	0.1256	0.0195	0.6162	0.1268	0.0193	0.6273
0.7	0.0650	0.0156	0.4643	0.0724	0.0150	0.5379	0.0736	0.0148	0.5529
0.8	0.0046	0.0104	0.0559	0.0116	0.0098	0.1513	0.0127	0.0096	0.1688
Skew46									
J	MS			FS10			FS20		
	K_T	K_Q	η_0	K_T	K_Q	η_0	K_T	K_Q	η_0
0.1	0.3456	0.0393	0.1399	0.359	0.0394	0.145	0.3626	0.0395	0.146
0.3	0.2498	0.0308	0.3868	0.2636	0.0312	0.4035	0.2666	0.0313	0.4073
0.5	0.1535	0.0225	0.5425	0.1659	0.0227	0.5809	0.1684	0.0227	0.5901
0.6	0.1021	0.0179	0.5436	0.1133	0.018	0.6023	0.1155	0.0179	0.6159
0.7	0.0449	0.0127	0.3926	0.0550	0.0126	0.4867	0.0570	0.0125	0.5074
0.8	-0.0176	0.0070	-0.3180	-0.0090	0.0067	-0.1674	-0.0070	0.0065	-0.1371

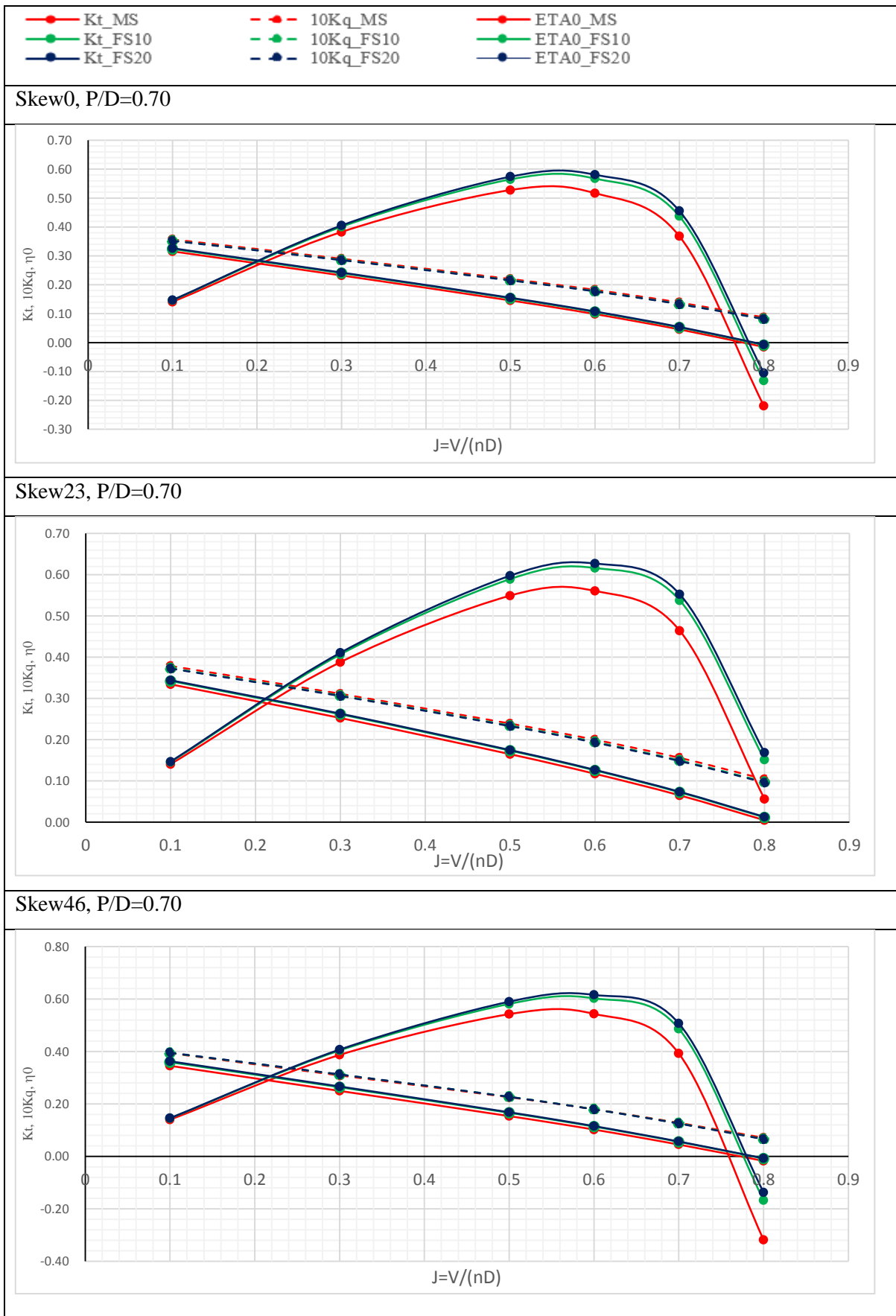


Figure 4.2.1 open water diagrams of scale effects study

Table 4.8 Pressure and friction components in total forces classified by different skews

J	K_T	Skew 0°			Skew 23°			Skew 46°		
		MS	FS10	FS20	MS	FS10	FS20	MS	FS10	FS20
0.30	Calc(Tot)	0.2327	0.2404	0.2425	0.2526	0.2616	0.2631	0.2498	0.2636	0.2666
	Pressure	0.2354	0.2422	0.2440	0.2553	0.2634	0.2646	0.2525	0.2654	0.2682
	Friction	-0.0027	-0.0018	-0.0015	-0.0027	-0.0017	-0.0015	-0.0027	-0.0018	-0.0015
0.50	Calc(Tot)	0.1460	0.1533	0.1553	0.1649	0.1736	0.1749	0.1535	0.1659	0.1684
	Pressure	0.1488	0.1551	0.1568	0.1677	0.1754	0.1764	0.1564	0.1678	0.1700
	Friction	-0.0028	-0.0018	-0.0016	-0.0028	-0.0018	-0.0016	-0.0029	-0.0019	-0.0017
0.70	Calc(Tot)	0.0459	0.0525	0.0543	0.0650	0.0724	0.0736	0.0449	0.0550	0.0570
	Pressure	0.0489	0.0545	0.0560	0.0680	0.0744	0.0753	0.0481	0.0572	0.0588
	Friction	-0.0031	-0.0020	-0.0017	-0.0031	-0.0020	-0.0017	-0.0032	-0.0022	-0.0018

4.2.2 Open water characteristics for different skews

The open water diagrams for the propellers with different scales are shown in Figure 4.2.1. As shown in the following figure, for propellers with different skews (skew0, skew23, skew46), the overall trends of thrust coefficient K_T , torque coefficient K_Q and efficiency η_0 are identical from one scale to another. Therefore, the propellers with different skews (skew0, skew23, skew46) in model scale were taken as analysis examples.

The diagram states that the propeller with a skew angle of 23 deg possesses the largest thrust force in a wide range of advance velocity ($J \geq 0.3$) and the efficiency of it is also higher than the other two propellers with the skew angle of 0 deg and 46 deg when $J \geq 0.5$. The propeller skew0 performed the minimal thrust force in almost the whole simulation range while the measured thrust force for Skew 46 shows the most obvious decrease as the increase of advance velocity.

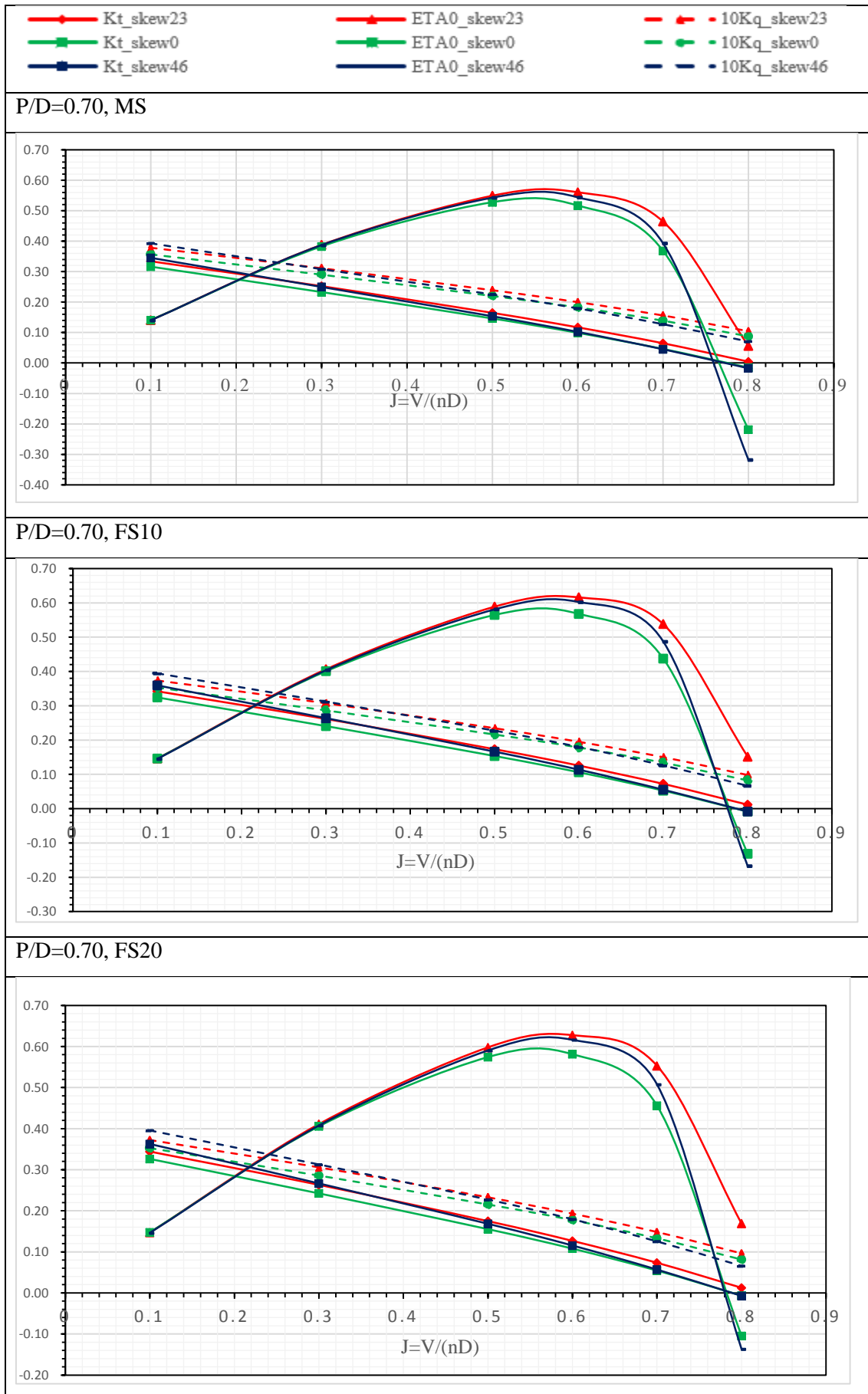


Figure 4.2.2 open water diagrams for propellers with different skews in both model and full scales

To understand the aforementioned behaviour of the characteristics, the two components of total forces – pressure and friction – were analyzed for both model scale and full scale propellers with different skews (refer to Table 4.9). The friction part of the total force shows negligible differences between different skews of propellers in the same scale, for instance, when $J = 0.3$, the friction component is -0.0027 for propellers with three different skews (skew0, skew23, skew46). Therefore, the differences for thrust force of propellers with different skews in one particular scale comes from the pressure component of the total force.

Table 4.9 Pressure and friction components in total forces classified by different scales

J	K_T	MS			FS10			FS20		
		Skew 0°	Skew 23°	Skew 46°	Skew 0°	Skew 23°	Skew 46°	Skew 0°	Skew 23°	Skew 46°
0.3	Calc(Tot)	0.2327	0.2526	0.2498	0.2404	0.2616	0.2636	0.2425	0.2631	0.2666
	Pressure	0.2354	0.2553	0.2525	0.2422	0.2634	0.2654	0.2440	0.2646	0.2682
	Friction	-0.0027	-0.0027	-0.0027	-0.0018	-0.0017	-0.0018	-0.0015	-0.0015	-0.0015
0.5	Calc(Tot)	0.1460	0.1649	0.1535	0.1533	0.1736	0.1659	0.1553	0.1749	0.1684
	Pressure	0.1488	0.1677	0.1564	0.1551	0.1754	0.1678	0.1568	0.1764	0.1700
	Friction	-0.0028	-0.0028	-0.0029	-0.0018	-0.0018	-0.0019	-0.0016	-0.0016	-0.0017
0.7	Calc(Tot)	0.0459	0.0650	0.0449	0.0525	0.0724	0.0550	0.0543	0.0736	0.0570
	Pressure	0.0489	0.0680	0.0481	0.0545	0.0744	0.0572	0.0560	0.0753	0.0588
	Friction	-0.0031	-0.0031	-0.0032	-0.0020	-0.0020	-0.0022	-0.0017	-0.0017	-0.0018

4.2.3 Pressure distribution on blade section

The pressure distribution on the propellers with different skews and scales along the chordwise of the blades are represented by the sections of 0.5R, 0.7R, 0.9R and 0.95R. Firstly, the scale effects of pressure distribution on propellers with different magnitude of skews were investigated on the blade sections of 0.7R under the condition of $J = 0.1$. The results are shown in Figure 4.2.3, and in this picture, c_p represents the pressure coefficient, x states the position of the point on the section along the chord and c indicates the chord length of the section $r/R = 0.70$.

For the propellers with the skew angle of 0 deg (skew 0), the pressure distribution shows negligible differences between propellers with various scales (MS, FS10, FS20). However, the differences increased as the rise of skew angle and the discrepancy mainly exists at the trailing edge area ($0 < x/c < 0.20$). For example, it is obvious that the differences of pressure coefficient C_p for propellers with the skew angle of 23 deg and different scales (MS, FS10, FS20) is larger than that of

the propellers with the skew angle of 0 deg but smaller than that of the propellers with the skew angle of 46 deg. The pressure distribution states coincidence at the range of $x/c > 0.20$. Therefore, the later pressure distribution analysis is mainly focused on the effects of blade section location (0.5R, 0.7R, 0.9R and 0.95R) and various of skews (skew0, skew23, skew46) at the same propeller scale – model scale. The pressure distribution diagrams of blade sections in various positions are shown in Figure 4.2.4.

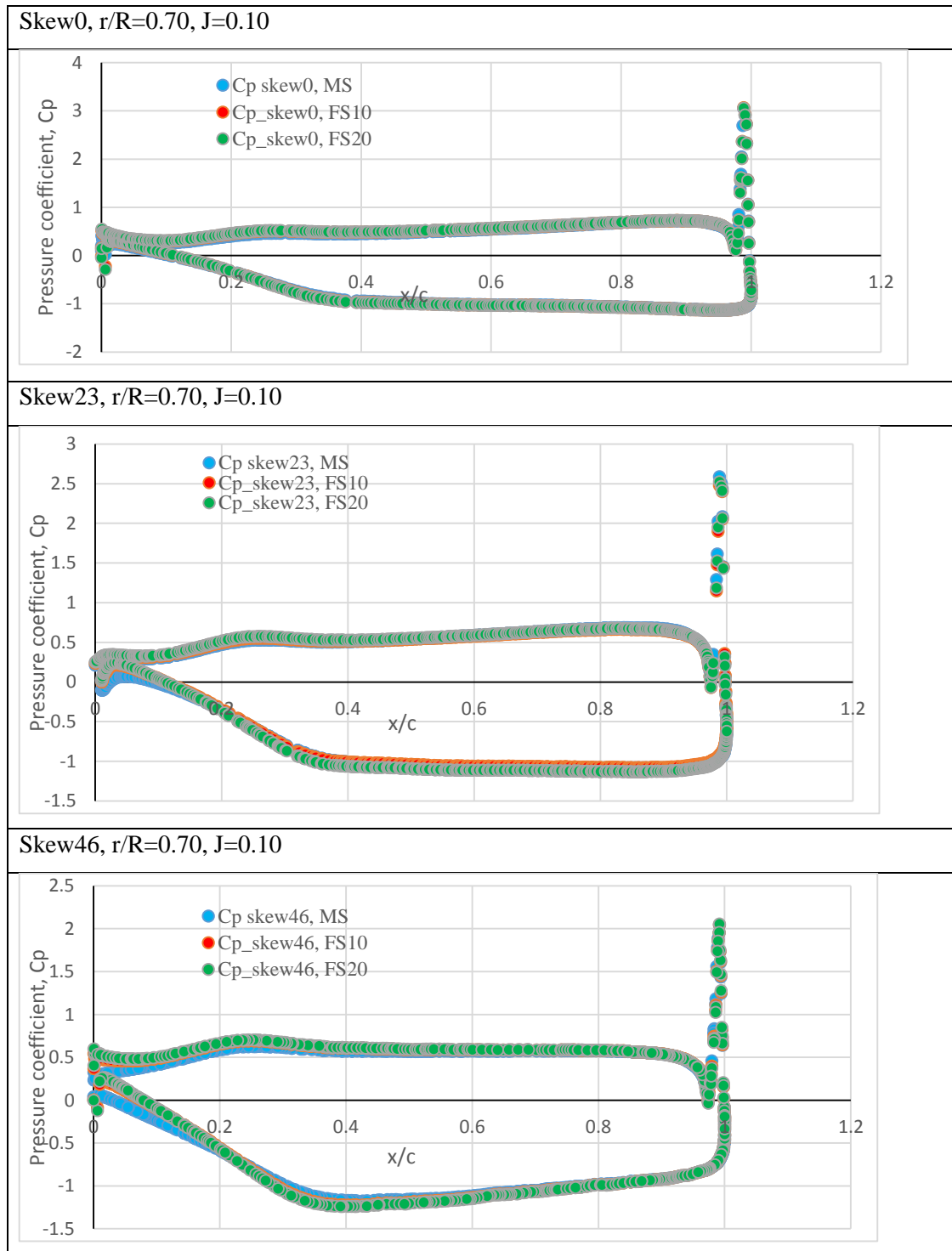


Figure 4.2.3 Pressure distribution on the section 0.7R for propellers with the same skews and different scales

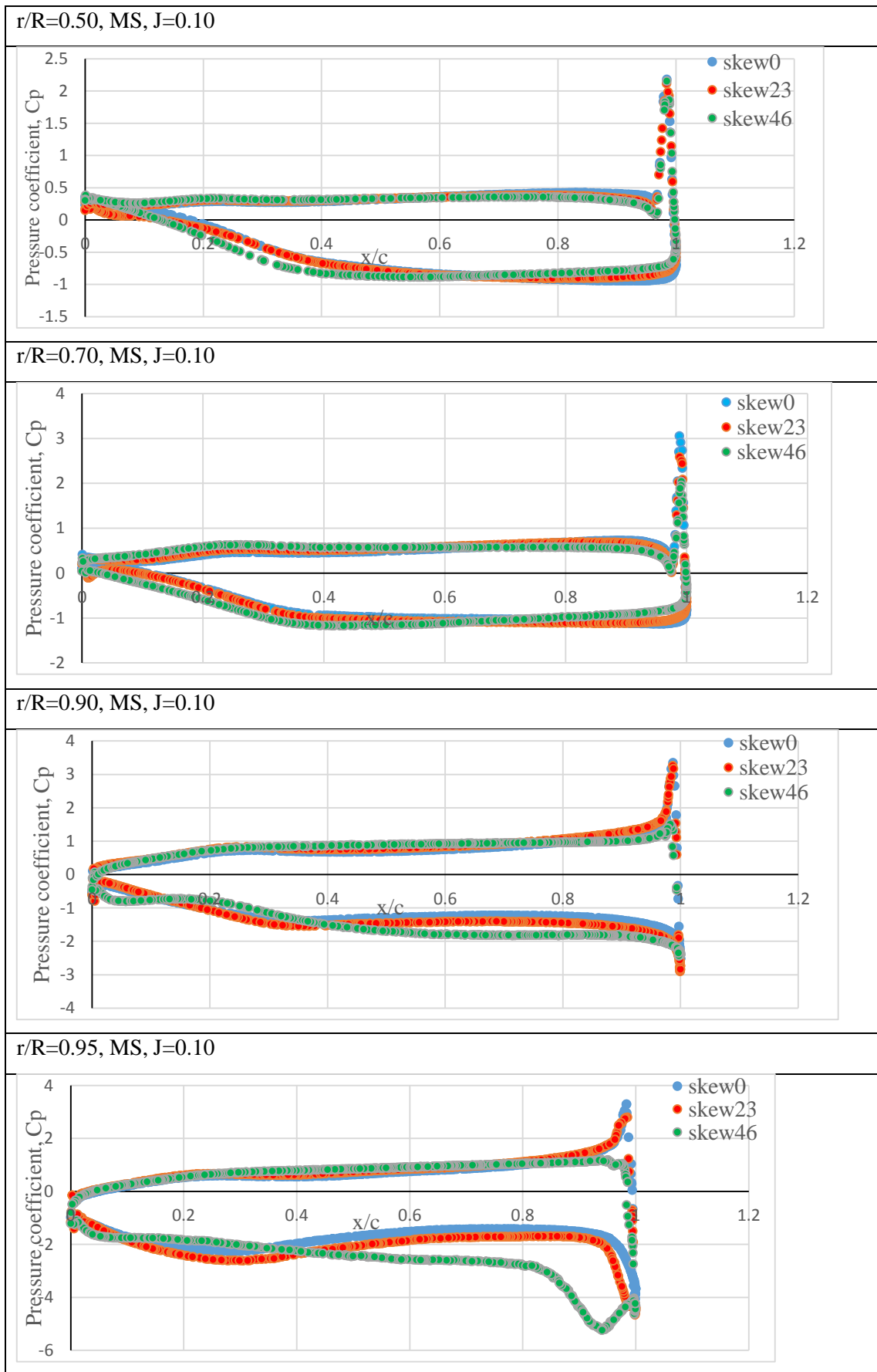


Figure 4.2.4 Pressure distribution of section 0.50R, 0.70R, 0.90R, 0.95R, model scale, J=0.10

In the blade location $r/R = 0.50$, the propeller skew46 (skew angle 46 deg) shows higher pressure on the suction side in the region of $0 < x/c < 0.5$ followed by the propeller skew23 (skew angle 23 deg) while propeller skew0 (skew angle 0 deg) possesses the minimal pressure in that region. However, this trend is reversed in the region of $0.5 < x/c < 1.0$ on the suction side, which means the propeller skew0 possesses the maximal pressure while skew46 has the minimum values. On the pressure side, the propeller skew46 shows the lowest pressure and skew0 shows the highest pressure in the region of $0 < x/c < 0.6$. This trend is also reversed in the area of $0.6 < x/c < 1.0$. Propeller skew46 shows the maximum pressure deduction in the region close to trailing edge ($0 < x/c < 0.6$) and propeller skew0 indicates the largest pressure deduction in the region close to leading edge are ($0.6 < x/c < 1.0$).

In the blade section $r/R = 0.70$, the pressure distribution states the similar tendency as that of the location $r/R = 0.50$. The pressure deduction along the chord length at $r/R = 0.70$ is more larger than that of the position $r/R = 0.50$.

The pressure distribution along the chord length at $r/R = 0.90$ shows greater differences than that of the previous two sections. The propeller skew46 shows the highest pressure in the mid-chord region ($0 < r/R < 0.70$) on the suction side while in the leading edge area ($0.70 < r/R < 1.0$), it indicates the lowest pressure. On the pressure side of the section, skew46 possesses the minimal pressure in the range of $0.40 < r/R < 1.0$. Therefore, in the region of $0.40 < r/R < 0.70$, propeller skew46 shows the largest pressure deduction. When $0.10 < r/R < 0.40$, on the pressure side of the section, propeller skew23 shows the most obvious pressure deduction.

As to the pressure distribution of the section $r/R = 0.95$, it is apparent that the propeller skew46 shows the lowest pressure in the range of $0.40 < r/R < 1.0$ on the pressure side and it also indicates the largest pressure gap in that range.

Generally speaking, the differences of pressure distribution between propellers with different magnitude of skews become larger when the blade section gets further outside of the blade. For example, the differences of pressure distribution between various skews for the section $r/R = 0.95$ is more evident than that of the section $r/R = 0.50$. The pressure deduction between suction side and pressure side for one particular propeller becomes larger when considering a more outer blade section. For instance, for the propeller skew23, the pressure deduction of the blade section $r/R = 0.50$ is smaller than that of the section $r/R = 0.90$.

4.2.4 Flow patterns

The pressure on both suction side and pressure side of model scale propellers with different magnitude of skews under the condition of $J = 0.1$ is captured in STAR-CCM+.

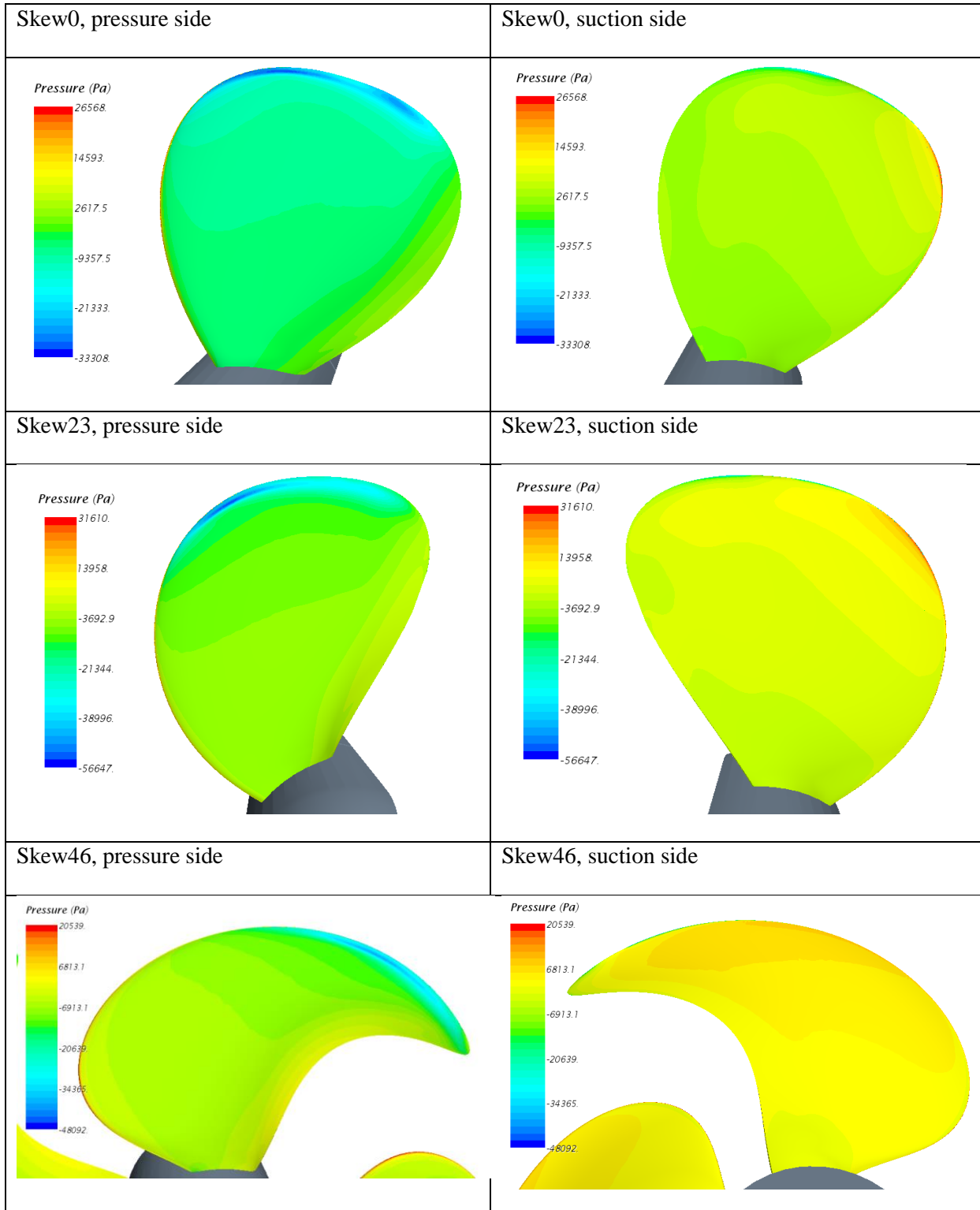
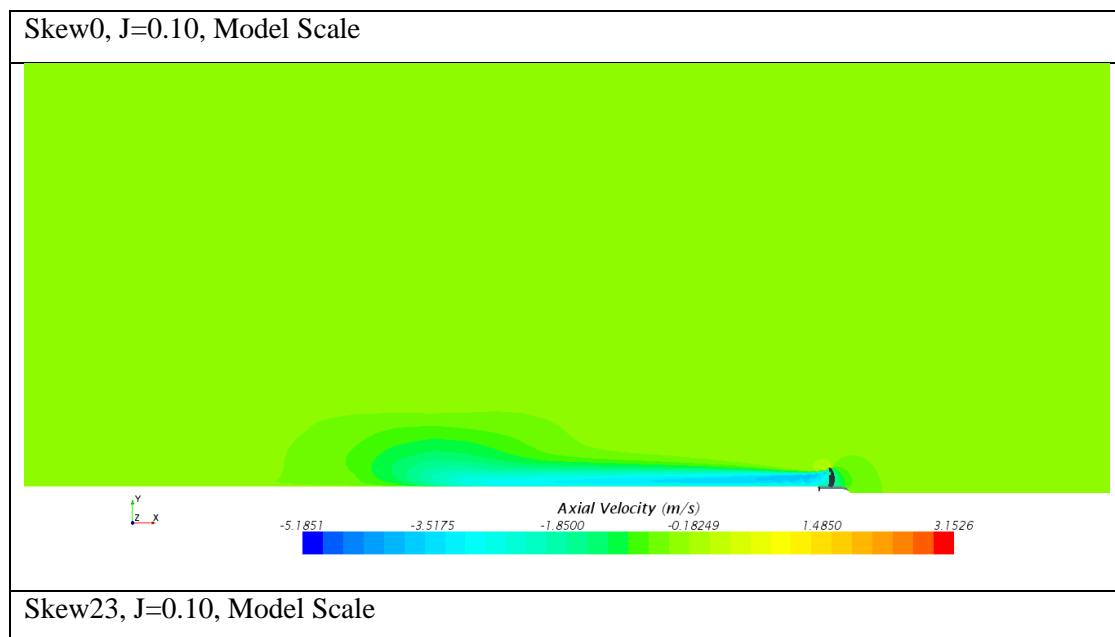


Figure 4.2.5 Pressure distribution on both pressure side and suction side (model scale, $J=0.10$)

The pressure distribution on pressure side and suction side expresses the pressure gap between those two sides. The pressure on the pressure side is obviously lower than that of the suction side. According to Figure 4.2.5, on the pressure side, in the tip region of the blade, the blue colour indicates the low pressure and a high velocity can be expected in that area. In the leading edge area, on the pressure side, the low values show up and on the suction side, the high pressure values are captured. Therefore, in the leading edge area, the large pressure deduction will produce efficient thrust force for the propellers. The outer portion of the blades show larger pressure deductions between suction sides and pressure sides, which indicates that the main thrust differences between propellers of various skews come from that region.

To introduce the flow patterns in the simulated region, the axial velocities for propellers (skew0, skew23, skew46) are shown in Figure 4.2.6. In Figure 4.2.6, the flow patterns are exhibited on a plane through the blade and shaft centerline of the propellers. The propellers with different skews angles show the similar flow pattern in a whole view. The axial velocities show relatively large changes after the flow accelerated by the blades. The detailed velocity patterns around the blade are shown in Figure 4.2.7.



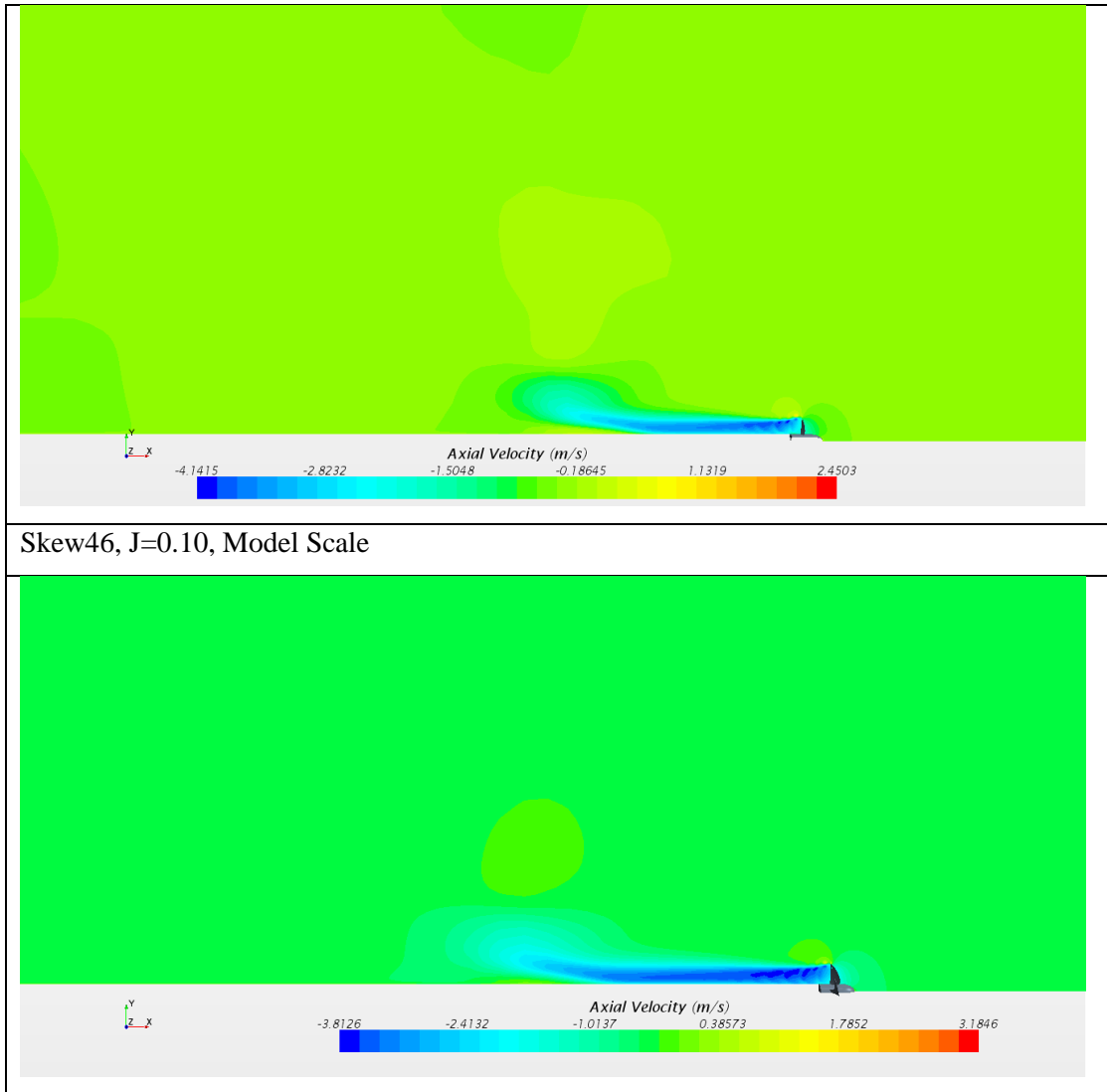
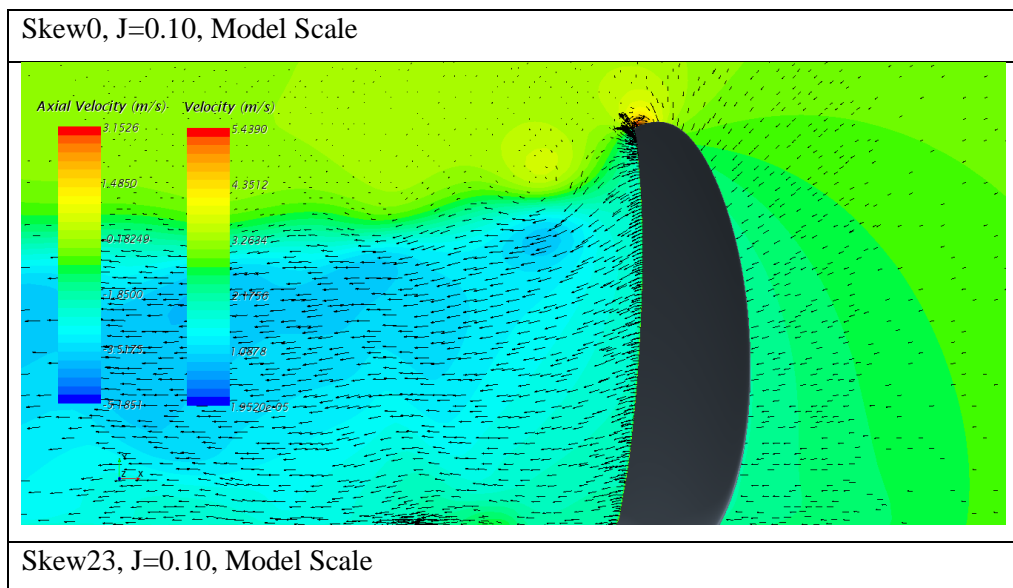


Figure 4.2.6 Axial velocity of model scale propellers (Propeller skew0, skew23, skew46) under J=0.10



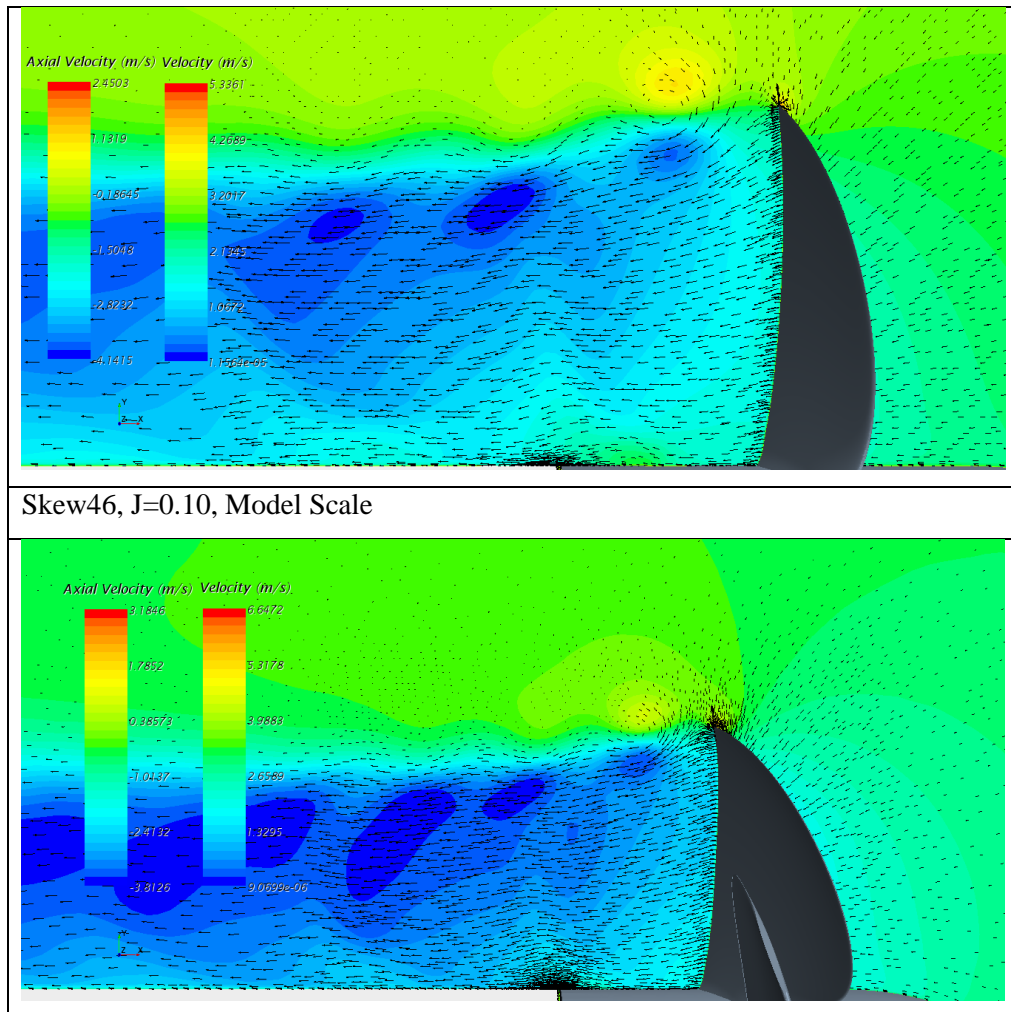


Figure 4.2.7 Velocity vectors around blades, Model scale (Propeller skew0, skew23, skew46) under $J=0.10$

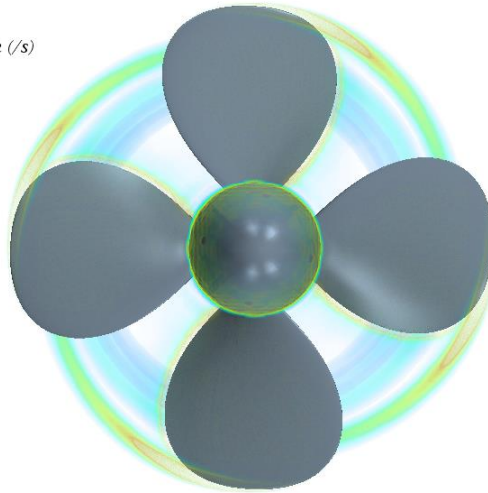
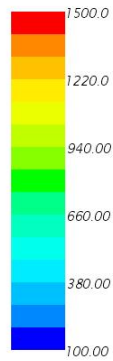
4.2.5 Vortex

The vortex in the region around the blades also shows some differences for propellers with various of skew angles and different scales.

The vortex analysis for propellers with the same scale is performed on model scale propellers with different skew angles (skew0, skew23, skew46) as shown in Figure 4.2.8. The tip vortex play an important part in the differences. For the symmetric blade propeller (skew0), in the present range of 100-1500 /s, it shows the weakest tip vortex while the propeller with a skew angle of 46 deg (skew46) states the strongest tip vortex. In the leading edge area, the propeller skew46 also shows the strongest vortex. The intensity of vortex increases as the skew angle increasing – from skew angle 0 deg to 46 deg, which is indicated by the widespread blue colour in the simulated vortex region of propeller skew46 followed by skew23.

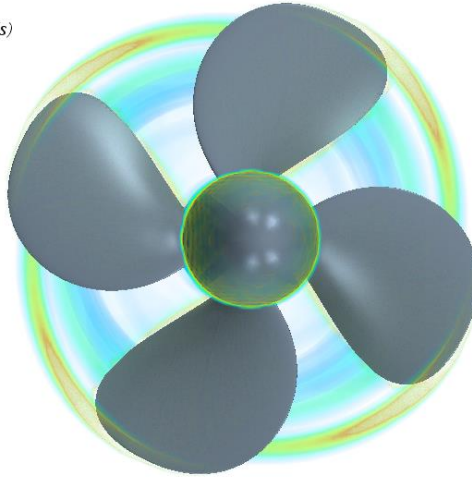
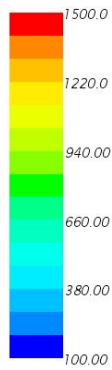
Skew0, model scale, $J=0.10$

Vorticity: Magnitude (/s)



Skew23, model scale, $J=0.10$

Vorticity: Magnitude (/s)



Skew46, model scale, $J=0.10$

Vorticity: Magnitude (/s)

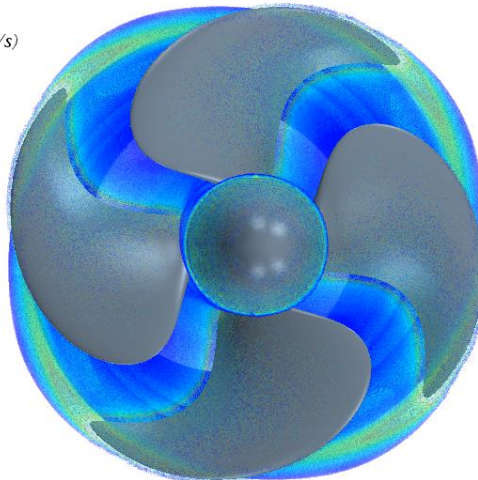
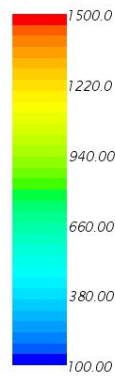
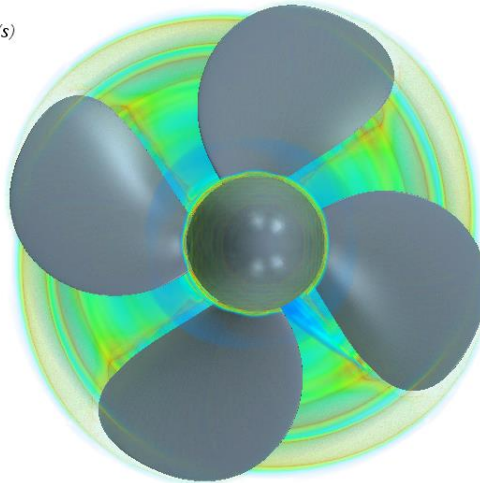
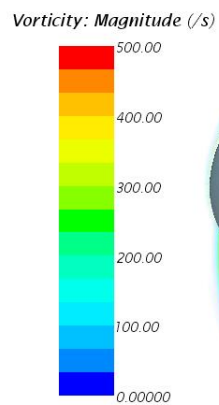


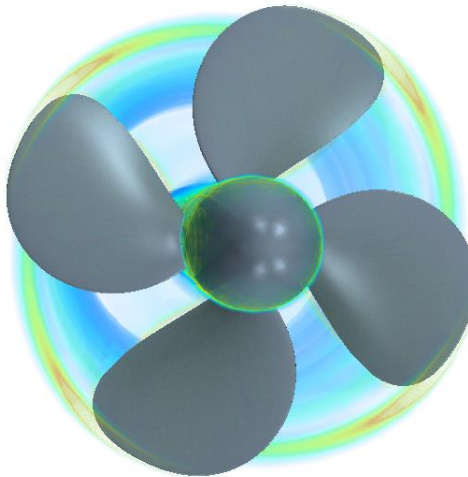
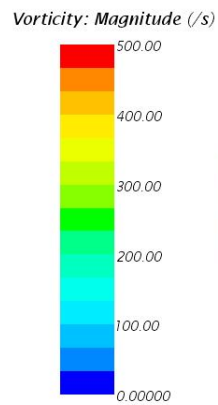
Figure 4.2.8 Vortex around the propellers with different skew angles (skew0, skew23, skew46) in model scale (coloured by the magnitude of vorticity)

For the vortex conditions produced by propellers at the same skew angle but different scales, the analysis was performed on the propeller with a skew angle of 23 deg (shown in Figure 4.2.9). It is obvious that in the range of 0 – 500 /s for vorticity magnitude, the model scale propeller performs the strongest vortex while the largest scale propeller (FS20, D = 5.0m) presents the weakest vortex.

Skew23, J=0.10, Model scale



Skew23, J=0.10, Full scale (M=10, FS10)



Skew23, J=0.10, Full scale (M=20, FS20)

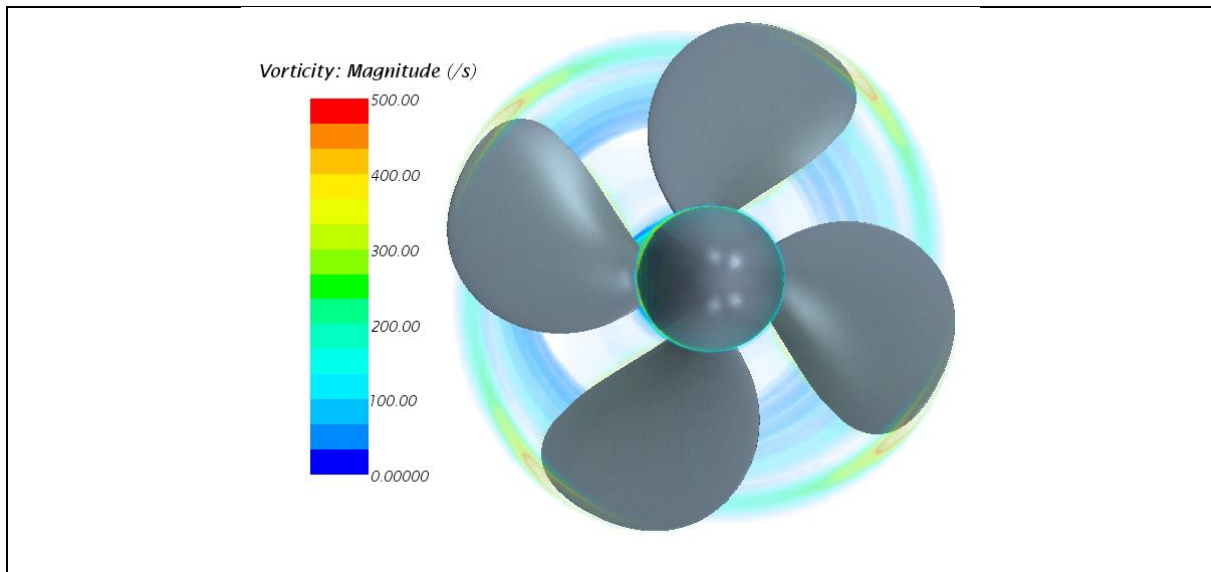
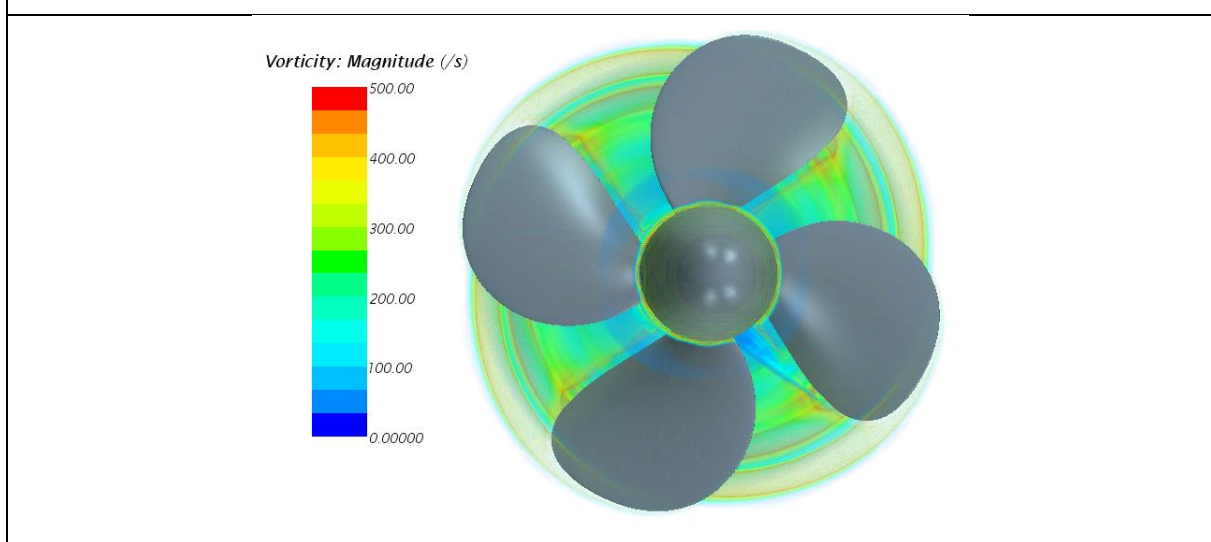


Figure 4.2.9 Vortex around the propellers with different scales (MS, FS10, FS20) and skew angle 23 deg (coloured by the magnitude of vorticity)

The propeller vortex condition at the specific propeller (with the same skew angle and size, here the propeller skew angle 23 deg in model scale is taken as an example) under various of advance velocities is also studied in the project. The represented advance ratios in the analysis are 0.1, 0.5 and 0.8 and the results are shown in Figure 4.2.10. As the velocity increases, the vortex produced by the propellers become stronger, for example, the intensity of vortex under the advance number 0.10 is heavier than that of the propeller under the advance ratio 0.50.

Skew23, model scale, $J=0.10$



Skew23, model scale, $J=0.50$

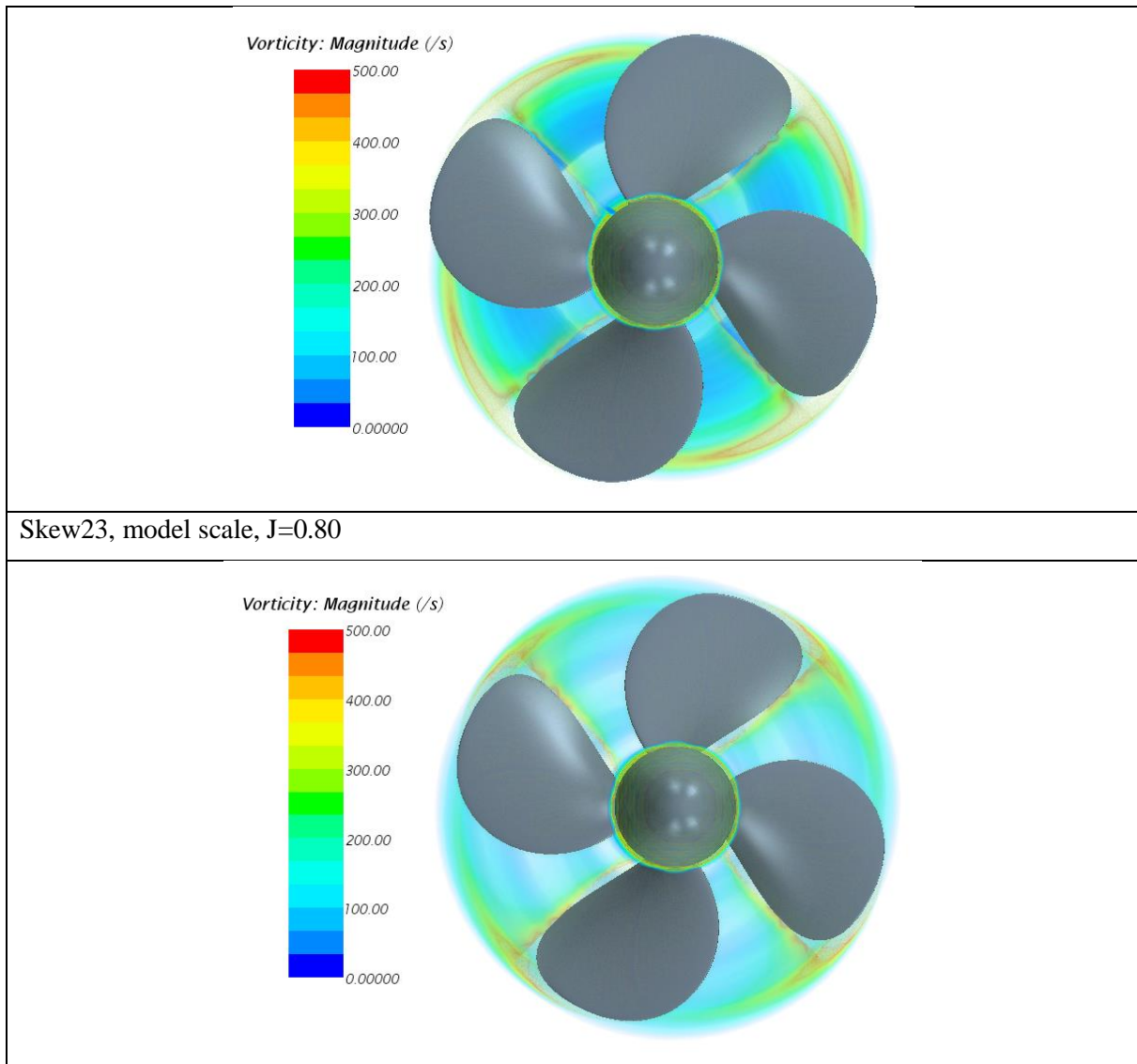


Figure 4.2.10 Vortex around the propeller with skew angle 23 deg in model scale under different advance velocities (coloured by the magnitude of vorticity)

4.2.6 ITTC correction for propeller scale effects

According to ITTC 78's recommendation, the scale effect expectation (this method has been introduced in Chapter 3) can be obtained which was used as a reference for the analysis. All the corrections of scale effects on open water characteristics will be received based on the model scale characteristics. In this project, only the correction for the propeller with a skew angle of 23 deg, at $J = 0.10$, $J = 0.30$, $J = 0.50$ and $J = 0.70$ are calculated.

The basic parameters used in Equ. 3.4, Equ. 3.5, Equ. 3.6 and Equ. 3.7 are shown in Table 4.10. Substituting all these parameters into the four equations, the scale effects correction for open water propellers are obtained (shown in Table 4.11). The results from ITTC method will be compared with the CFD results obtained in this project in next chapter.

Table 4.10 Parameters input in the equations for scale effects correction (ITTC 78's)

K_p [m]		3.00E-05
Density, ρ , [kg/m ³]		999.1
Dynamic viscosity, μ [Pa · s]		0.00114
chord length $c_{(r/R)}$, [m] (at $r/R = 0.75$)		0.0977
Maximum thickness t , [m] (at $r/R = 0.75$)		0.0035
Pitch ratio P/D (at $r/R = 0.70$)		0.70
Propeller diameter D , [m]		0.25
Propeller RPS, n [Hz]		15
Velocity, V , [m/s]	$J = 0.10$	0.375
	$J = 0.30$	1.125
	$J = 0.50$	1.875
	$J = 0.60$	2.250
	$J = 0.70$	2.625
	$J = 0.80$	3.000

Table 4.11 scale effects correction for propeller recommended by ITTC

J	R_{nco}	C_{DM}	C_{DS}	ΔC_D
0.1	757479.2717	0.007691415	0.0135	-0.00586
0.3	762907.6925	0.007686858	0.0135	-0.00586
0.5	773650.2749	0.007677889	0.0135	-0.00587
0.6	780950.0852	0.00767183	0.0135	-0.00588
0.7	789490.1194	0.007664778	0.0135	-0.00588
0.8	799230.6216	0.007656784	0.0135	-0.00589
J	ΔK_T	ΔK_Q	ΔK_T Reference difference (%)	ΔK_Q Reference difference (%)
0.1	0.001923	0.002289	0.575	6.048
0.3	0.001925	0.002291	0.790	7.538
0.5	0.001928	0.002295	1.183	9.667
0.6	0.001930	0.002297	1.645	11.499
0.7	0.001932	0.002300	2.974	14.755
0.8	0.001935	0.002303	42.284	22.115

5 DISCUSSION

5.1 Work quality

5.1.1 CFD results compared with experimental data

As the study limitation, no experimental data was received for the propellers with the skew angle of 0 deg and 46 deg. However, some experimental data was provided by MARINTEK for the propeller P1374 (skew angle 23 deg). Therefore, more discussions were performed on this propeller.

In the validation process, the CFD results (open water characteristics, thrust coefficient K_T , torque coefficient K_Q and efficiency η_0) have been used to compare with the CFD results for P1374 with the pitch ratio of 1.10 ($P/D = 1.10$) at the rotational speed RPS, $n = 9$ Hz. For further study, the CFD results at $n = 15$ Hz were also be compared with the experimental data at $n = 9$ Hz, but not much differences were found even the propellers performed at different rotational speed.

In this section, the CFD data for propeller P1374 in pitch ratio $P/D = 0.70$ will be compared with the experimental results for P1374 at two different pitch ratios – $P/D = 0.90$ and $P/D = 1.10$. The comparison results can reveal the change tendency of open water characteristics on various pitch ratios, which can be used as a reference for controllable pitch propeller (CPP) design.

The thrust coefficient K_T for both experimental results and CFD results is shown in Figure 5.1.1. In this figure, it is evident that, with the increase of pitch ratio, the total force produced by the propeller will increase, for example, when $J = 0.50$, the thrust coefficient K_T at $P/D = 1.10$ is approximately 0.38 and the value at $P/D = 0.90$ is about 0.27 while the thrust coefficient at $P/D = 0.70$ is around 0.17. Another phenomenon the range of advance velocity that the propeller can provide efficient thrust will increase while the pitch ratio increases. The range for the pitch ratio $P/D = 1.10$ is $J = 0 - 1.20$ and the ranges for $P/D = 0.90$ and $P/D = 0.70$ are about $J = 0 - 1.0$ and $J = 0 - 0.80$ respectively.

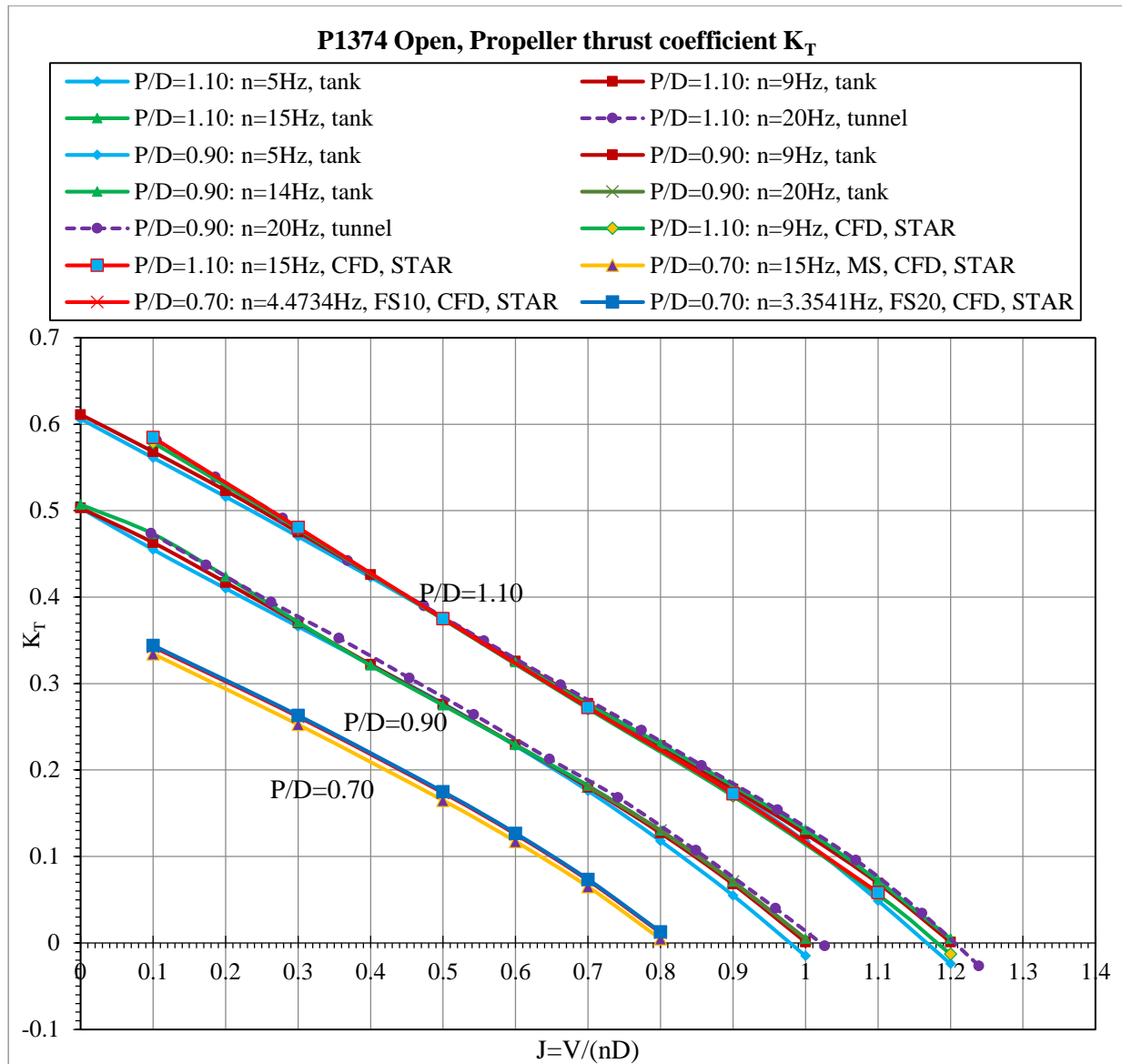


Figure 5.1.1 Thrust coefficient K_T for P1374 with different pitch ratios (0.70, 0.90, 1.10) (experimental data and CFD data)

The torque coefficient K_Q for both experimental data and CFD results are shown in Figure 5.1.2. The figure shows the similar tendency of K_Q to that of thrust coefficient K_T . Torque coefficient K_Q shows the largest values at $P/D = 1.10$ for all the advance ratios while the values at $P/D = 0.70$ represents the smallest ones.

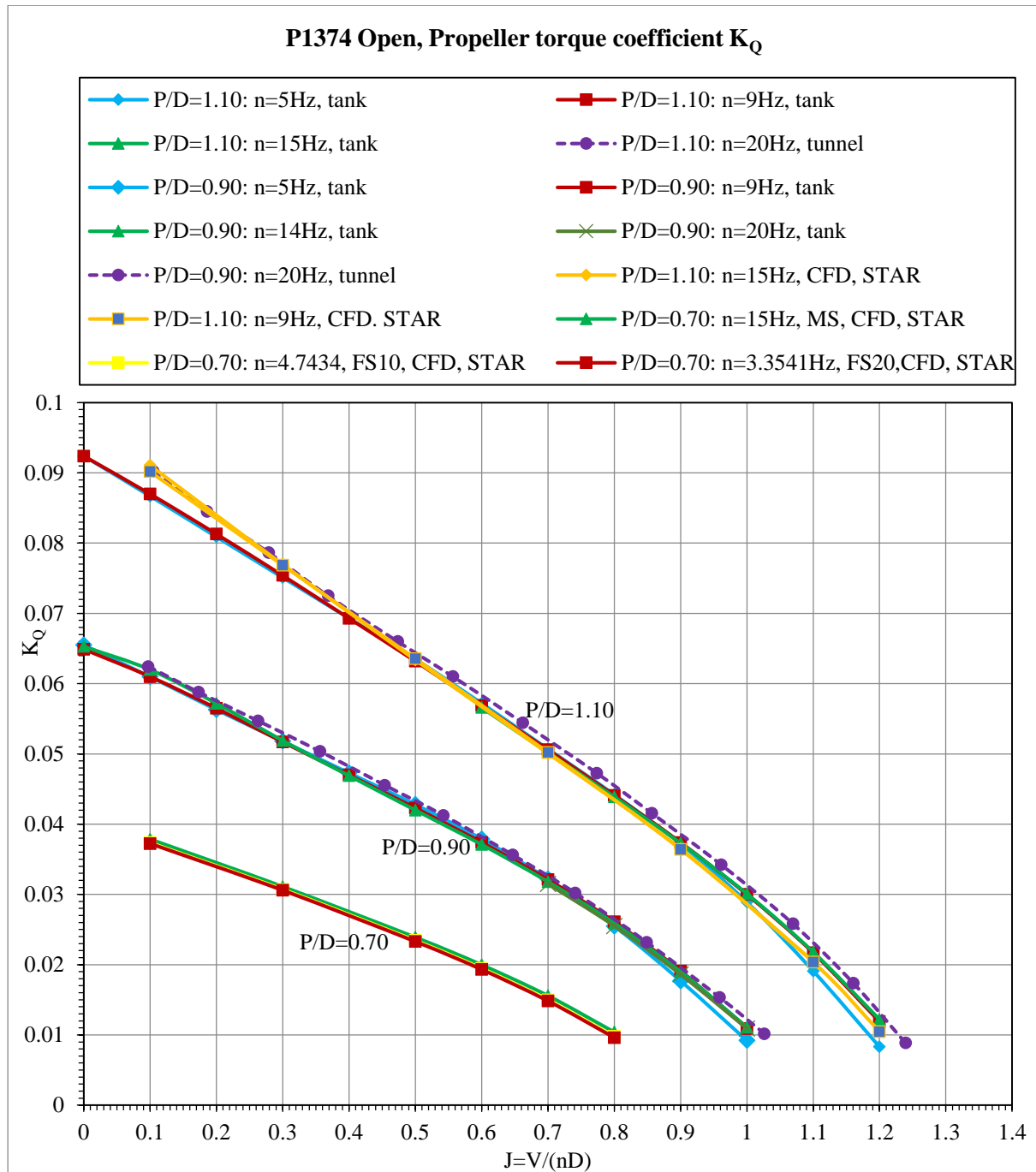


Figure 5.1.2 Torque coefficient K_Q for P1374 with different pitch ratios (0.70, 0.90, 1.10) (experimental data and CFD data)

The open water efficiency η_0 diagrams for both experimental and CFD results are shown in Figure 5.1.3. For the experimental data, the results obtained by various of tests (different rotational speed n , performed in tank or tunnel) for one particular pitch ratio (e.g. $P / D = 1.10$) show little difference at the relatively lower speed region (e.g. in the range of $0 < J < 0.80$ for $P / D = 1.10$, in the range of $0 < J < 0.60$ for $P / D = 0.90$). The odds are increased as the advance velocities rise.

For the CFD results calculated in this project, the model scale propeller reveals larger differences than that between the two full-scale propellers with different scale factors ($M = 10$ and $M = 20$). The efficiency increases when the size of the propeller get bigger.

In the range of $0 < J < 0.64$, the propeller with a pitch ratio of $P / D = 0.70$ shows the highest efficiency η_0 . In the range of $0.64 < J < 0.80$, the propeller with the pitch of $P / D = 0.90$ shows the highest efficiency. When $0.80 < J < 1.20$, the propeller with the pitch ratio $P / D = 1.10$ shows the highest values. Therefore, for the controllable pitch propeller (CPP) P1374, to keep the most efficient thrust, the pitch should be changed for different advance velocities. The theoretical way to change the pitch derived from that is when the propeller loading is increased, the used pitch should be decreased. This has also been confirmed by some practical CPP applications although there are more factors influencing the choose of proper pitch for the propeller when it comes to practical use.

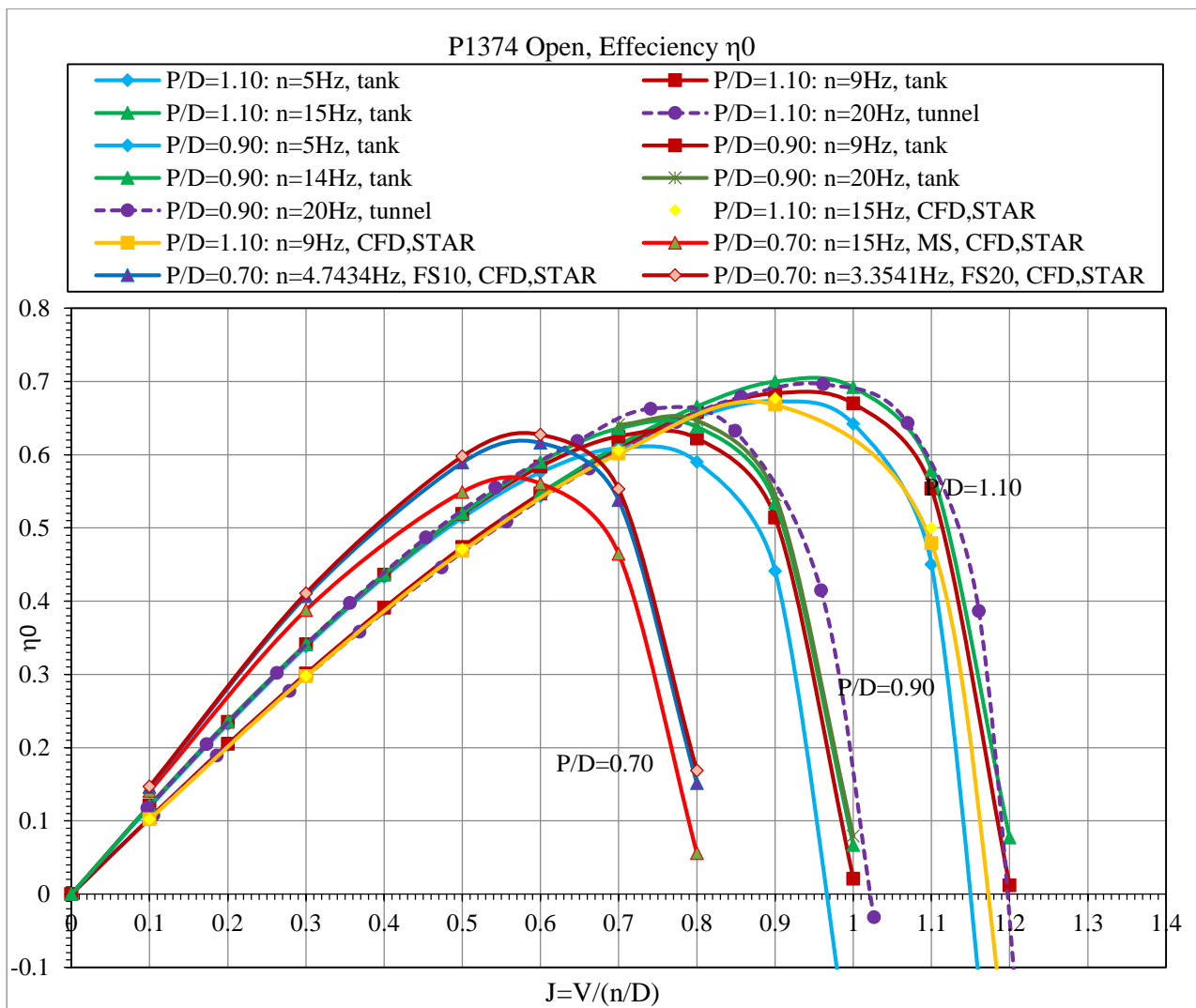


Figure 5.1.3 Open water efficiency η_0 for P1374 with different pitch ratios (0.70, 0.90, 1.10) (experimental data and CFD data)

5.1.2 Scale effects on propellers with different skew angles

The scale effects on propellers with different magnitude of skews (0 deg, 23 deg and 46 deg) were measured by the relative differences of the open water characteristics between model scale and full scale propellers. The relative difference is calculated as:

$$\Delta K = \left| \frac{K_M - K_{FS}}{K_M} \right| * 100\% \quad (\text{Equ. 5.1})$$

Where

K_M – the open water characteristic (e.g. thrust coefficient K_T , torque coefficient K_Q and efficiency η_0) for model scale propeller;

K_{FS} – the open water characteristics for full scale propellers (FS10 and FS20);

All the CFD results for these characteristics have been shown in last chapter.

5.1.2.1 Skew angle 0 deg

For the symmetric blade propeller (skew angle 0 deg), the relative differences of thrust coefficient ΔK_T is shown in Figure 5.1.4. The values for ΔK_T keep increasing with the rise of advance ratios. At $J = 0.80$, it goes up dramatically. But that does not mean the absolute difference rise up in the same way, because a little difference is magnified by the small dividend (according to Equ. 5.1, the small characteristic values of model scale propellers will be used as the dividend). The relative difference of full scale propeller with the scale factor of 20 (FS20) is larger than the corresponding values of propeller FS10 (the scale factor is 10) at the same advance ratio. The similar tendency is found for the relative difference of torque coefficient K_Q and efficiency η_0 as shown in Figure 5.1.5 and Figure 5.1.6.

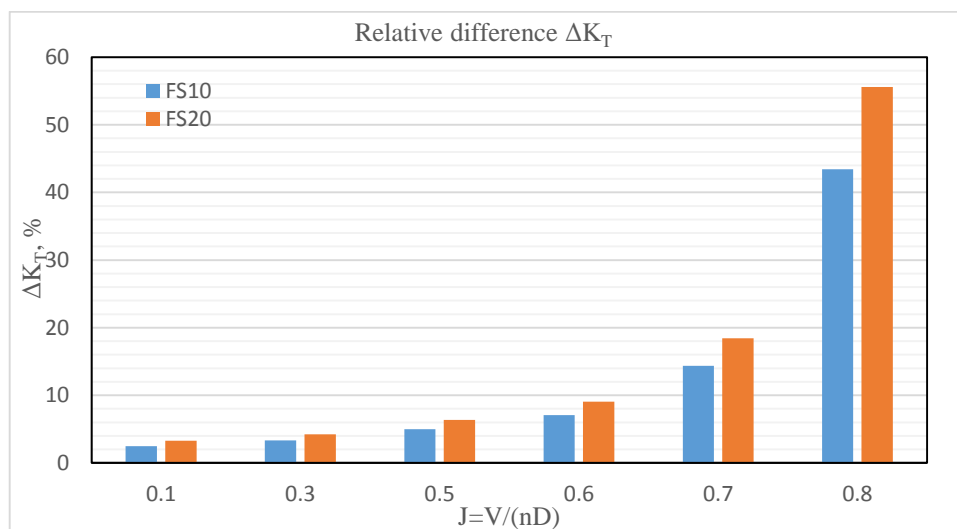


Figure 5.1.4 Relative differences for thrust coefficient K_T , skew angle 0 deg

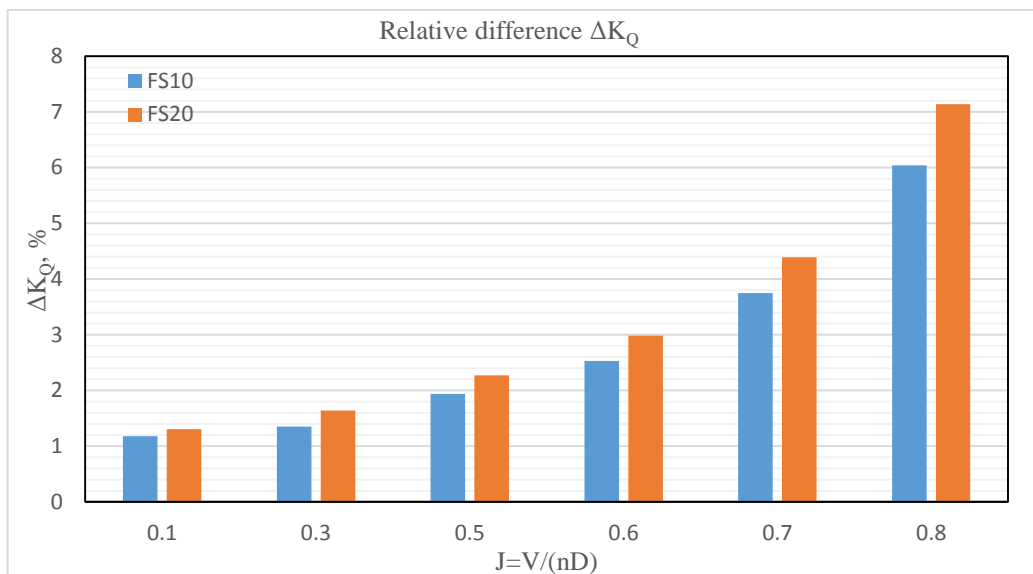


Figure 5.1.5 Relative differences for torque coefficient K_Q , skew angle 0 deg

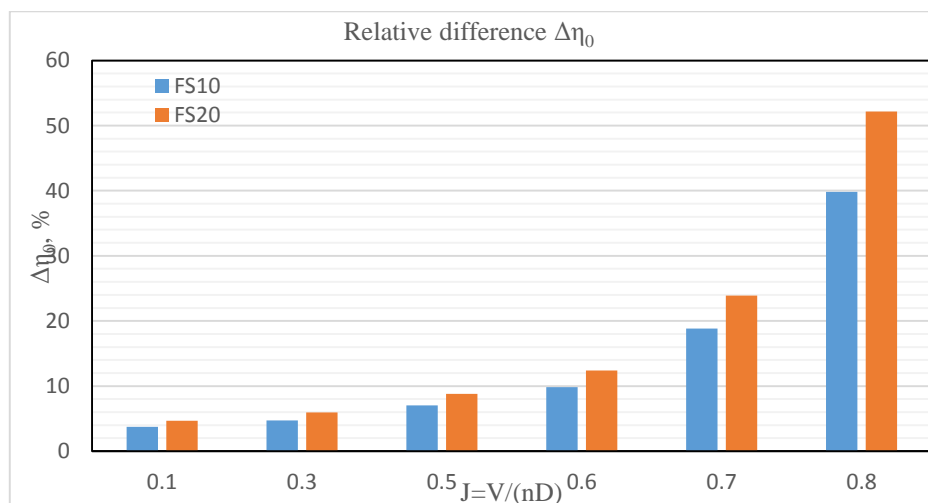


Figure 5.1.6 Relative differences for efficiency η_0 , skew angle 0 deg

5.1.2.2 Skew angle 23 deg

As the propeller P1374 with skew angle of 23 deg is the parent propeller, there are more data obtained for it. In last chapter, the ITTC scale effects correction has been calculated as a reference for this propeller (shown in Table 4.11).

The relative difference of thrust coefficient ΔK_T is shown in Figure 5.1.7. In the advance ratio $J = 0.80$, the values rise up significantly and the reason for this has been explained in last section (skew angle 0 deg). According to the ITTC algorithm, the relative differences for scale effects is much smaller than the resultant values from CFD methods applied in this project.

The relative difference ΔK_T is increasing with the increase of advance ratio for the same propeller. The relative difference for the propeller with a bigger scale (FS20) is larger than that of the propeller FS10 for all the advance ratios.

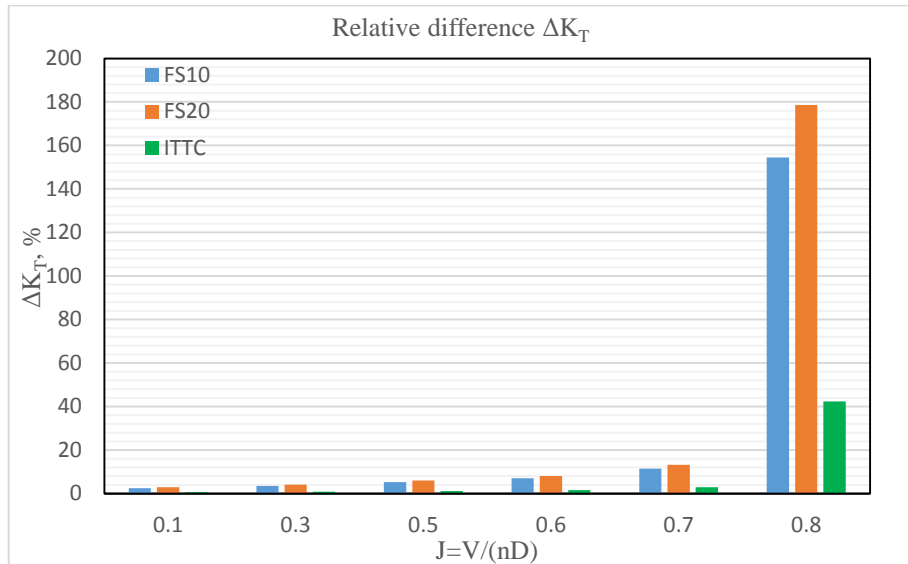


Figure 5.1.7 Relative differences for thrust coefficient K_T , skew angle 23 deg

The relative difference of torque coefficient ΔK_Q is shown in Figure 5.1.8. The ITTC expectation for that is much larger than the CFD results.

As the ITTC method only take the effects of Reynolds number Re on drag neglecting the effects on section lift, this difference can be proper.

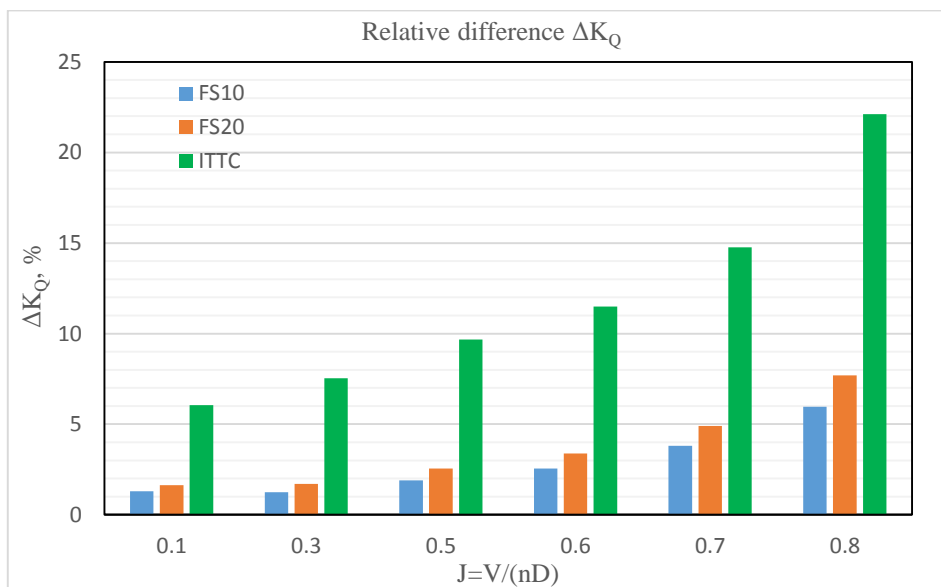


Figure 5.1.8 Relative differences for torque coefficient K_Q , skew angle 23 deg

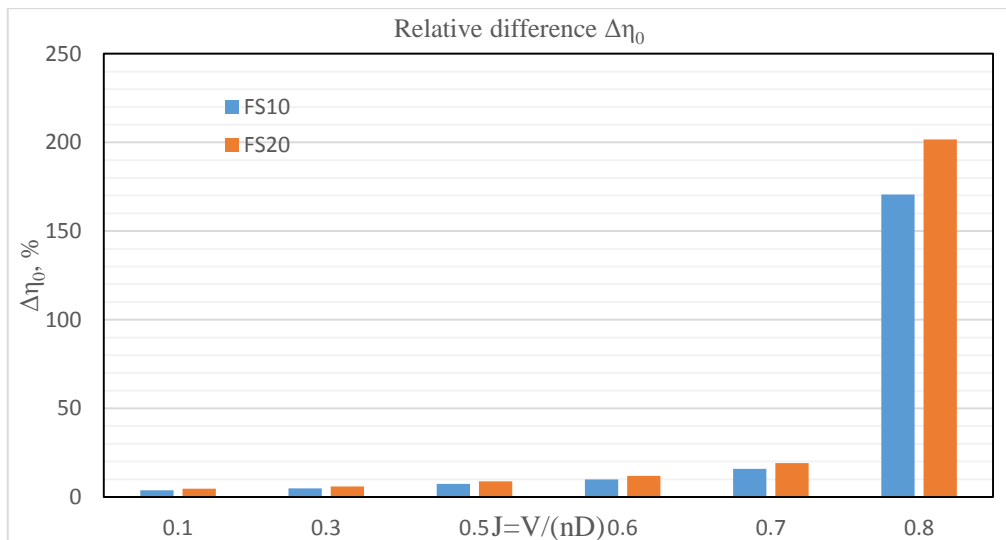


Figure 5.1.9 Relative differences for efficiency η_0 , skew angle 23 deg

5.1.2.3 Skew angle 46 deg

For the propeller with a skew angle of 46 deg, the scale effects on the torque coefficient shows big difference from the other two propellers (skew0, skew23) for the torque coefficient difference ΔK_Q . However, according to Figure 4.2.1, the absolute differences for torque coefficient is negligible and the little unique difference even can not change the efficiency tendency as shown in Figure 4.2.1 and Figure 5.1.12. Therefore, the different tendency for relative difference of torque coefficient K_Q can be considered as some errors within tolerated scope.

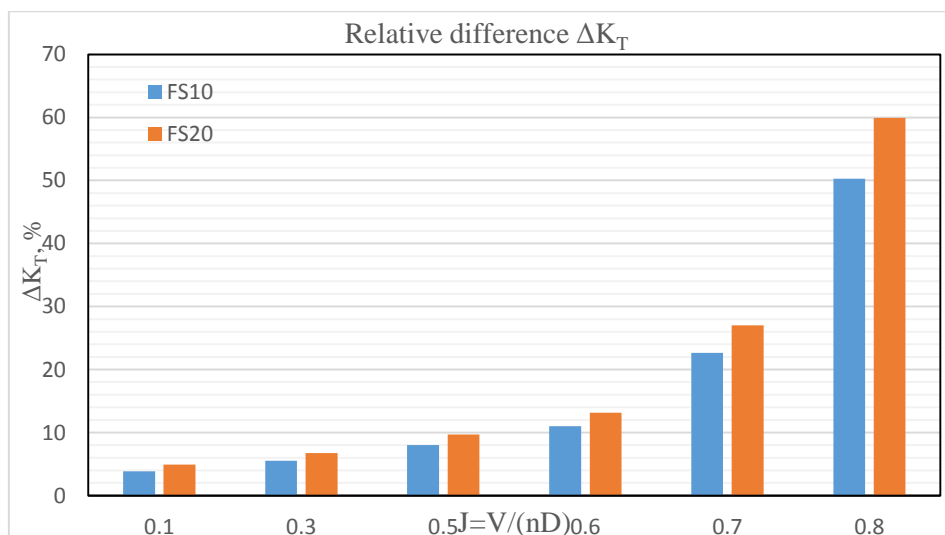


Figure 5.1.10 Relative differences for thrust coefficient K_T , skew angle 46 deg

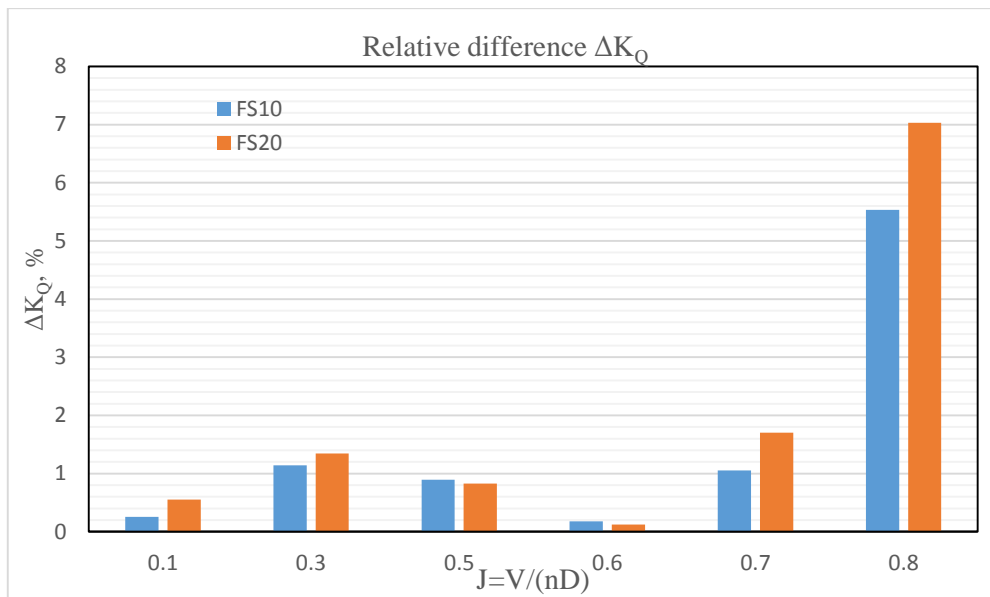


Figure 5.1.11 Relative differences for torque coefficient K_Q , skew angle 46 deg

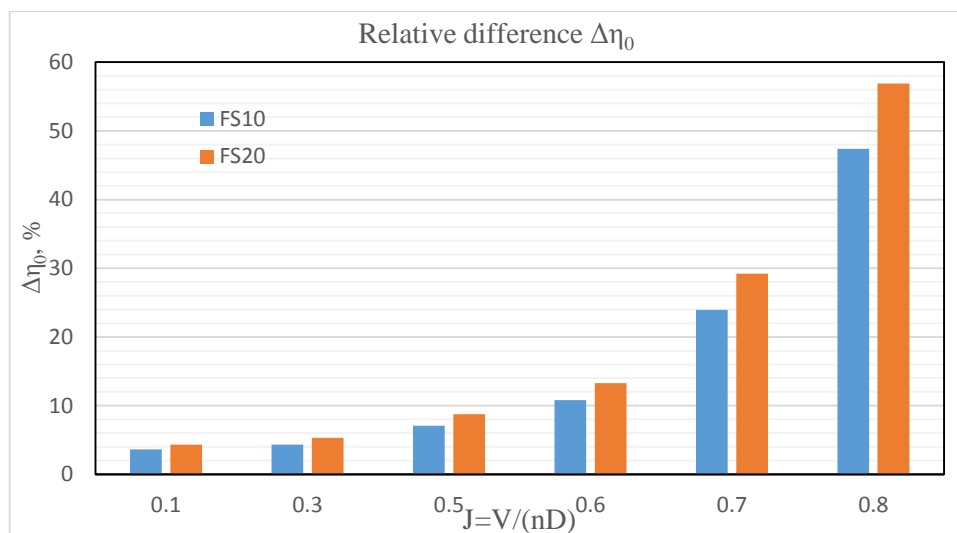


Figure 5.1.12 Relative differences for efficiency η_0 , skew angle 46 deg

5.2 Project process

The main simulation of the propellers were proceeded in STAR-CCM+ and some results can directly exported as a file format that can be edited in other tool software. The MicroOffice tools, especially Excel played an important role in data processing.

To ensure all the settings for the open water simulation is proper, the validation process is firstly performed at the propeller P1374 (skew angle 23 deg) with the pitch ratio of $P/D = 1.10$. The

experimental data and simulation model for STAR-CCM+ of P1374 were provided by MARINTEK. That is why it was chosen as the validation example. In the validation process, at $n = 9$ Hz (because the experimental data at this rotational speed and $P / D = 1.10$ was available, it was selected in the validation process), the mesh base size in the CFD simulation was set to 0.20 m. The high consistency of the CFD results with experimental data revealed that the settings in the simulation could lead to appropriate results. However, the huge cell quantity in the simulated region makes the simulation excessively time-consuming. To balance the required time and the accuracy of result, the compromised mesh settings (the mesh base size was set to 0.25 m) were used. The CFD results were then compared to the experimental again and indicated that the mesh setting can satisfy the accuracy requirements. Therefore, in the CFD simulation process, the result accuracy is not the only limitation for the project. A proper mesh setting can result in accurate enough results and save the computational time.

After the validation process, the basic numerical setups were almost decided for all the propellers with different scales and skew angles. Some changes were required when change the advance velocity, propeller scale and skew angles. All these methods have been introduced in Chapter 3. In the process of changing these parameters, details are always important especially when replacing the blade model. It is important to check if every part of the replaced blade was assigned into the corresponding simulated region.

The proper time arrangement and plan of data processing are important requirements for the completion of the project. All the CFD results for propellers with different scales and magnitude of skews were summarized to find the interesting points that can explain the scale effects. The meticulous attitude is the first requirement for a successful technical research.

6 CONCLUSIONS

For propellers with the same skew angle, the thrust coefficient K_T and efficiency η_0 will increase with the increasing propeller scale, for example, at the same advance ratio J , the thrust coefficient K_T of propeller P1374 in full scale with the scale factor of 20 (FS20) has the highest value followed by that of the full scale propeller with the scale factor of 10 (FS10), and the model scale propeller P1374 shows the lowest K_T .

For the propellers with the same scale, the open water characteristics (thrust coefficient K_T , torque coefficient K_Q and efficiency η_0) are different from one skew to another. Propeller P1374 (skew angle 23 deg) is always larger than that of the symmetric blade propeller (skew angle 0 deg). However, the characteristics of propeller with the skew angle of 46 deg changes fast along the different advance ratio. In the low advance ratio range ($0 < J < 0.3$), the propeller with skew angle 46 deg has the largest open water characteristics compared the other two propellers with different skews, but in high advance ratio scope ($J > 0.6$), it possesses the lowest values. Thus the changes of open water performance for propeller skew angle 46 deg is fast.

The analysis on pressure distribution for different blade sections and vortex reveals that the main differences of open water performance result from the outer portion of the blades. The flow pattern of the region near the blade tip is also more complex than that of other regions.

The scale effects analysis indicates that the larger the size of full scale propeller is, the larger differences of open water performance from model scale propellers will be resulted in. Compared with the ITTC expectation, the CFD results still reveals big differences especially for high advance ratios. As the ITTC method only take the effects of Reynolds number Re on drag neglecting the effects on section lift, this difference can be proper.

7 FURTHER WORK

For further study, the scale effects on open water propellers with different magnitude of skews in the higher pitch ratio, for example, $P_{(0.7)}/D = 1.3$ and $P_{(0.7)}/D = 1.5$. This further research can be useful for controllable pitch propeller (CPP) design.

More research work can focus on the open water performance of propellers under different rotational speed, for example, for model scale propellers, the rotational speed RPS can be changed to $n = 5$ Hz, 10 Hz and 20 Hz.

In the CFD calculation, two different kinds on domain were used. For the propellers with the skew angle of 0 deg and 23 deg, the domain can cover one whole blade of the propeller while for the propeller of skew angle 46 deg, the blade was split as the it is too wide to be included in the domain. This difference can affect the results. To reduce the possible error resulted from CFD setups, the propellers with skew angle of 0 deg and 23 deg can be calculated at the same domain setups as the propeller with skew angle of 46 deg. The resultant open water performance from CFD methods may be slightly changed. Then the discussion for which kind of domain is better for the propeller can be performed by the comparison of results with experimental data.

REFERENCES

- [1] John Carlton, Marine Propellers and Propulsion, 2007, Page 200-201
- [2] Vladimir Krasilnikov, Jiaying Sun & Karl Henning Halse, CFD Investigation in Scale Effect on Propellers with Different Magnitude of Skew in Turbulent Flow, 2009, Page 1-11
- [3] John Carlton, Marine Propellers and Propulsion, 2007, Page 33-39
- [4] John Carlton, Marine Propellers and Propulsion, 2007, Page 95-98
- [5] Vladimir I. Krasilnikov, First Introduction into Computational Fluid Dynamics for Marine Applications, 2011, Page 3
- [6] Vladimir I. Krasilnikov, First Introduction into Computational Fluid Dynamics for Marine Applications, 2011, Page 72-152
- [7] John Carlton, Marine Propellers and Propulsion, 2007, Page 89-94
- [8] Performance, Propulsion 1978 ITTC Performance Prediction Method, 7.5-02-03-01.4, Page 3-5

Appendix A Experimental data of P1374 at P/D=0.90

Open water tests in the towing tank, April 2014

n=5 Hz				n=9 Hz			
J	K_T	K_Q	η₀	J	K_T	K_Q	η₀
0.0	0.503	0.0655	0	0.0	0.503	0.0649	0
0.1	0.455	0.061	0.119	0.1	0.463	0.061	0.121
0.2	0.41	0.0563	0.232	0.2	0.417	0.0565	0.235
0.3	0.366	0.0518	0.338	0.3	0.37	0.0517	0.341
0.4	0.322	0.0473	0.433	0.4	0.322	0.047	0.436
0.5	0.277	0.0428	0.514	0.5	0.276	0.0423	0.519
0.6	0.228	0.0379	0.576	0.6	0.229	0.0374	0.584
0.7	0.176	0.0322	0.609	0.7	0.18	0.0321	0.625
0.8	0.118	0.0255	0.59	0.8	0.127	0.0261	0.622
0.9	0.055	0.0177	0.441	0.9	0.068	0.0191	0.514
1.0	-0.015	0.0092	-0.259	1.0	0.001	0.0109	0.021

n=14 Hz				n=20 Hz			
J	K_T	K_Q	η₀	J	K_T	K_Q	η₀
0.0	0.507	0.0653	0	-	-	-	-
0.1	0.473	0.062	0.121	-	-	-	-
0.2	0.424	0.0572	0.236	-	-	-	-
0.3	0.371	0.0519	0.341	-	-	-	-
0.4	0.321	0.0469	0.437	-	-	-	-
0.5	0.275	0.042	0.52	-	-	-	-
0.6	0.229	0.0371	0.59	-	-	-	-
0.7	0.182	0.0318	0.636	0.7	0.181	0.0315	0.641
0.8	0.13	0.0259	0.638	0.8	0.13	0.0255	0.647
0.9	0.071	0.019	0.534	0.9	0.071	0.0186	0.545
1.0	0.005	0.0111	0.067	1.0	0.005	0.0109	0.079

Open water tests in the cavitation tunnel, March 2006

n=20 Hz			
J	K_T	K_Q	η₀
0.09730	0.47380	0.06244	0.1175
0.17300	0.43700	0.05879	0.2047
0.26290	0.39410	0.05469	0.3015
0.35620	0.35250	0.05036	0.3968
0.45360	0.30630	0.04555	0.4855
0.54230	0.26420	0.04125	0.5528
0.64700	0.21270	0.03561	0.6151
0.74110	0.16830	0.03020	0.6573
0.84880	0.10710	0.02320	0.6236
0.95880	0.04010	0.01533	0.3992
1.02640	-0.00340	0.01016	-0.0547

Appendix B Publication version of the thesis

Investigation in Scale Effects on Propellers with Different Magnitude of Skew by CFD Methods

Yaning Zhao, Supervision at Aalesund UC.: Karl Henning Halse

ABSTRACT

Scale effects on the open-water performance of marine propellers are the problems to be investigated to the researchers and ship designers. Present thesis analyse the scale effects of marine propellers by CFD methods. The main focus is on the aspects related to propeller blade skews. The ambient flow around the propeller is assumed to be fully turbulent and the Reynolds-averaged Navier-Stokes (RANS) equations are applied in the turbulent flow. Propellers with different scales and skew angles operating in open-water conditions will be simulated in the CFD software – STAR-CCM+. The differences in open-water characteristics (e.g. thrust coefficient K_T , torque coefficient K_Q and efficiency η_0) of propellers with different skew angles are demonstrated and explained through the analysis of simulated flow patterns around the blades, as well as through the reasonable estimations of percentage of pressure and friction force contributions. The CFD results are compared with some experimental data for verifications.

Keyword

Scale effect, Propeller skew, CFD, RANS

1. INTRODUCTION

In nowadays, to achieve the best propulsion performance for commercial ship owners, an excellent propeller design is one of the most economical saving ways. A large numbers of factors may affect the characteristics and performance of propellers e.g. the levels of periodic forces, blade structural strengths, cavitation, as well as the noises and vibrations induced by the propellers. Among those factors, the different magnitudes and distributions of blade skews and the overall influence on the propeller performance by these parameters will be investigated in details in the thesis. Skewed propellers have been used for many years. However, the scale effects of different magnitudes of blade skews need further investigations.

In marine propeller related hydrodynamics, the two fundamental non-dimensional governing-flow parameters are the Froude number and the Reynolds number. In both the model scale and full scale cases for propellers rotating in an open-water, we want to keep the Froude number and Reynolds number the same, at the same time, due to the dynamic similarity of water. Froude number is a non-dimensional parameter that represents the ratio

of inertia force of water to the gravity force. The Reynolds number represents the viscous of water and flow separations.

There are some different procedures used by practitioners to predict the scale effects from model test. The main one is the ITTC procedure which take only take Reynolds number into consideration, as Reynolds number is always applied to measure the boundary layer phenomena. Some other methods also take propeller loading into account. Significantly different results can arise from the various procedures. To get more accurate results about scale effect of model propeller performance characteristics, much more analysis about the flow structure within the boundary layer and the lift and drag properties in the flow field is needed. ^[4]

Computational fluid dynamics (CFD) are becoming an increasingly important way for propeller tests in the propeller pre-design phase. Among different propeller-flow simulation techniques, the RANS method are found to be the most favorable because the computational times are rather lower than the other methods.

Hopefully, the results in this paper can be a valid reference for propeller designers or engineers, as there will be a validation process of the results compared with the information from Norwegian Marine Technology Research Institute (MARINTEK).

One concern is that this project is a complete CFD application in studies of open water propellers and the results are either compared with some experimental data or some CFD results. In expectations, there are differences for the results may come from the different settings of CFD software or even the exact test condition. But with a larger database, we can always try to find a way to get propeller characteristics as accurate as possible. In this paper, propellers with different skew (0 deg, 23 deg, 46 deg) are investigated in both model scale and full scale (with the scale number 10 and 20). Their thrust characteristics such as thrust coefficient K_T , Torque coefficient K_Q , open water efficiency η_0 , pressure and velocity of the flow in the wake filed will be obtained and compared to get the scale effect of different magnitude of blade skew. The flow are assumed to be 100% turbulent in the whole analysis process.

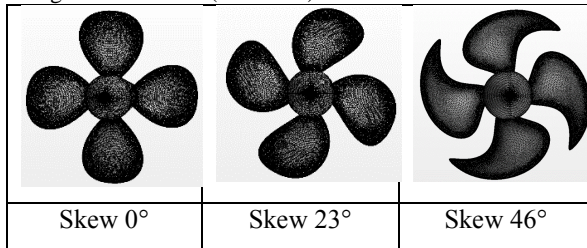
The original parent propeller P1374 is a controllable pitch propeller (CPP). It has four blades, and the blade area ratio is 0.60. Skew angle

23 deg (balanced skew distribution) and design pitch i.e. $P(0.7)/D=1.10$. It's hub ratio at the propeller plane is 0.24 and direction of propeller rotation is right-handed. The model tests performed with this propeller in the PROPSALE project are those of CPP propeller. In the systematic CFD analyses, propellers are considered as fixed-pitch propellers (FPP). The parameters of the propeller series are shown in Table 1.1.

Table 0.1 Skew series parameters

Skew Series	
A_E/A_0	0.60
P/D	0.70 (FPP - Fixed Pitch Propeller)
Skew	0 deg; 23 deg; 46 deg
Z	4

Table 0.2 Model scale propellers with different magnitude of skew (rear view)



Preliminary calculations done with the parent propeller P1374 have shown quite heavy loading of the outer blade sections, resulting in strong tip vortex. This result is thought to be related to the radial distributions of chord length and pitch at the outer blade sections, which may not be typical for conventional open propeller designs (it should be remembered that propeller P1374 was conceived as a compromise design to be used in the tests with both open and ducted propulsors). Obviously, the aforementioned phenomena may have considerable influence on scale effects. Therefore, it is planned to include in the investigations some alternative distributions of chord length and pitch along the radius.

2. METHOD

The equations of the RANS method for incompressible viscous flow are derived by averaging of the Navier-Stokes equations. The governing equations of the method to be solved are written in the following form:

$$\frac{\partial \rho}{\partial t} + \frac{\partial(\rho u_i)}{\partial x_i} = 0, \quad (\text{Equation 1})$$

$$\frac{\partial(\rho u_i)}{\partial t} + \frac{\partial(\rho u_i u_j)}{\partial x_j} = -\frac{\partial p}{\partial x_i} + \frac{\partial}{\partial x_j} \left[\mu \left(\frac{\partial u_i}{\partial x_j} + \frac{\partial u_j}{\partial x_i} - \frac{2}{3} \delta_{ij} \frac{\partial u_l}{\partial x_l} \right) \right] + \frac{\partial}{\partial x_j} (-\rho \overline{u'_i u'_j}),$$

$$(\text{Equation 2})$$

Where x_i is the i -th Cartesian component of the absolute velocity vector, p is the static pressure, μ

is the molecular viscosity, δ_{ij} is the Kronecker delta and $-\rho \overline{u'_i u'_j}$ is the Reynolds stress. The Reynolds stress must be modeled to close the governing equation by using an appropriate turbulence model. In the present work, the SST (Shear Stress Transport) $k-\omega$ turbulence model is chosen for turbulence closure. The $k-\omega$ turbulence models represent a group of two-equation turbulence models in which the transport equation are solved for the turbulent kinetic energy k and its specific dissipation rate ω .

The tests in this project can be classified as two parts. The first part is validation. To ensure the results of STAR-CCM+ for this project is reliable and all the settings are appropriate for the specific simulation condition, the propeller P1374 (skew angle 23 deg) in a model scale with a rotational speed RPS, $n = 9 \text{ Hz}$, pitch ratio $P/D = 1.10$, will be calculated in a series of advance ratio J . The results from the CFD method will be compared with that of the experimental method as a validation. The second part is the main part of this project: simulations of propeller with different skew angles (0 deg, 23 deg and 46 deg), different diameters (model scale propeller with the diameter of 0.25 m, full scale propeller with the scale factor of 10 and 20, and the propeller diameters for full scale propellers are 2.5 m and 5 m respectively) and the pitch ratio of $P/D = 1.10$ under all work conditions (with different advance ratio J).

When modelling propeller in a straight-flow open-water condition, one can take advantage of flow's axial symmetric property, and use only one blade passage domain with setting up appropriate periodic boundaries. The most straightforward setup for one blade passage flow simulation implies the use of a fan-shaped sector, having angular dimension of $360/Z$ deg (Z is the number of propeller blades). The sector is cut from a cylinder and includes only one whole blade, as shown in Figure 3.1.1a). Such a setup also makes the post-processing work simpler. However, if propeller blades are wide, they may not be entirely accommodated in the domain as described above.

The simplest way to solve the problem is to use an alternative one blade passage setup that includes the same cylindrical sector, but instead splits two neighbouring blades. Such a setup will ensure that complete blade geometry will be accommodated in the one blade passage domain, and flow periodicity will be observed.

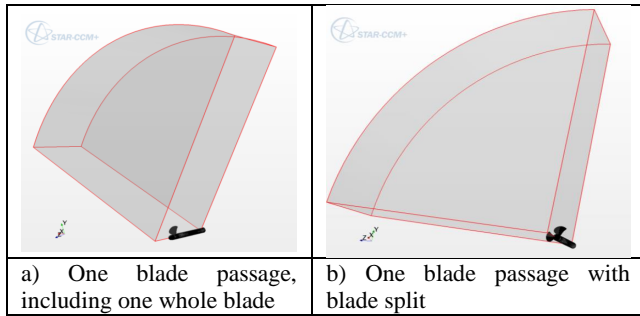


Fig.2.1 Two kinds of the domain setup

Depending on the complexity of the blade surface, minor surface flaws may occur at the intersection of the blade with periodic boundaries. The Surface Remesher tries to repair these flaws, often resulting in unnecessary locally increased mesh density and higher overall cell count, if special treatment is not applied to the blade surface mesh. One remedy is to make use of feature curves. The setup with the first variant of one blade passage domain allows in principal only one (combined) feature curve for all geometry parts. Surface remeshing on the blade is then entirely guided by the values of target size and minimum surface size set up for blade, tip and TE (Trailing Edge) boundaries. Such meshing model may result in the aforementioned issues when using the alternative setup with blade split. To remedy this one can, at the stage of preparation of geometry parts, produce a separate set of feature curves describing blade patch perimeters and following the blade edges. The blade edges and tip region are the areas where finer mesh is needed. Then one can set up both the target size and minimum size for the blade surface to the same desired value and instruct Surface Remesher to do mesh refinement only along the Blade Patch Perimeter feature curves, on the blade tip and blade TE. The rest of the blade surface and regions on the periodic boundaries where they intersect with the blade will be unaffected, resulting in good quality mesh as shown in Fig.2.2.

In this project, four different kinds of mesh models are selected: Surface Remesher, Prism Layer Mesher, Polyhedral Mesher and Extruder. The volume mesh scene is shown in Fig.2.3.

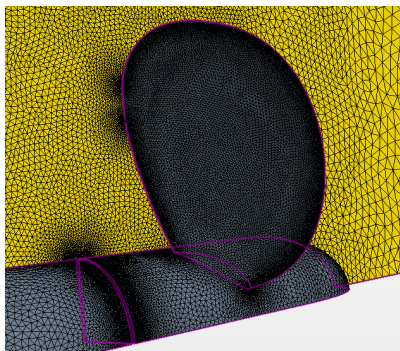


Fig.2.2 Introduction of feature curves in the one blade passage domain

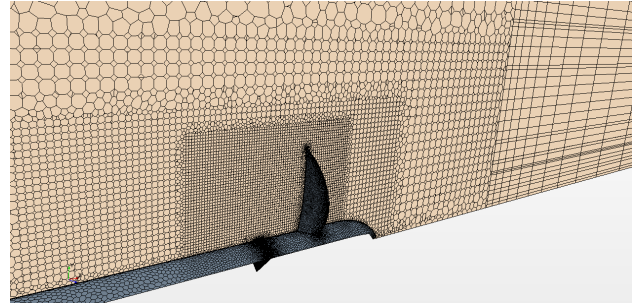


Fig.2.3 Volume mesh around P1374, model scale

The flow near the solid propeller geometry is not turbulent while in the turbulent model, the flow is assumed to be 100% turbulent. To solve the near-wall problem, Y^+ near wall treatment is applied in the simulation. Y^+ represents the local Reynolds number.

$$Y^+ = \frac{VL}{\nu} \quad (\text{Equation 3})$$

Where V is the velocity of the cell centroid (m / s), L is the distance between the cell centroid and the solid boundary (m), ν is the kinematic viscosity of the fluid ($\nu = \mu/\rho$) (m^2 / s).

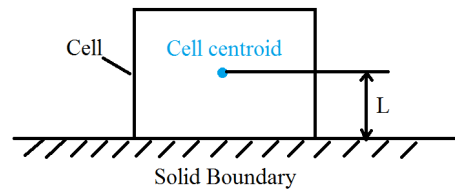


Fig.2.4 Near-wall cell of the prism layer

For the model scale propeller, the rotational speed in RPS is $n = 15$ Hz. The full scale propeller will be obtained by Froude scaling method.

$$\text{Froude number: } Fr = \frac{V}{\sqrt{gL}} \quad (\text{Equation 4})$$

$$Fr = \frac{\pi \cdot n_M \cdot D_M}{\sqrt{g \cdot D_M}} = \frac{\pi \cdot n_S \cdot D_S}{\sqrt{g \cdot D_S}}$$

$$n_S = n_M \cdot \sqrt{\frac{D_M}{D_S}} = \frac{n_M}{\sqrt{M}}$$

Where V states the characteristic flow velocity (m/s); g is acceleration of gravity (m^2/s) and L is the characteristic length of the object (m). The subscript M and S indicate model scale and full scale propeller respectively. M is the scale factor, which represents how many times of the size of full scale propeller is compared to the model scale size.

Table 0.3 Propeller sizes and rotational speed

Propeller scale	Model scale	Full scale (M=10)	Full scale (M=20)
Diameter [m]	0.25	2.5	5.0
Rotational speed RPS, n, [Hz]	15.0	4.7434	3.3541

3. RESULTS

The results obtained from CFD methods can be affected by some simulation errors and

uncertainties, such as the model errors and uncertainties, discretization (numerical) errors, iteration (convergence) errors, round-off errors, application uncertainties, user errors and code errors. Therefore, the simulation results from STAR-CCM+ will be compared with some experimental data provided by MARINTEK. If the results errors are within the acceptable range, some detailed setups will be proceeded with in the following simulations.

The experimental data is based on the model scale propeller P1374 (skew angle 23 deg) with a pitch ratio of $P/D = 1.10$, and rotational speed, RPS, $n = 9\text{Hz}$. The CFD simulations P1374 possess the same parameters as aforementioned. To get the proper mesh setups in STAR-CCM+, the author has investigated two different base size of mesh – 0.20m and 0.25m (mesh results are shown in Table 3.1). The simulation results show little difference on the open water characteristics as shown in Table 3.2.

Table 0.4 Different mesh results for two mesh sizes

P/D = 1.10, skew angle $\theta_{sp} = 23^\circ$, model scale			
Base size of mesh [m]		0.20	0.25
Volume mesh representations	Cells	$2.17 \cdot 10^6$	$1.36 \cdot 10^6$
	Interior Faces	$12.0 \cdot 10^6$	$7.20 \cdot 10^6$
	Vertices	$8.96 \cdot 10^6$	$5.25 \cdot 10^6$

Table 0.5 Simulation results of different mesh sizes

J	K_T		K_Q	
	0.20 m	0.25 m	0.20 m	0.25 m
0.1	0.5787	0.5803	0.0902	0.0909
0.3	0.4787	0.4777	0.0769	0.0770
0.5	0.3743	0.3727	0.0636	0.0634
0.7	0.2710	0.2695	0.0502	0.0500
0.9	0.1699	0.1693	0.0364	0.0364
1.1	0.0557	0.0551	0.0204	0.0204
1.2	-0.0129	-0.0140	0.0105	0.0104

There is only a marginal difference between the results for a specific advance ratio J, for example, when $J = 0.70$, the difference of thrust coefficient expressed by percentage is:

$$\Delta K_T = \frac{0.2710 - 0.2695}{0.2710} \times 100\% = 0.55\%$$

However, the required time of the simulation for the case with the base size of 0.20 m (about 40 hours) is approximately twice of the case with the base size of 0.25 m. Therefore, the base size 0.25m will be applied to all the simulations for model scale propellers and the base size of the full scale

propellers will be this value multiplied by the scale factor ($M=10, 20$).

The CFD results are compared with the experimental data (Fig.3.1) and the consistency of the CFD results and experimental data indicates the CFD setups are proper.

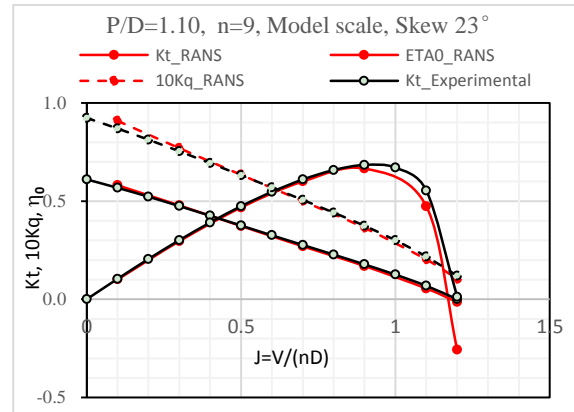
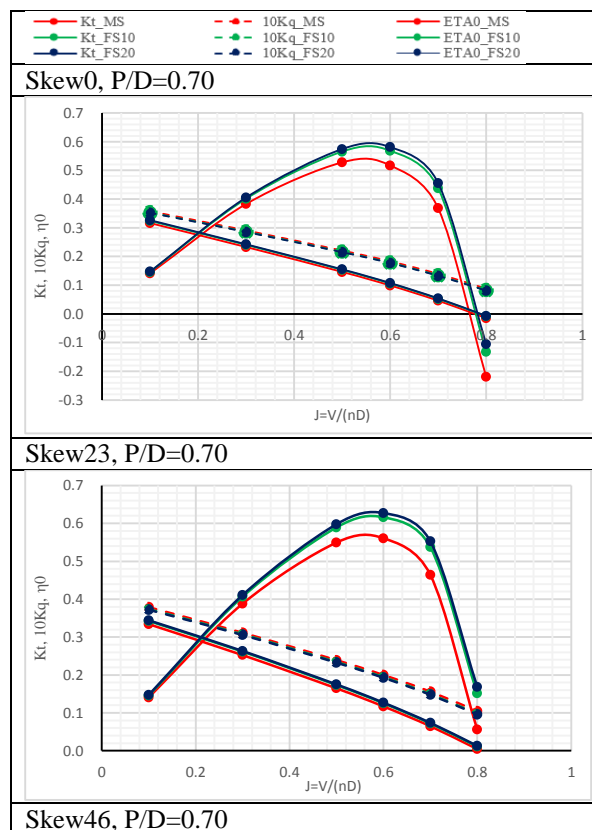


Fig.3.1 Comparison of CFD results and experimental data

The scale effects on open water performance of propellers with different skew angles are shown in Fig.3.2.



Skew46, P/D=0.70

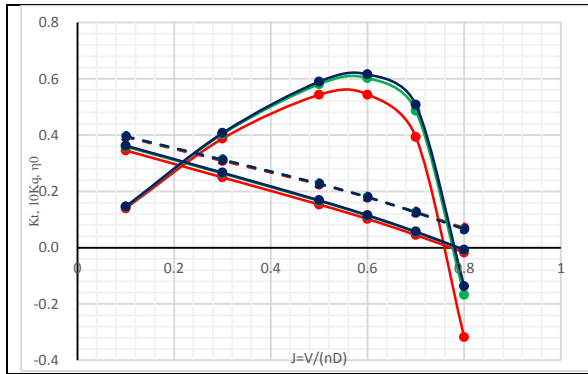


Fig.3.2 open water diagrams of scale effects study

The open water diagrams show the same tendency in the characteristics (thrust coefficient K_T , torque coefficient K_Q and efficiency η_0) of different scale propellers with the same skew angle. The thrust coefficient K_T and efficiency η_0 of the model scale propeller is always lower than that of the full scale propellers at the same skew. The propellers of two different full scales (FS10, FS20) show little difference in terms of thrust coefficient K_T and efficiency η_0 compared with that of propellers in corresponding model scale. The propeller with the largest diameter (FS20, $D = 5.0$ m) indicates the maximal thrust coefficient K_T , minimal torque coefficient K_Q and highest efficiency η_0 in comparison with the propellers in the other two scales at the same skew.

The skew effects of propellers in the same size have also been investigated (shown in Fig.3.3). for propellers with different skews (skew0, skew23, skew46), the overall trends of thrust coefficient K_T , torque coefficient K_Q and efficiency η_0 are identical from one scale to another. Therefore, the propellers with different skews (skew0, skew23, skew46) in model scale were taken as analysis examples. The diagram states that the propeller with a skew angle of 23 deg possesses the largest thrust force in a wide range of advance velocity ($J \geq 0.3$) and the efficiency of it is also higher than the other two propellers with the skew angle of 0 deg and 46 deg when $J \geq 0.5$. The propeller skew0 performed the minimal thrust force in almost the whole simulation range while the measured thrust force for Skew 46 shows the most obvious decrease as the increase of advance velocity.

To understand the aforementioned behaviour of the characteristics, the two components of total forces – pressure and friction – were analyzed for both model scale and full scale propellers with different skews (refer to Table 3.3). The friction part of the total force shows negligible differences between different skews of propellers in the same scale, for instance, when $J = 0.3$, the friction component is -0.0027 for propellers with three different skews (skew0, skew23, skew46). Therefore, the differences for thrust force of propellers with

different skews in one particular scale comes from the pressure component of the total force.

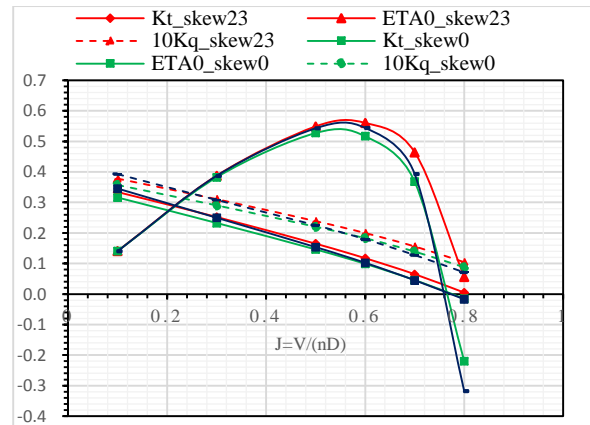


Fig.3.3 Skew effects analysis, model scale, open water diagram

Table 0.6 Pressure and friction components in total forces of model scale propellers

J	K_T	MS		
		Skew 0°	Skew 23°	Skew 46°
0.3	Calc(Tot)	0.2327	0.2526	0.2498
	Pressure	0.2354	0.2553	0.2525
	Friction	-0.0027	-0.0027	-0.0027
0.5	Calc(Tot)	0.1460	0.1649	0.1535
	Pressure	0.1488	0.1677	0.1564
	Friction	-0.0028	-0.0028	-0.0029
0.7	Calc(Tot)	0.0459	0.0650	0.0449
	Pressure	0.0489	0.0680	0.0481
	Friction	-0.0031	-0.0031	-0.0032

The pressure distribution on the propellers with different skews and scales along the chord length of the blades are represented by the sections of 0.5R, 0.7R, 0.9R and 0.95R. Firstly, the scale effects of pressure distribution on propellers with different magnitude of skews were investigated on the blade sections of 0.7R under the condition of $J = 0.1$. The results are shown in Figure 4.2.33.4, and in this picture, c_p represents the pressure coefficient, x states the position of the point on the section along the chord and c indicates the chord length of the section $r/R = 0.70$. The pressure distribution shows negligible differences between propellers with various scales (MS, FS10, FS20). The pressure distribution is independent on scale effects.

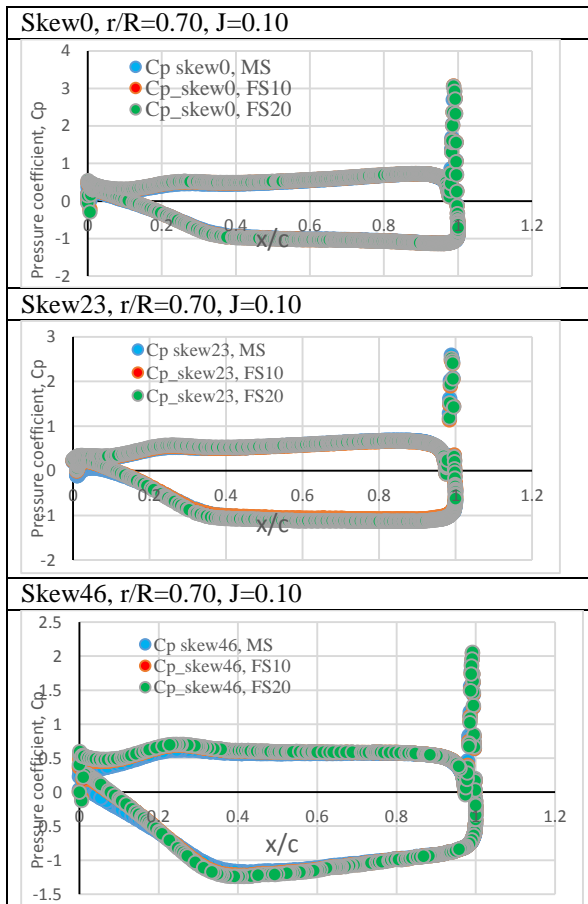


Fig.3.4 Pressure distribution on the section 0.7R for propellers with the same skews and different scales

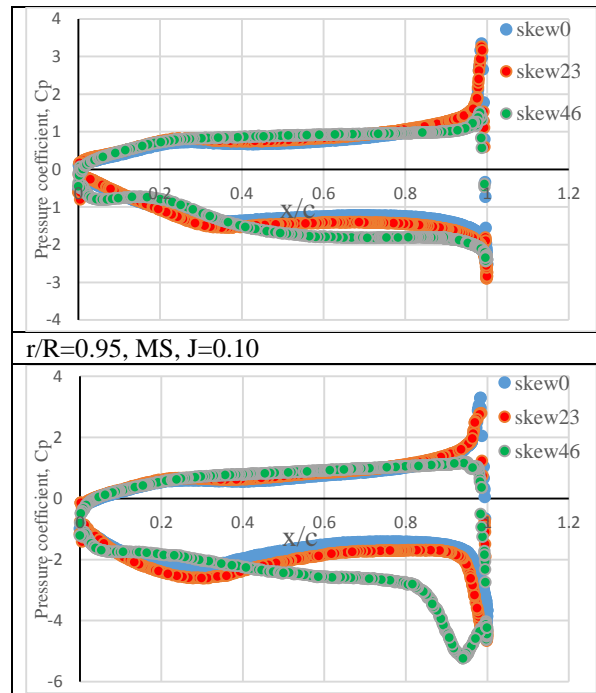
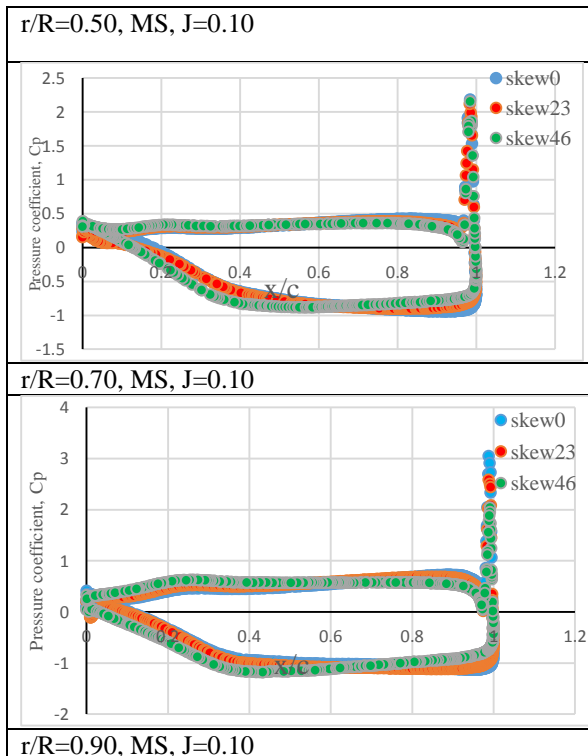


Fig.3.5 Pressure distribution of section 0.50R, 0.70R, 0.90R, 0.95R, model scale, J=0.10

The later pressure distribution analysis is mainly focused on the effects of blade section location (0.5R,0.7R, 0.9R and 0.95R) and various of skews (skew0, skew23, skew46) at the same propeller scale – model scale. The pressure distribution diagrams of blade sections in various positions are shown in Figure 4.2.43.5.

In the blade location $r/R = 0.50$, the propeller skew46 (skew angle 46 deg) shows higher pressure on the suction side in the region of $0 < x/c < 0.5$ followed by the propeller skew23 (skew angle 23 deg). On the pressure side, the propeller skew46 shows the lowest pressure and skew0 shows the highest pressure in the region of $0 < x/c < 0.6$. This trend is reversed in the area of $0.6 < x/c < 1.0$. Propeller skew46 shows the maximum pressure deduction in the region close to trailing edge ($0 < x/c < 0.6$) and propeller skew0 indicates the largest pressure deduction in the region close to leading edge are ($0.6 < x/c < 1.0$). In the blade section $r/R = 0.70$, the pressure distribution states the similar tendency as that of the location $r/R = 0.50$. The pressure deduction along the chord length at $r/R = 0.70$ is more larger than that of the position $r/R = 0.50$.

The pressure distribution along the chord length at $r/R = 0.90$ shows greater differences than that of the previous two sections. The propeller skew46 shows the highest pressure in the mid-chord region ($0 < r/R < 0.70$) on the suction side while in the leading edge area ($0.70 < r/R < 1.0$), it indicates the lowest pressure. In the region of $0.40 < r/R < 0.70$, propeller skew46 shows the largest pressure deduction. When $0.10 < r/R < 0.40$, on the pressure side of the section, propeller skew23

shows the most obvious pressure deduction. As to the pressure distribution of the section $r/R = 0.95$, it is apparent that the propeller skew46 shows the lowest pressure in the range of $0.40 < r/R < 1.0$ on the pressure side and it also indicates the largest pressure gap in that range.

The vortex in the region around the blades also shows some differences for propellers with various of skew angles and different scales. The vortex analysis for propellers with the same scale is performed on model scale propellers with different skew angles (skew0, skew23, skew46) as shown in Figure 4.2.83.6. The tip vortex play an important part in the differences. For the symmetric blade propeller (skew0), in the present range of 100-1500 /s, it shows the weakest tip vortex while the propeller with a skew angle of 46 deg (skew46) states the strongest tip vortex. In the leading edge area, the propeller skew46 also shows the strongest vortex. The intensity of vortex increases as the skew angle increasing – from skew angle 0 deg to 46 deg, which is indicated by the widespread blue colour in the simulated vortex region of propeller skew46 followed by skew23.

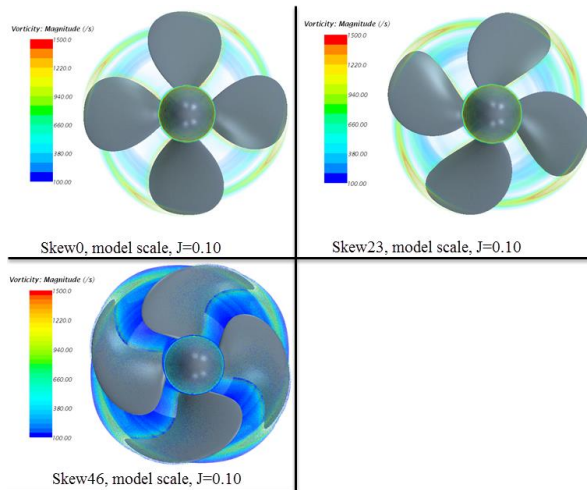


Fig.3.6 Vortex around the propellers with different skew angles (skew0, skew23, skew46) in model scale

For the vortex conditions produced by propellers at the same skew angle but different scales, the analysis was performed on the propeller with a skew angle of 23 deg (shown in Figure 4.2.93.7). It is obvious that in the range of 0 – 500 /s for vorticity magnitude, the model scale propeller performs the strongest vortex while the largest scale propeller (FS20, $D = 5.0\text{m}$) presents the weakest vortex.

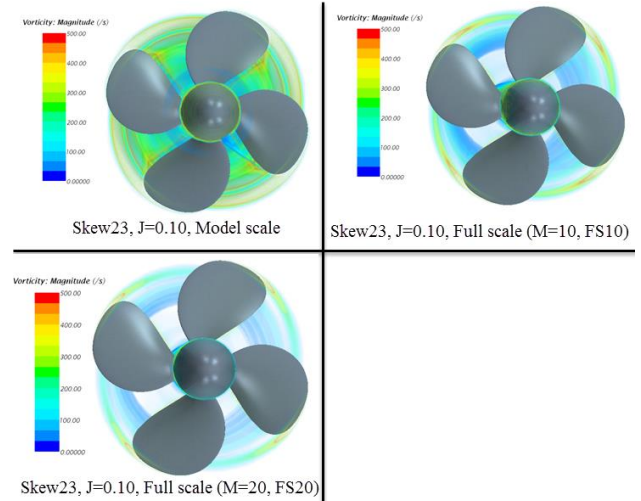


Fig.3.7 Vortex around the propellers with different scales (MS, FS10, FS20) and skew angle 23 deg

As the propeller P1374 with skew angle of 23 deg is the parent propeller, there are more data obtained for it. In last chapter, the ITTC scale effects correction has been calculated as a reference for this propeller.

The relative difference of thrust coefficient ΔK_T is shown in Figure 5.1.73.8. In the advance ratio $J = 0.80$, the values rise up significantly and the reason for this has been explained in last section (skew angle 0 deg). According to the ITTC algorithm, the relative differences for scale effects is much smaller than the resultant values from CFD methods applied in this project. The relative difference ΔK_T is increasing with the increase of advance ratio for the same propeller. The relative difference for the propeller with a bigger scale (FS20) is larger than that of the propeller FS10 for all the advance ratios. The relative difference of torque coefficient ΔK_Q is shown in Figure 5.1.83.9. The ITTC expectation for that is much larger than the CFD results. As the ITTC method only take the effects of Reynolds number Re on drag neglecting the effects on section lift, this difference can be proper.

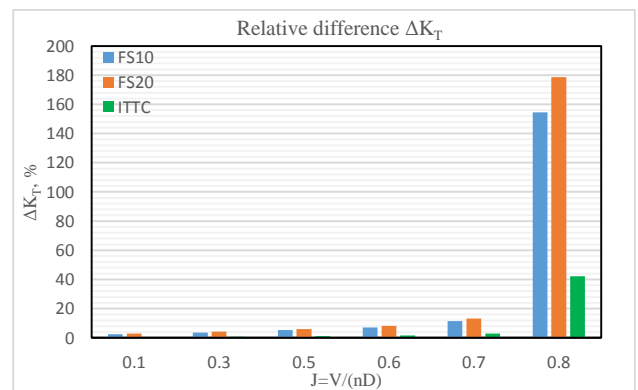


Fig.3.8 Relative differences for thrust coefficient K_T , skew angle 23 deg

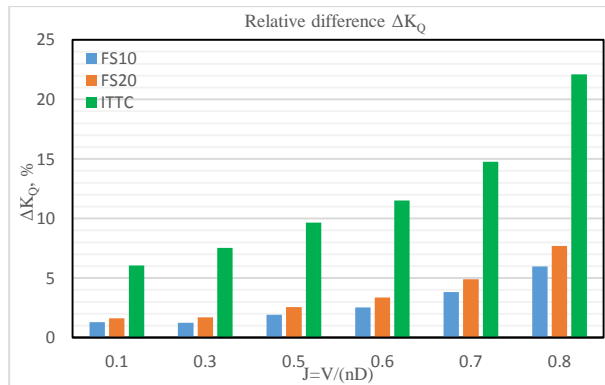


Fig.3.9 Relative differences for torque coefficient K_Q , skew angle 23 deg

4. CONCLUSION

For propellers with the same skew angle, the thrust coefficient K_T and efficiency η_0 will increase with the increasing propeller scale, for example, at the same advance ratio J , the thrust coefficient K_T of propeller P1374 in full scale with the scale factor of 20 (FS20) has the highest value followed by that of the full scale propeller with the scale factor of 10 (FS10), and the model scale propeller P1374 shows the lowest K_T .

For the propellers with the same scale, the open water characteristics (thrust coefficient K_T , torque coefficient K_Q and efficiency η_0) are different from one skew to another. Propeller P1374 (skew angle 23 deg) is always larger than that of the symmetric blade propeller (skew angle 0 deg). However, the characteristics of propeller with the skew angle of 46 deg changes fast along the different advance ratio. In the low advance ratio range ($0 < J < 0.3$), the propeller with skew angle 46 deg has the largest open water characteristics compared the other two propellers with different skews, but in high advance ratio scope ($J > 0.6$), it possesses the lowest values. Thus the changes of open water performance for propeller skew angle 46 deg is fast. The analysis on pressure distribution for different blade sections and vortex reveals that the main differences of open water performance result from the outer portion of the blades. The flow pattern of the region near the blade tip is also more complex than that of other regions.

The scale effects analysis indicates that the larger the size of full scale propeller is, the larger differences of open water performance from model scale propellers will be resulted in. Compared with the ITTC expectation, the CFD results still reveals big differences especially for high advance ratios. As the ITTC method only take the effects of Reynolds number Re on drag neglecting the effects on section lift, this difference can be proper.

REFERENCES

- [1] John Carlton, Marine Propellers and Propulsion, 2007, Page 200-201
- [2] Vladimir Krasilnikov, Jiaying Sun & Karl Henning Halse, CFD Investigation in

Scale Effect on Propellers with Different Magnitude of Skew in Turbulent Flow, 2009, Page 1-11

- [3] John Carlton, Marine Propellers and Propulsion, 2007, Page 33-39
- [4] John Carlton, Marine Propellers and Propulsion, 2007, Page 95-98
- [5] Vladimir I. Krasilnikov, First Introduction into Computational Fluid Dynamics for Marine Applications, 2011, Page 3
- [6] Vladimir I. Krasilnikov, First Introduction into Computational Fluid Dynamics for Marine Applications, 2011, Page 72-152
- [7] John Carlton, Marine Propellers and Propulsion, 2007, Page 89-94
- [8] Performance, Propulsion 1978 ITTC Performance Prediction Method, 7.5-02-03-01.4, Page 3-5